An alloy selection and processing framework for nanocrystalline materials

by

Arvind R. Kalidindi

B.S. Mechanical Engineering
Drexel University, 2013

SUBMITTED TO THE DEPARTMENT OF MATERIALS SCIENCE AND ENGINEERING
IN PARTIAL FULFILLMENT OF THE REQUIREMENTS OF THE DEGREE OF

Doctor in Philosophy in Materials Science and Engineering

at the

MASSACHUSETTS INSTITUTE OF TECHNOLOGY

September 2018

Signature of Author: ……
Department of Materials Science and Engineering
March 22, 2018

Certified by: ……
Christopher A. Schuh
Danae and Vasilios Salapatas Professor of Metallurgy
Thesis Supervisor

Accepted by: …….
Donald Sadoway
Chair, Departmental Committee for Graduate Studies

An alloy selection and processing framework for nanocrystalline materials

by

Arvind R. Kalidindi

Submitted to the Department of Materials Science and Engineering
on March 22, 2018 in Partial Fulfillment of the Requirements for the
Degree of Doctor of Philosophy in Materials Science and Engineering

ABSTRACT

Nanocrystalline materials have a unique set of properties due to their nanometer-scale grain size. To harness these properties, grain growth in these materials needs to be suppressed, particularly in order to process bulk nanocrystalline components and to use them reliably. Alloying the material with the right elements has the potential to produce remarkably stable nanocrystalline states, particularly if the nanocrystalline state is thermodynamically stable against grain growth. This thesis builds upon previous models for selecting alloy combinations that lead to thermodynamic stability against grain growth, by developing frameworks that extend to negative enthalpy of mixing systems and ordered grain boundary complexions. These models are used to develop a generalized stability criterion based on bulk thermodynamic parameters, which can be used to select alloy systems that are formally stable against grain growth. A robust statistical mechanics framework is developed for reliable thermodynamic observations using Monte Carlo simulations to produce free energy diagrams and phase diagrams for stable nanocrystalline alloys.

Thesis Supervisor: Christopher A. Schuh

Title: Danae and Vasilios Salapatas Professor of Metallurgy

ACKNOWLEDGEMENTS

The research presented in this work would not have been possible without the support of several colleagues, advisors, friends, and family.

When I started in the Schuh Group, I was new to the study of metallurgy. I want to thank Tongjai Chookajorn, Michael Gibson, and Zachary Cordero for taking me under their wing and bringing me up to speed on the thermodynamics and metals processing that led to the developments in this thesis. I also want to thank many other members of the Schuh Group – Oliver, Kathleen, Alan, Ting-Yun, Mostafa, Kathrin, Dor, Peter, Wenting, Eddie, Isabel, Ashley, Kat, Thomas, and others – for being supportive and helpful throughout my Ph.D. You have all had a great impact on this work and my wonderful time at MIT; it has truly been an honor and a privilege being your groupmate!

My advisor, Chris Schuh, provided constant guidance, inspiration, and wisdom throughout my Ph.D. When I joined the materials science department, I chose the Schuh Group because I believed Chris was an exceptional advisor and a brilliant researcher – looking back this was one of the best decision I have made in my life. Thank you Chris for helping me become the person I am today and for giving me the environment to thrive as a researcher over the past 5 years.

I want to thank Profs. Carl Thompson and Ju Li for advising me on the direction of this thesis as part of my thesis committee, and for lively discussions on grain boundaries and complexions that always gave me ample ideas to work on. I also want to thank Aslan Ahadi for collaborating on NiTi-W nanocrystalline alloys. My Ph.D. experience was made possible by the National Science Foundation Graduate Research Fellowship and the National Defense Science and Engineering Graduate Fellowship.

My time at MIT was marked by great friendship. To my roommates, Alex and Frank, our time at 45 Union St. was incredibly fun and enriching, and will be some of my fondest memories from MIT. Abigail, Ross, and Yang Yang, thank you for always being there when I wanted some company over soup dumplings, and Olivia, Seth, Jeremy, Brendan, Kate, and Jane, I will miss our Cambridge adventures and game nights. Neha, through the final year of my Ph.D. you have been an incredible new part of my life and have revealed in me an entirely new part of myself; I love you and am excited for our next steps together.

My parents, Manju and Surya, and my brother, Bharath – your enduring love and support is the reason that I am who I am today and why I could even imagine embarking on this Ph.D. at MIT. Mom and Dad, thank you for giving me the confidence in my abilities and investing in my education to make all of this possible. Bharath, you will always be my better half and I will never enjoy anything more than watching sports with you at home eating chicken curry. And to my broader family, Mrudu, Anil, Meghana, Sanjana, Phani, Kiran, Sudeep, Anish, Pedda, Jayanthi, Siddhardth, Meera, Tattaya and Ammamma, I am incredibly grateful for having all of you be such big parts of my life and supporting me in everything I do.

Table of Contents

List of Figures

List of Tables

Chapter 1: Introduction

Section 1.1: What are nanocrystalline materials and why are they interesting?

Most structural materials used commercially are polycrystalline, meaning that they contain several crystalline regions, called grains, which each have different lattice orientations. At the intersection of grains, there is a planar defect due to the misorientiation of the two adjoining lattices, called a grain boundary. Structural materials produced through conventional processing methods, e.g. casting or sintering, typically have grain sizes in the 10s of microns and up to millimeter length scales. On the other hand, polycrystalline materials prepared through thin film fabrication methods, such as sputtering or electrodeposition, generally have grain sizes that are orders of magnitude smaller, and can be as small as a few nanometers [1-3].

These materials, when possessing grain sizes less than 100 nm, are referred to as nanocrystalline materials. The structural properties of these nanocrystalline materials have been studied in thin film form quite extensively. Most notably, nanocrystalline materials have a high yield strength, as described by the Hall-Petch relationship (Figure 1) [4-7], an empirical observation that the yield strength, σ_y, increases with decreasing grain size, d, as $\sigma_y = \sigma_0 + k\frac{1}{\sqrt{d}}$, where k and σ_0 are material-specific constants.

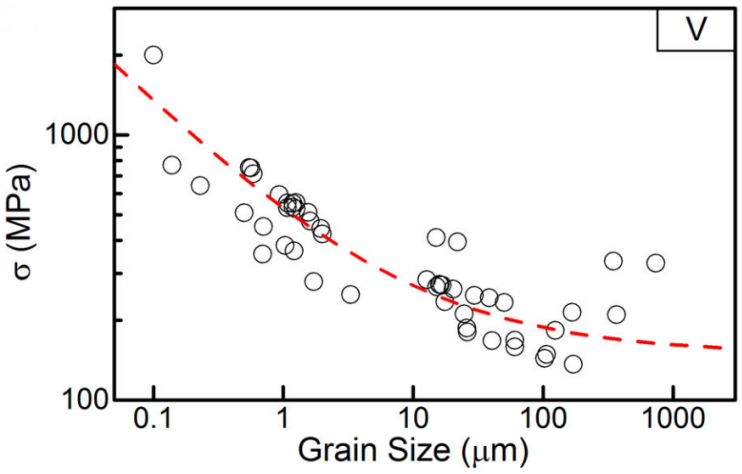

Figure 1: An example of the Hall-Petch relationship as observed through tensile and/or compression tests in vanadium, where the yield strength increases with decreasing grain size. This trend has been observed for several material systems, many of which are outlined in a review paper by Cordero et. al. from which this figure is reproduced with permission [7].

The high yield strength of nanocrystalline materials has several promising applications. For instance, in material applications where plastic deformation constitutes failure, one can use a fraction for the same material to meet load tolerances if the material is nanocrystalline. As a result, producing nanocrystalline materials can enable light-weighting in structural applications such as automobiles and aircrafts. Additionally, certain applications, such as tooling or coatings, are limited by the yield strength of the material. Today, W-carbide and diamond films are often used in these applications where the material hardness is critical to performance. Refining the grain structure can enable alternate pathways to producing material hardness that rivals and potentially surpasses that of current high-hardness materials. This has the potential to decrease costs, increase material performance, and offer more diversity in materials for high hardness applications, which can decrease reliance on rare or hazardous materials (such as depleted uranium or chromium [8, 9]).

Section 1.2: Suppressing grain growth is the challenge to producing bulk nanocrystalline materials

Grain sizes in the nanocrystalline regime can be readily formed in thin films. However, producing a bulk part that is nanocrystalline is a serious challenge, due to the propensity of nanocrystalline materials to undergo grain growth at low homologous temperatures. Nanocrystalline materials have a much higher density of grain boundaries, which carry an excess energy (~ 1 J/m^2) as defects [10], than a courser grained material. Due to the high density of grain boundaries, the driving force for grain growth is substantially higher for nanocrystalline materials compared to course grained materials: doubling the grain size of a nanocrystalline material leads to a ~1000 times larger decrease in grain boundary area than does doubling a micron-scale grain size.

As a result, nanocrystalline materials undergo rapid grain growth at relatively low temperatures (Figure 2) [11]. For instance, nanocrystalline Ni undergoes grain growth from grain sizes in 10s of nanometers to 100s of nanometers in just 30 minutes at 300 °C [11]. The use of conventional routes for producing bulk parts generally require time at elevated temperatures. Solidifying into the nanocrystalline regime from a liquid phase requires a high nucleation rate and a low coarsening and growth rate, conditions that either require unreasonable cooling rates, or in

glass-formers require avoiding glass transitions. Alternatively, one can produce nanocrystalline materials from bulk metallic glasses, but producing bulk metallic glasses is in itself a challenge and such devitrified materials can be brittle due to a strong tendency to form intermetallics [12]. Powder-route processing by sintering nanocrystalline powders into a bulk part requires avoiding substantial grain growth at sintering temperatures.

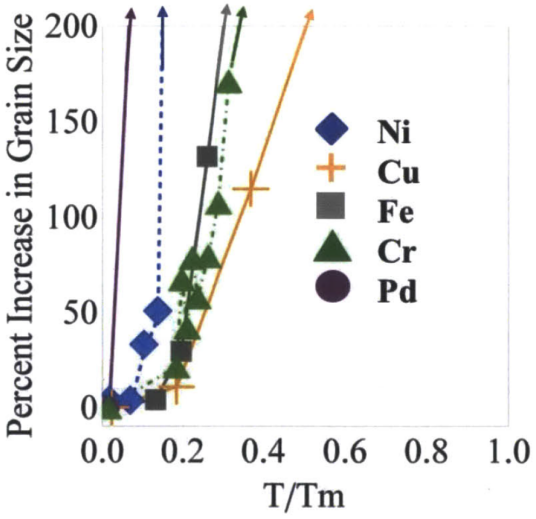

Figure 2: Rapid grain growth occurs at relatively low homologous temperatures in unalloyed nanocrystalline materials (Reproduced from the thesis of Heather Murdoch [11]).

The key challenge to producing bulk nanocrystalline materials is therefore to mitigate grain growth at elevated temperatures. Grain growth is enabled by grain boundary motion, the speed (v) of which can be described by:

$$v = M\gamma\kappa \tag{1}$$

where M is the mobility of the grain boundary (and is expected to have an Arrhenius behavior), γ is the grain boundary energy (decreases linearly with temperature), and κ is the curvature of the grain boundary (high in bulk nanocrystalline materials) [13]. Therefore, to avoid substantial grain growth at low temperatures in nanocrystalline materials, either the mobility needs to be drastically reduced so that grain boundaries cannot move easily or the excess energy of the grain boundary itself needs to be reduced so that grain boundaries have a smaller driving force to move and cause grain growth.

Section 1.3: Alloying to suppress grain growth in nanocrystalline materials

Alloying is a powerful way to reduce grain growth as it can both reduce the grain boundary mobility and decrease the grain boundary energy. Grain boundary mobility is decreased by two different mechanisms in alloys. In multiphase alloys, precipitates of secondary phases can pin grain boundaries [14,15], known as Zener pinning, providing an obstacle which grain boundaries must pass through, thereby increasing the activation energy for grain boundary motion. To stabilize nanocrystalline alloys against grain growth through Zener pinning, the precipitate size must be nanometer scaled as well [14,15]. This poses a secondary challenge in preventing coarsening of fine precipitates, particularly since these precipitates reside on grain boundaries which can act as fast diffusion pathways for coarsening. As a result, second phases such as oxides and carbides that are more likely to be interface-limited in coarsening are generally required for Zener pinning to be successful in nanocrystalline materials [16,17]. Grain boundary mobility can also be decreased by solute drag, where solute species in solid solution provide resistance to grain boundary motion as the grain boundary must incorporate the solute into its free volume and then reject the solute as it passes by [18-20]. This mechanism similarly can increase the activation energy for grain boundary motion.

Suppressing grain boundary motion is referred to as a "kinetic" route to stabilizing nanocrystalline materials against grain growth at elevated temperatures [21]. Due to the Arrhenius relationships underlying these kinetic mechanisms, increasing the activation energy by a factor, X, allows the alloy to be stable against grain growth up to temperatures of roughly a factor of X higher than for the pure solvent material. While such increases in the temperature at which grain growth occurs has the potential to enable the processing of bulk nanocrystalline alloys, identifying the right alloying elements is complicated by the difficulty in assessing activation energies of grain boundary motion in alloys [22]. Thus, even though these mechanisms are well-established, they have not yet enabled the systematic development of bulk nanocrystalline alloys.

Alloying can also decrease the grain boundary energy when alloying elements segregate to the grain boundary, decreasing the driving force for grain growth [23-25]. Grain boundary segregation is the presence of an excess concentration of solutes in the grain boundary with respect to the bulk concentration of that solute element. The magnitude of the decrease in energy at the grain boundary is measured by the enthalpy of grain boundary segregation for an alloy system.

The enthalpy of grain boundary segregation is defined as the change in energy between a random distribution of solutes in the system and the equilibrium, grain boundary segregated state on a per mole basis.

Designing alloys based on the grain boundary segregation effect as a means to suppress grain boundary motion is referred to as a "thermodynamic" route to stabilizing nanocrystalline materials [21]. The enthalpy of segregation decreases the grain boundary energy linear manner, and so this effect is generally weaker than the kinetic drag and pinning effects which have exponential effects on grain boundary motion. However, unlike the kinetic route, the thermodynamic route has the potential to produce a formally stable nanocrystalline state.

The concept of a formally stable nanocrystalline alloy was first introduced by Weissmüller [26-27]. Using the Gibbs adsorption isotherm, Weissmüller showed that if the segregation of solute species is energetically favorable enough to offset the excess free energy associated with the grain boundary, then the segregated grain boundary states would be stable against grain growth. Using classical thermodynamics, Weissmüller derived an expression for the grain boundary energy, γ, for a dilute binary alloy with solute segregation at the grain boundaries:

$$\gamma = \gamma_0 - \Gamma_{\mathrm{sat}}\left[\Delta H_{\mathrm{seg}} + RT\ln(x_{\mathrm{c}})\right] \tag{2}$$

In this expression, γ_0 is the pure solvent grain boundary energy, which can be offset by an alloying addition with a positive enthalpy of grain boundary segregation, ΔH_{seg}, defined here as the enthalpy required to take a single solute atom from the crystalline region and place it into the grain boundary in the dilute limit. Γ_{sat} is the specific solute excess at the solute-saturated grain boundary, and x_{c} is the solute concentration in the crystalline region. This equation shows that the grain boundary energy is decreased linearly with the enthalpy of grain boundary segregation. Based on this expression, Weissmüller showed that strongly segregating solute species can reduce the grain boundary energy to zero, or more specifically, can lead to a minimum in the free energy of the alloy with respect to grain boundary area, $\frac{\mathrm{d}G}{\mathrm{d}A} = 0$, at a finite grain size as shown in Figure 3. Such a nanocrystalline state in the alloy has no driving force to change its grain boundary area when the grain size is equal to the equilibrium grain size; the nanocrystalline state is stable against grain growth, because grain growth would require ejection of some solute into the grain interiors at an energy penalty.

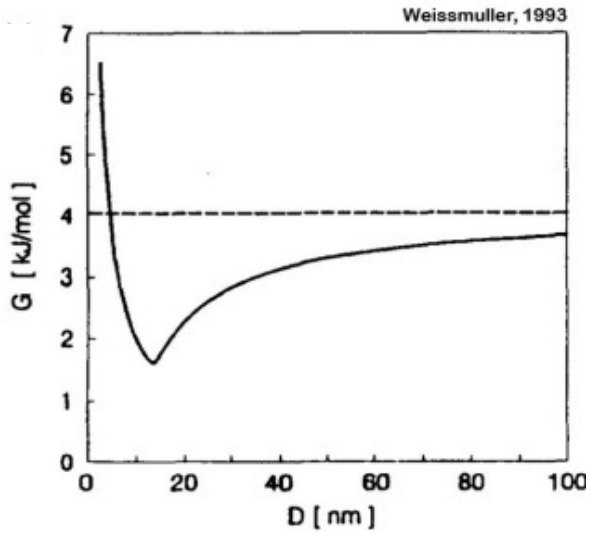

Figure 3: This figure shows the free energy of a nanocrystalline alloy (with a large enough enthalpy of segregation to be thermodynamically stable) as a function of grain size. The minimum in free energy occurs at a finite, nanocrystalline grain size from which there is no driving force for grain growth (Reproduced with permission from [27]).

Unlike the kinetic route, the enthalpy of grain boundary segregation can be estimated theoretically through density functional theory calculations, embedded atom-type potentials, as well as empirical Miedema models [27-31]. As a result, identifying alloy systems that are stable thermodynamically against grain growth is a more viable route to developing bulk nanocrystalline materials systematically. In the next section, previous models for identifying and developing such alloy systems are discussed, which form the foundation on which the frameworks in this thesis are developed.

Section 1.4: Existing frameworks for designing nanocrystalline materials

Section 1.4.1: Analytical models for stability against grain growth and solute precipitation

Early alloy systems developed using the Weissmüller framework were typically observed to exhibit stability of nanocrystalline grain sizes at low annealing temperatures. However, at the elevated tempreatures required for processing bulk nanocrystalline parts, these alloys were often observed to undergo rapid grain growth [32-38]. Experiments monitoring grain growth often

observed that second phases would form at the instance when rapid grain growth was initiated, an example of which is shown in the Fe-Cu system in Figure 4 [38].

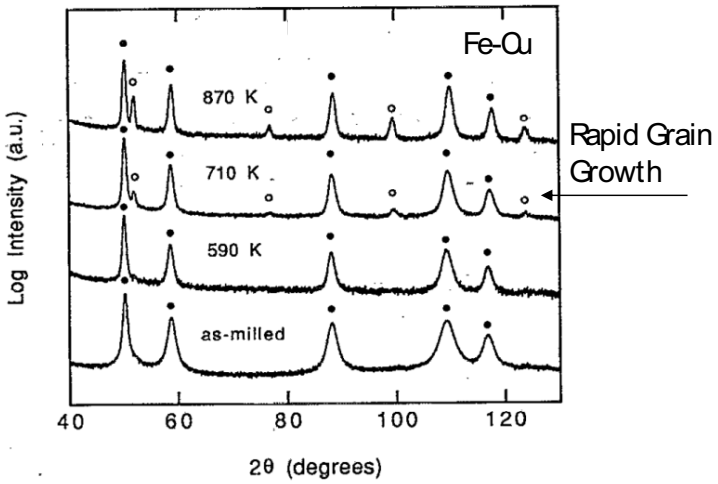

Figure 4: Diffraction patterns for Fe-Cu during annealing (heating at 20 K/min). Grain growth out of the nanocrystalline regime is observed following a phase transformation (white dots) in the Fe-Cu alloy (reproduced with permission from [38]).

This revealed a key limitation of the model developed by Weissmüller for thermodynamic stability of the nanocrystalline state: the assumption that the solutes are in dilute concentrations. Because the Weissmüller model does not account for the potential for solutes to form a second phase, it effectively only compares the free energy of the nanocrystalline state to that of a single crystal solid solution at the same concentration. To be truly stable, the nanocrystalline state needs to be energetically preferred to any single crystalline state, including those containing second phases.

To begin to alleviate the dilute limit assumption from Weissmüller's model, Trelewicz and Schuh [39] used a regular solution approach to develop the regular nanocrystalline solution (RNS) model. In addition to a crystalline grain interior region, the RNS model includes a grain boundary region, defined by two variables. This first variable is the grain boundary volume fraction, which in their model mapped monotonically to grain size. The second variable is the grain boundary solute concentration, which is a measure of the degree of grain boundary segregation. As in the classical regular solution model, the free energy of the alloy state is determined from the internal energy, calculated by summing the energies of the bonds (assuming a random distribution of solute in the crystalline and grain boundary regions and considering nearest-neighbor pairwise

interactions), and from the configurational entropy of the full system. A particular alloy system can be described by interaction parameters, ω, which are used to define the solute-solvent bond energies within the crystal (c) and grain boundary (gb) regions:

$$\omega_{\mathrm{c}} = E_{\mathrm{AB}}^{\mathrm{c}} - \frac{E_{\mathrm{AA}}^{\mathrm{c}} + E_{\mathrm{BB}}^{\mathrm{c}}}{2} \tag{3}$$

$$\omega_{\mathrm{gb}} = E_{\mathrm{AB}}^{\mathrm{gb}} - \frac{E_{\mathrm{AA}}^{\mathrm{gb}} + E_{\mathrm{BB}}^{\mathrm{gb}}}{2} \tag{4}$$

where E is the energy per bond classified by the subscript which represents the types of species bonded (A – solvent, and B – solute) and the superscript which denotes the bond type. The two interaction parameters can be related to the enthalpy of mixing and enthalpy of segregation to link model predictions of stability to actual alloys [39,40]:

$$\Delta H_{mix} = z\omega_c \tag{5}$$

$$\Delta H_{seg} = z\left[\omega_c - \frac{\omega_{gb}}{2} - \frac{1}{2zt}(\Omega^B\gamma_0^B - \Omega^A\gamma_0^A\right] \tag{6}$$

where Ω is the atomic volume of an element, z is the coordination number, and t is the thickness of the grain boundary.

The free energy calculated by the RNS model is not restricted to dilute solutions or saturated grain boundaries. The equilibrium state is the one that minimizes the free energy, but unlike in the Weissmüller model where the only degree of freedom is the grain size, in the RNS model both the grain size and the concentration at the grain boundary are equilibrium quantities. The free energy landscape for a particular alloy chemistry is shown in Figure 5 [41]. The Trelewicz-Schuh RNS model has also been refined and extended by other authors to different more specific situations, with similar general outputs in each case [42-45].

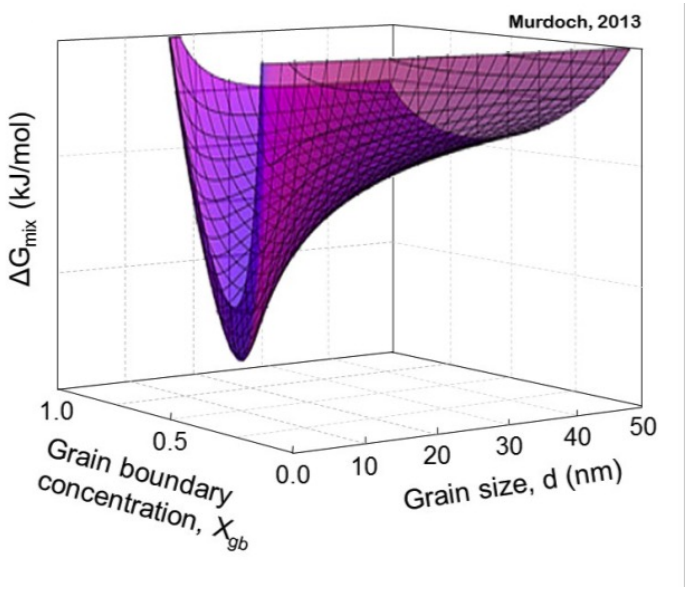

Figure 5: The free energy landscape of a stable nanocrystalline alloy as calculated by the regular nanocrystalline solution model, where a minimum in free energy exists at a finite grain size in the nanocrystalline regime (Reproduced with permission from [41]).

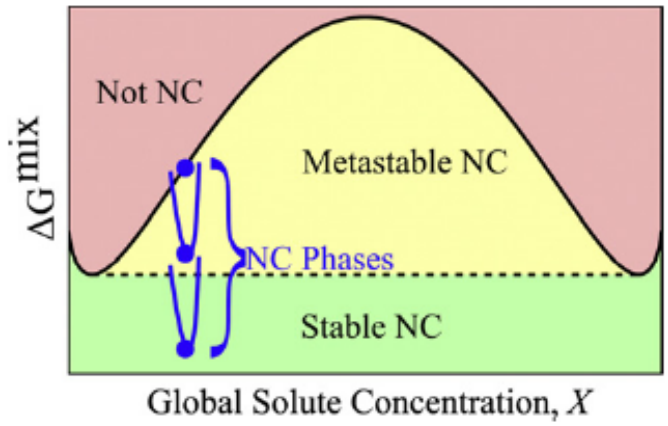

Figure 6: The free energy diagram schematic for a binary alloy with the inclusion of nanocrystalline free energy curves (blue curve, which would be calculated from the RNS model). If the nanocrystalline free energy curve lies below the miscibility gap, the nanocrystalline state is formally stable against grain growth, but if it falls in the yellow, metastable, region it is unstable against forming a second phase (Reproduced with permission from [41]).

Murdoch and Schuh used the RNS model to explicitly define metastability and stability of nanocrystalline alloys against grain growth [41]. In order for the nanocrystalline state to be stable, the free energy of the nanocrystalline state has to reside below the free energy of any bulk

equilibrium state on the free energy diagram. As shown in Figure 6, Murdoch and Schuh used a regular solution treatment for the bulk miscibility gap and defined a nanocrystalline state as stable if it lies below the miscibility gap.

This is an immensely valuable insight for the selection of alloying elements for stabilizing nanocrystalline alloys against grain growth, as it improves upon the largest shortcoming of the Weissmüller model by accounting for driving forces for forming second phases. As a result, nanocrystalline alloys that are found to be stable under this criterion would be expected to be formally stable against grain growth up to elevated temperatures and ideal candidates for producing bulk nanocrystalline materials. Through a series of simulations, Murdoch and Schuh found that the stability criterion can be written as:

$$\Delta H_{\text{seg}} > c(\Delta H_{\text{mix}})^{a} \tag{7}$$

where the coefficients *a* and *c* depend on the homologous temperature and were fitted to the results of the RNS model.

Chookajorn et al. [46] developed a stability map for W alloys using this analytical approach, shown in Figure 7 with corresponding free energy diagrams illustrating the difference between a predicted stable nanocrystalline alloy, W-Sc, and a classical bulk stable alloy, W-Ag. The map delineates the alloy pairs for which at least one nanocrystalline alloy has an energy lying below the miscibility gap free energy. This map was used to identify W-Ti as a candidate for exhibiting thermodynamic stability at 1100 °C. This system was subsequently explored with a W-20 at.% Ti alloy that exhibited no significant changes in grain size after annealing at 1100 °C for 1 week. The results of Chookajorn et al. [46] show that a simple analytical model such as the RNS model can be used to rapidly screen possible alloys that may exhibit nanocrystalline ground states.

The RNS framework also has the potential to guide the processing of nanocrystalline alloys by describing how the free energy landscape of nanocrystalline states is affected by processing parameters such as temperature and composition. Zhou and Luo [47] extended the approach of Murdoch and coworkers [41,46] by using a CALPHAD evaluation of free energies to produce a phase diagram for Fe-Zr alloys, shown in Figure 8. They included nanocrystalline states computed using a regular solution model for grain boundary segregation developed by Wynblatt and Chatain [23]. In this case, the segregated nanocrystalline states were less energetically favorable than the $Fe_{23}Zr_6$ compound, and thus only metastable grain size information could be provided. In an alloy

exhibiting true nanocrystalline stability, phase diagrams are expected to include phase transitions between bulk phases and nanostructured states, as well as two-phase regions possessing unique nanostructural features.

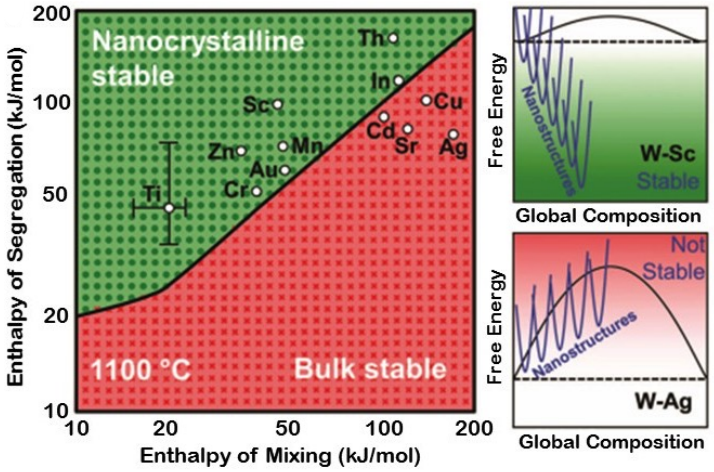

Figure 7: Alloy selection map for W-based alloys produced using the RNS model based on enthalpies of mixing and grain boundary segregation for binary W alloys. On the right are free energy diagrams for two such binary alloys that show how the distinction between stable and unstable alloy systems were made by comparing the nanocrystalline free energy to the bulk miscibility gap. (Reproduced with permission from [46]).

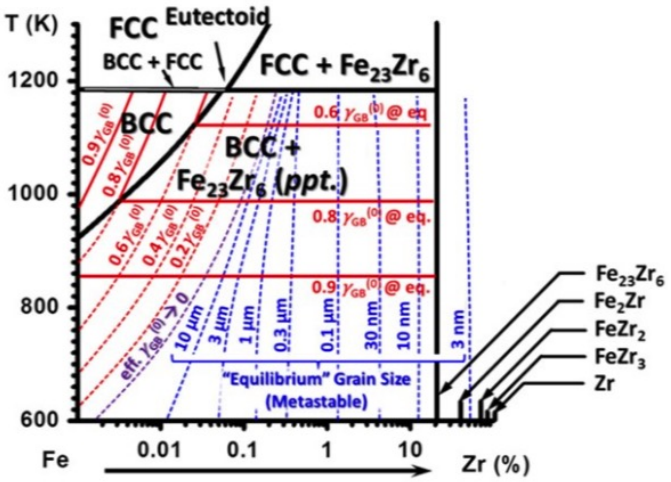

Figure 8: Phase diagram of Fe-Zr including the consideration of nanocrystalline states using the CALPHAD method. This diagram shows the metastable nanocrystalline states using blue dashed lines (reproduced from [47] with permission).

While these analytical models have been useful to advancing the development of nanocrystalline alloys, they are limited by regular solution assumptions. In order for regular solution assumptions to be reasonably valid, the interaction parameters should be of relatively low magnitudes in order for there to be a random distribution of solute in a region. However, stable nanocrystalline states are formed due to a high tendency for grain boundary segregation, which means that they inherently possess large interaction parameters for solutes at the grain boundary.

In effect, the constraint of random distributions within the grains and at the grain boundaries of nanocrystalline states in the RNS model strongly limits the possible configurations of nanocrystalline states considered in these models [48]. Expanding the configuration space (or the phase space in statistical mechanics terms) considered in nanocrystalline alloys is critical to understand the thermodynamics of nanocrystalline alloys []. This larger configuration space is too complex to capture analytically, so we must build thermodynamic simulations.

Section 1.4.2: Defining the configuration space of nanocrystalline alloys for improved thermodynamic models

Before exploring the methods available to perform a thermodynamic exploration of the nanocrystalline alloy configuration space, let's define what the configuration space for a nanocrystalline alloy is, and what reasonable simplifications can be made.

In bulk alloys, the configuration space to be considered in determining the equilibrium state can often be reduced to the distribution of chemical species on a lattice. However, to consider grain boundary segregation, the portion of the phase space surveyed for free energy minima must be expanded. This is a multi-scale challenge: grain boundaries are disordered regions of the lattice at the atomic scale and form a complex network throughout the system at the topological, meso-scale level, as illustrated in Figure 9. Details at these different scales are all important to a full assessment of equilibrium. At the topological level, the grain boundary network determines the equilibrium average grain size, the solute interaction with the grain boundaries, and whether nanocrystalline states are preferable to bulk phases. At the atomic-scale, the local positioning of atoms in the inhomogeneous environment of the grain boundary is important for capturing segregation phenomena accurately.

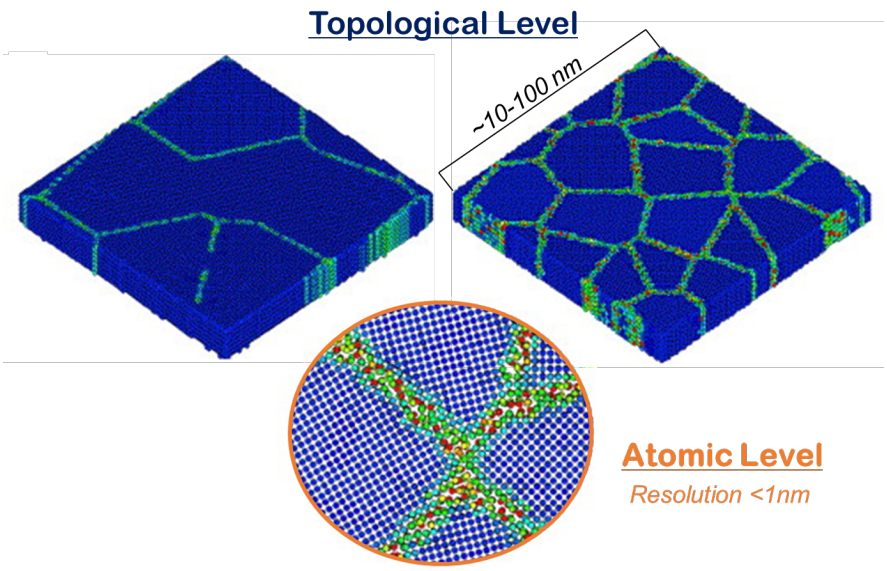

Figure 9: Schematic of the multi-scale considerations of nanocrystalline states in describing the thermodynamic configuration (or phase) space (images are from the work of Millett et al. [50], reproduced with permission of the publisher).

A multi-scale description of the grain boundary state is difficult to capture analytically, and as such the analytical models discussed in the previous subsection rely on the definition of a single average grain boundary site, and the fraction of those sites in the system then becomes the core descriptor of a nanocrystalline structure. Atomistic simulations, on the other hand, have demonstrated great utility at both describing the atomistic environment of the grain boundaries of nanocrystalline states, as well as the grain topology in studies of grain growth. Taking advantage of this, Millett and coworkers performed molecular statics and molecular dynamics (MD) studies of stability against grain growth [50-52]. Using a Lennard-Jones potential, their simulations showed that placing sufficiently larger solute atoms at the grain boundaries successfully arrested grain growth by reducing the excess grain boundary energy to zero. However, from a thermodynamic perspective, there are two critical features missing from such an approach for studying nanocrystalline ground states. First, grain boundary segregation should occur thermodynamically, such that the chemical potential of the alloy is constant throughout the system, which is not obeyed by artificially placing solute at the grain boundary. Second, the simulation must be sufficiently long such that bulk phases can nucleate, which is not easy to capture in an

MD simulation due to the longer time-scales associated with diffusion. For the time and length scales required to study the thermodynamics of nanostructured states, a statistical mechanics-based approach offers many advantages, and it is to these models that we turn our attention.

Section 1.4.3: Introduction to Monte Carlo simulations of alloy statistical mechanics

In statistical mechanics, the equilibrium behavior of an alloy is determined by taking thermal averages at the atomic level. For closed systems at a fixed temperature (i.e. in the canonical ensemble), the probability that a particular alloy configuration, m, is the equilibrium state depends on the energy of the configuration, E_m, as $P_m = \left(\mathrm{e}^{-\frac{E_m}{kT}}\right)/Q$, where k is the Boltzmann constant, and T is the absolute temperature. The partition function, $Q = \sum_i e^{-\frac{E_i}{kT}}$, represents the size of the configuration space and can be related to thermodynamic quantities, such as entropy and free energy. Thus if the energies of all configurations are known, the canonical ensemble partition function and the probabilities of each configuration can be determined and used to identify the preferred state of the alloy and calculate relevant thermodynamic information.

Monte Carlo is a stochastic method for approximating the thermal averages of statistical mechanics, capturing statistical fluctuations and connecting this information to macroscopic thermodynamic quantities. Sampling the configuration space is not a trivial task, as most configurations in the space contribute insignificantly (have very low probabilities) to the equilibrium, and thus simple sampling methods can be prohibitively inefficient. Monte Carlo simulations can be devised to instead sample configurations in the phase space at a rate corresponding to their probability of occurring in the ensemble, which is termed importance sampling. This is done by sampling the space through transitions, where a new configuration, j, is considered for sampling by applying a transformation to the current configuration, i. The Metropolis algorithm [40] then provides stochastic rules for accepting the transition from state i to j by the transition probabilities:

$$P_{i\to j} = \begin{cases} \mathrm{e}^{-\frac{E_j - E_i}{kT}}, & \text{if } E_j > E_i \\ 1, & \text{otherwise} \end{cases} \tag{8}$$

According to this method, if the new configuration has a lower energy, the system always transitions into it, but if it has a higher energy the transition only occurs with a probability determined by the energy increase and the temperature (with transitions to higher-energy states more probable at elevated temperatures). Typically, an initial configuration is chosen, and transitions are attempted and performed according to the Metropolis algorithm until the system reaches equilibrium, at which point any dependence on the choice of initial configuration has been eliminated. For more background on Monte Carlo simulations, I highly suggest reading [53].

When defining transitions, the goal is to efficiently explore the configuration space with respect to its degrees of freedom. For example, for bulk crystalline alloys the alloy configuration space can be simplified to consider the distribution of solute on a lattice, as is done in the Ising model [54]. In closed systems, atom swaps are used to transition through the configuration space, where a random solute atom and solvent atom from within the lattice have their lattice positions exchanged, leading to a new configuration. The nature of this transition has two important features. First, this mechanism is not meant to represent a physical process, but rather to sample the configuration space without getting trapped in metastable states corresponding to local minima in the free energy, which is assisted by the long-range nature of these swaps. At the same time, a single atom swap does not produce an independent sample configuration from the phase space; it is highly dependent on the previous configuration. Therefore, to collect uncorrelated samples of the phase space, and to satisfy the ergodic hypothesis, many swaps must be performed in between samples before including a new state in calculations of macroscopic thermodynamic quantities. At moderate temperatures, it has been demonstrated in a number of studies that this sampling approach successfully finds the global minimum in free energy and captures the expected phase equilibria as well as enthalpic and entropic behavior of binary alloys [55-58].

Section 1.4.4: Monte Carlo simulations for designing nanocrystalline materials

This general Monte Carlo formulism can be adapted to include grain boundaries in the description of the configurational space of the alloy. As discussed in Section 1.4.2, the presence of grain boundaries and their interaction with segregants introduces additional degrees of freedom at both the atomistic scale, related to the structure of the grain boundary, and at the meso-scale, related to the topology and crystallography of the grain boundary network. Two types of Monte

Carlo simulations have been developed, each designed to focus at a particular scale, and to provide a different level of information regarding the stability of nanocrystalline states.

Section 1.4.4.1 Monte Carlo Simulations at the Atomic Level of Grain Boundaries

A particular grain boundary can take on different equilibrium atomic configurations, known as complexions [59-60], with varying grain boundary thicknesses, disorder, and chemistry. As such, Monte Carlo studies of grain boundary segregation at the atomic level should consider the added positional degrees of freedom available for atoms at the grain boundary by including appropriate transition operations to reach the equilibrium grain boundary structures for a particular nanocrystalline alloy. Simulations to study grain boundary segregation in this way were first developed to measure the extent of segregation at different grain boundaries, and to analyze structural transitions that occur within the grain boundary [28,29,61-64]. Such methods have been more recently adapted by Detor and Schuh [65], and Purohit and coworkers [66,67] to study the thermodynamics of nanocrystalline alloys.

The transition event used to sample the phase space of the alloy must allow atoms to relax locally. A common approach is to accompany each solute-solvent atom swap with atomic relaxation of the system to maintain zero hydrostatic stress, for example by straining the system incrementally and using conjugate gradient relaxations to allow the atoms to utilize the off-lattice degrees of freedom at the grain boundary. The new, depressurized state is then considered for transition according to the Metropolis algorithm, where the energies of each state are typically calculated using many-body potentials. Such a simulation produces the lowest free energy state for the alloy, but is constrained to the initial grain topology provided, since the transition event does not create or remove grain boundary area, and the relaxations permitted do not allow for large atomic reconfiguration. Thus in order to assess nanocrystalline stability, simulations at fixed grain sizes must be compared to single crystal simulations to determine the more favorable state, as these states are not considered simultaneously in the Monte Carlo framework. Figure 10 shows the work of Detor and Schuh on Ni-W using this approach to understand the composition ranges in which the internal energy of the nanocrystalline states (considering systems with average grain sizes of 2, 3, and 4 nm) was lower than that of a single crystalline (the SC curve) system [65]. However, only the enthalpies are considered in such a calculation. Because the free energies are not known,

accurate assessment of thermodynamic stability at finite temperatures is difficult with this approach.

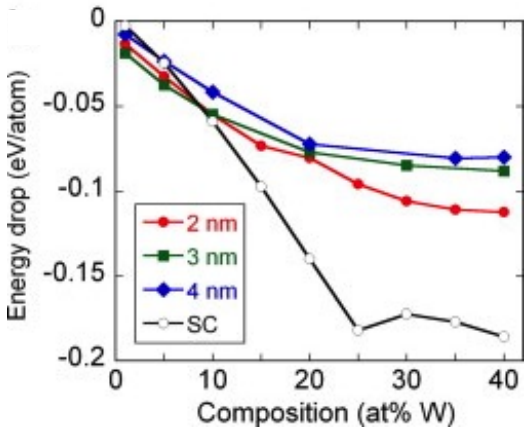

Figure 10: An assessment of the thermodynamic stability of nanocrystalline Ni-W using an atomistic Monte Carlo simulation, where internal energies of nanocrystalline systems with grain sizes of 2, 3, and 4 nm are compared to a single crystalline (black line) system. Reproduced with permission of the publisher from [65].

Another shortcoming of atomistic Monte Carlo simulations for considering the stability of nanocrystalline states is that the portion of the phase space considered in a given simulation does not simultaneously include both nanocrystalline and single crystalline states. Therefore, to identify the stable nanocrystalline state, all possible nanocrystalline configurations at the topological level should be considered in the free energy minimization to identify the nanostructure of the equilibrated state. As a result, while the atomic position degrees of freedom at the grain boundary are important at the grain boundary structure level, the topological degrees of freedom of the grain boundary network should be explored as part of the Monte Carlo sample space in order to determine if a nanocrystalline state exists at equilibrium and to assess the meso-scale structure of the state.

Section 1.4.4.2 Monte Carlo Simulations at the Topological Level of Grain Boundaries

In order for a Monte Carlo simulation to provide information on the stability of nanocrystalline states, the sampling method should have the freedom to add or remove grain boundary area in search of the lowest free energy nanostructure. To make such a description of the configuration space more computationally feasible, it is convenient to start from a more coarse-

grained approach that foregoes the atomic level description of grain boundary structure and its dependence on local factors, such as the adjoining grain orientations, in favor of describing the effects of alloying on a larger network of average grain boundaries. Chookajorn and Schuh [68] modified the Ising approach to incorporate the possibility of stable nanocrystalline states. Unlike the original Ising model, each lattice site in the alloy is not only prescribed with an occupying chemical species, but is also associated with a particular grain, denoted by a grain number, such that nearest neighbor bonds between two lattice sites with different grain numbers constitute a grain boundary, as shown in Figure 11.

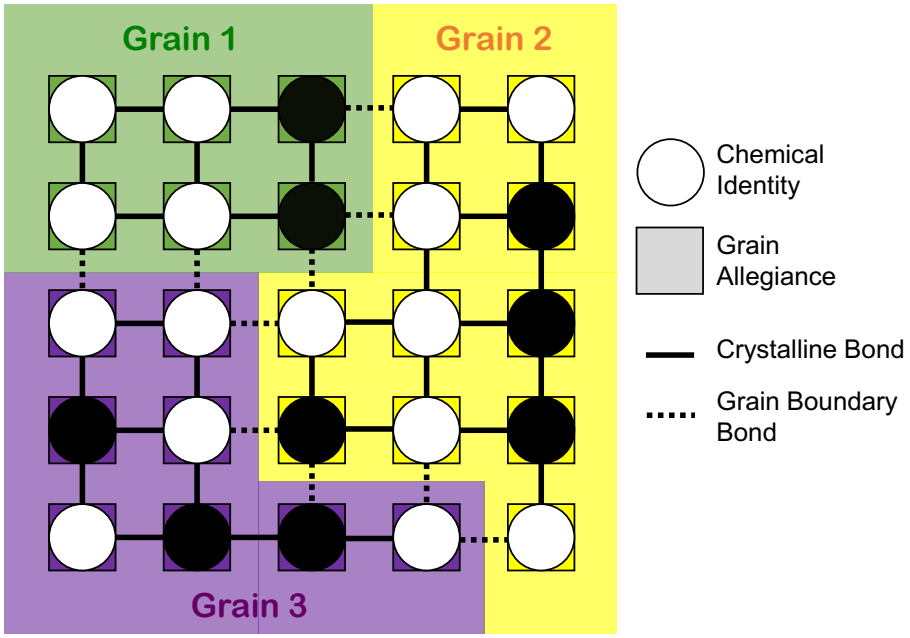

Figure 11: A schematic of the lattice-based nanocrystalline alloy model developed by Chookajorn and Schuh [68], where each lattice site contains chemical and grain allegiance information. The configuration space of this model can explore topological degrees of freedom for the grain boundary network, enabling a more direct method for analyzing thermodynamic stability of nanocrystalline alloys.

Under this description, the internal energy of a particular configuration, E_m, can be written by summing nearest neighbor bonds, as was done in the RNS model:

$$E_m = N_{\mathrm{AA}}^{\mathrm{c}} E_{\mathrm{AA}}^{\mathrm{c}} + N_{\mathrm{AB}}^{\mathrm{c}} E_{\mathrm{AB}}^{\mathrm{c}} + N_{\mathrm{BB}}^{\mathrm{c}} E_{\mathrm{BB}}^{\mathrm{c}} + N_{\mathrm{AA}}^{\mathrm{gb}} E_{\mathrm{AA}}^{\mathrm{gb}} + N_{\mathrm{AB}}^{\mathrm{gb}} E_{\mathrm{AB}}^{\mathrm{gb}} + N_{\mathrm{BB}}^{\mathrm{gb}} E_{\mathrm{BB}}^{\mathrm{gb}} \quad (9)$$

where E is the pairwise bond energy between the species specified by the subscript and with the bonding type delineated by the superscript, with N being the number of such bonds. The consideration of different possible grain boundary configurations increases the size of the phase space that is explored by Monte Carlo in search of the minimum free energy state with respect to the RNS model.

To sample configurations with different grain boundary topologies, in addition to atom swaps, two types of grain swaps were proposed by Chookajorn and Schuh: a random grain boundary site can change its grain number to that of an adjacent grain (grain boundary motion) or to an entirely new grain number (nucleation of a new grain). This evolution of the grain topology is based on the classical Potts model [69], and is likewise vulnerable to grain faceting and pinning [70], which increases the likelihood of being trapped in a local energy minimum and falsely identifying a stable nanocrystalline state. To address this, the temperature can be slowly decreased at the beginning of each simulation in order to facilitate grain boundary motion during the early stage. In Chookajorn's model, the temperature starts at 10,000 K and is decreased to the desired temperature for thermodynamic analysis at a rate of 0.1%.

In the cases where stable nanostructures are not thermodynamically the most favorable state, this model replicates bulk alloy thermodynamics that are consistent with the Ising model. The resulting state that forms has no grain boundaries, representing a single crystal. For alloys that favor grain boundary segregation strongly, however, the Monte Carlo method provides results that are consistent with the analytical models introduced earlier; nanocrystalline states emerge as preferred structures.

This model uncovers unique behaviors that arise from the synchronicity between the equilibration of both grain and chemical structures, which are not predicted by regular solution models, and to this point, remain unique predictions of the Monte Carlo model. To systematically probe the different types of stable nanostructures that can be found by the simulation, one can use a perspective based on the bond energies available to the model, which can be related using the alloy interaction parameters (cf. Eqs. 4 and 5). These two interaction energies along with the grain boundary energy penalty of the unalloyed components determine the relative preference for different bond environments, and can be used to estimate the enthalpically preferred structural

configuration. A stability map outlining several behavioral trends on the interaction parameter space was proposed by Chookajorn and Schuh [68] to provide guidelines of regions in which distinct types of nanostructures are expected (Figure 12).

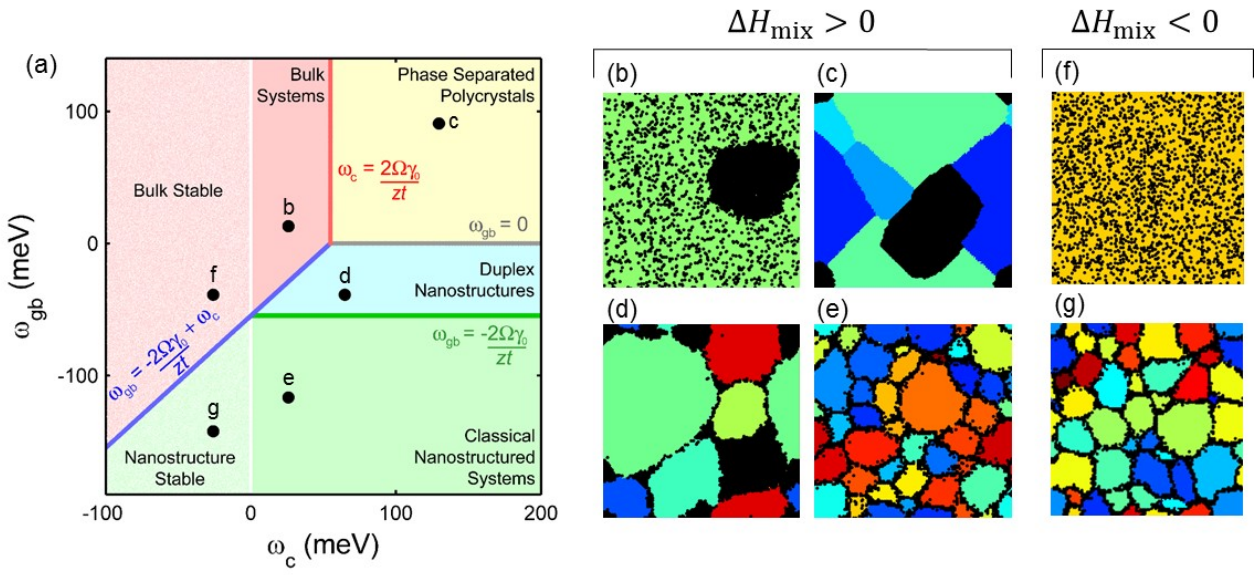

Figure 12: (a) Stability map of six general regions of nanocrystalline stability identified using the lattice-based Monte Carlo simulation: (b) bulk, single crystalline alloy with positive enthalpy of mixing, (c) phase separated polycrystal with undoped grain boundaries, (d) duplex nanostructured states with segregated grain boundaries, (e) segregated nanocrystalline state with positive enthalpy of mixing, (f) bulk. single crystalline alloy with negative enthalpy of mixing, (g) segregated nanocrystalline state with negative enthalpy of mixing.

In Figure 12, the regions denoted 'bulk structure' (red region, Figure 12(b)), and 'segregated nanocrystalline structure' (green region, Figure 12(e)) are the classical states predicted by the RNS model, and are similar to the RNS-based map regions plotted on different axes in Fig. 7. The simulations are, however, not limited to studying fully segregated grain boundary states and bulk phases. Duplex nanostructures (blue region, Figure 12(d)) exhibit simultaneous solute segregation and precipitation, and phase separated polycrystals (yellow region, Figure 12(c)) do not exhibit segregation but are characterized by precipitates as well as grain boundaries. The latter two nanostructures, which have solute precipitates as well as grain boundaries at equilibrium, are not the minimum internal energy configurations possible; in both cases the lowest internal energy

state would be a single crystal, precipitated state. However, in the duplex and phase separated polycrystal regions of the stability map, grain boundary states exist with internal energies that are in between the precipitated and disordered single crystal states, and as such at intermediate temperatures the higher entropy available in duplex nanostructures and phase separated polycrystals leads to a minimum free energy polycrystalline state. The ability of the lattice-based simulation to predict the stability of a wide range of structures makes it a valuable tool for alloy design, and has been shown to compare well with some limited experimental studies of W-Ti (segregated nanocrystal) [71] and W-Cr (duplex nanostructure) [72].

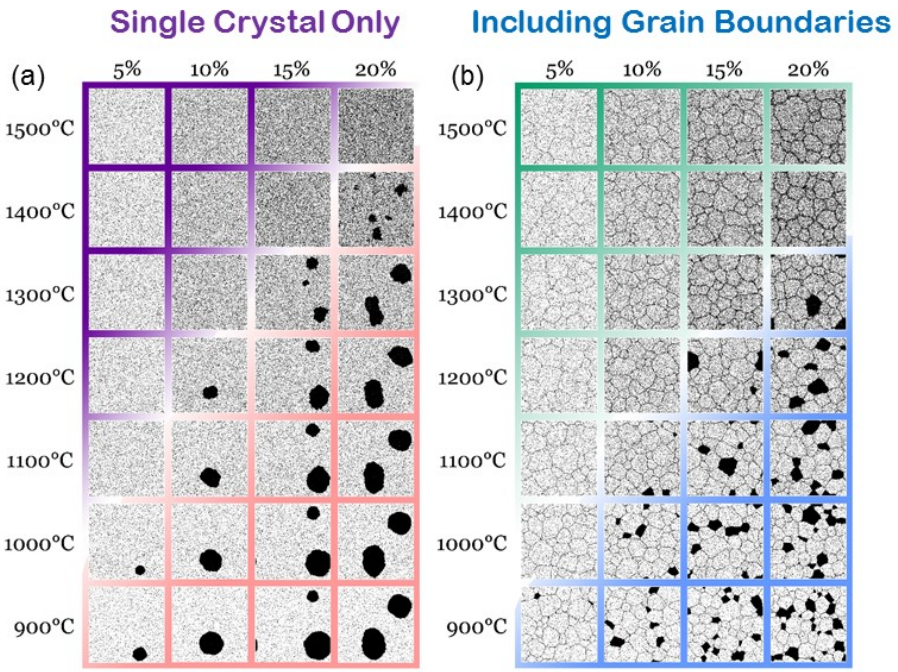

Figure 13: Pictorial representations of phase diagrams for a duplex nanocrystalline alloy constructed through Monte Carlo simulations at different compositions and temperatures first (a) without allowing for nanocrystalline states and (b) then allowing for nanocrystalline states in the configuration space considered (Reproduced with permission from [72]).

Monte Carlo simulations of this kind provide valuable thermodynamic insight as they are able to capture the entropy of the different equilibrium states, which is useful for constructing phase diagrams of alloys accounting for potential nanocrystalline stability. Using this method, Chookajorn and coworkers constructed a phase diagram of an alloy from the duplex region of the stability map, illustrated pictorially in Figure 13 [72]. For comparison, simulations were conducted

with an artificially-imposed single crystal state (Figure 13(a)) as well as using the full grain-evolving model as described above (Figure 13(b)). When the system was constrained against the formation of grain boundary states, this positive enthalpy of mixing alloy was verified to exhibit bulk precipitation at low temperatures which evolved to a solid solution at high temperatures (Figure 13(a)). However, when nanocrystalline states were allowed to evolve, at intermediate temperatures a duplex nanostructured phase emerged, which disordered into a segregated nanocrystalline state at higher temperatures (Figure 13(b)). The existence of an intermediate energy level associated with the grain boundary state leads to an interesting new phase diagram that includes nanostructured states at equilibrium.

Section 1.4.5: Challenges of existing models for selection and processing of nanocrystalline materials to be addressed in this thesis

Models for developing stable nanocrystalline alloys, to enable their processing into bulk parts, were reviewed in this section. Analytical models using regular solution assumptions provide a simple method for screening alloy systems and can identify systems that are formally stable against grain growth (i.e. they are also stable against forming a second phase leading to grain growth). However, regular solution assumptions are too restrictive, which has led to the use of Monte Carlo simulations to explore a larger part of the rich alloy configuration space possible in nanocrystalline alloys. These Monte Carlo simulations have enabled more detailed analysis of stability, leading to more accurate treatments of grain boundary chemistry and the identification of new equilibrium states of engineering interest, for example duplex nanocrystalline states.

A few significant challenges limit the capabilities of the Monte Carlo simulations. First, the Monte Carlo simulations have been limited to consider positive enthalpy of mixing alloys, as negative enthalpy of mixing alloys require the incorporation of more long-range bonds to capture the enthalpic preferences to form ordered compounds. Thus, even though the stability map in Figure 12 extends to negative enthalpies of mixing, it isn't accurate to use these models under these conditions and thus the map is not reliable in this regime. Extending the models to negative enthalpy of mixing systems opens up the space of potential alloys substantially and is expected to reveal interesting new equilibrium nanostructures.

Secondly, verifying thermodynamic stability in the Monte Carlo simulations remains a major challenge. In the 'atomic-level' simulations (Figure 10), the equilibrium state is assessed by

looking at internal energies, completely missing entropic considerations in stability. Without measures of entropy, it is difficult to truly identify the equilibrium nanostructure using these simulations. In the 'topological-level' simulations, the equilibrium state is only valid if the Monte Carlo simulation achieves ergodicity. This is a difficult challenge due to the local nature of the grain swaps, and it is common for the simulations to get trapped in a local metastable equilibrium. The method of cooling into the equilibrium state is an imperfect one, which hurts the reliability of this model. Particularly, the equilibrium grain sizes observed in the simulations can often be due to the grain swaps being kinematically constrained, making alloy processing guides such as phase diagrams (see Figure 12) created from this method too inaccurate to be useful.

The goal of this thesis is to improve the thermodynamic models used to design nanocrystalline alloys by making them applicable to a broader range of alloys and to make them more thermodynamically accurate to better guide alloy selection and processing.

Section 1.5: Outline of the main contributions of this thesis

This thesis develops improved thermodynamic models for nanocrystalline alloys that enable their applicability to a broader range of alloys and more accurate in determining the important features of equilibrium nanocrystalline states. The outline of the thesis is:

- *Chapter 2: Generalized Stability Criterion for Stable Nanocrystalline Alloys*. A generalized stability criterion is developed analytically to describe formal stability of the nanocrystalline state with respect to grain growth for any binary alloy system. This criterion informs the extension of the lattice Monte Carlo simulations to systems that have stable ordered compounds. The Monte Carlo simulation is verified to behave according to the generalized stability criterion, but also is found to reveal new nanostructured states that could not be modelled analytically.
- *Chapter 3: Thermodynamics of Ni-Ti-W Nanocrystalline Alloys: A Case Study*. The ability of the new model to capture the alloy thermodynamics of complex nanocrystalline materials is evaluated on the Ni-Ti-W alloy system.
- *Chapter 4: Developing Phase Diagrams of Nanocrystalline Alloys*. A more rigorous method for developing phase diagrams of stable nanocrystalline alloys is presented. This method extracts the free energy of the nanocrystalline alloy from

simulations and uses this to both better understand the free energy landscape of nanocrystalline materials and to construct more accurate phase diagrams.

- *Chapter 5: Pathways for Grain Refinement in Alloys with Nanocrystalline Ground States*. If a nanocrystalline alloy is formally stable, it is predicted from thermodynamics that certain annealing steps should lead to grain refinement without leaving the solid state. This chapter explores this concept.

Chapter 2: Generalized stability criterion for stable nanocrystalline alloys

In this chapter, criteria for metastability and stability of the nanocrystalline state against grain growth are derived by treating grain boundary segregation as a form of ordering that is available in nanocrystalline materials [73]. These criteria are valid for both positive and negative enthalpy of mixing alloys and take into account the formation enthalpies of ordered compounds. The lattice Monte Carlo simulation is modified to account for ordered states, allowing for consideration of any binary alloy pair.

Section 2.1: An analytical stability criterion for nanocrystalline alloys

Section 2.1.1: Formulation of the stability criterion

Grain boundary segregation, like precipitation, is largely believed to be an enthalpic effect, and is thus a form of chemical ordering. The competition between different ordered states can be resolved by determining which ordered state provides the lowest enthalpy for the alloy system, as is typically done for ordered compounds in developing 0 K phase diagrams [74-76]. The energies of ordered states as a function of composition can be compared on an energy diagram such as Figure 14 to determine regimes of stability.

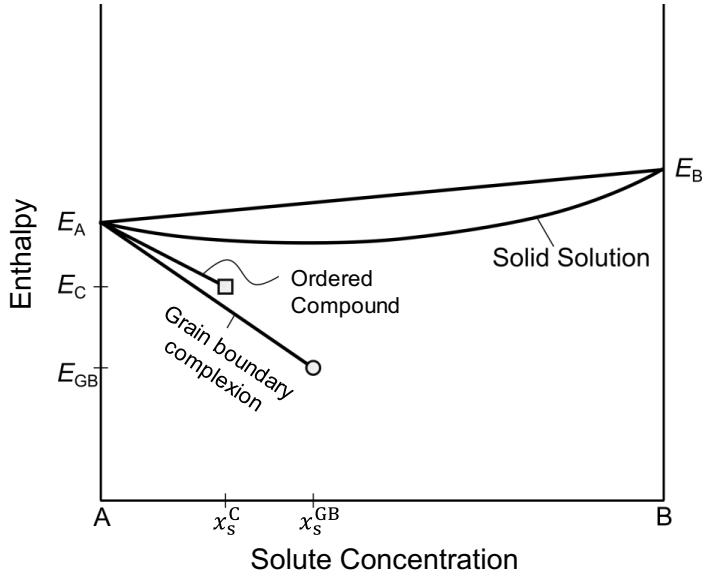

Figure 14: Schematic of the binary alloy energy diagram including an ordered phase (square) and a 2D grain boundary compound/complexion (circle) where the energy of non-stoichiometric compositions is calculated by the lever rule (lines).

Here, we particularly focus on solute-lean compositions without loss of generality. The enthalpy of the binary alloy system with an ordered phase, H_{ord}, can generally be written as:

$$H_{\mathrm{ord}} = \left(1 - \frac{X}{x_{\mathrm{s}}^{\mathrm{C}}}\right) E_{\mathrm{A}} + \frac{X}{x_{\mathrm{s}}^{\mathrm{C}}} E_{\mathrm{C}} \tag{10}$$

where E_{A} and E_{C} are the enthalpy per atom of the pure solvent and ordered compound, respectively, X is the global solute concentration, and $x_{\mathrm{s}}^{\mathrm{C}}$ is the stoichiometry of the compound (i.e. the fraction of atoms in the compound that are solute atoms). This expression defines the common tangent line of an ordered phase and the pure solvent phase, and is also applicable to positive enthalpy of mixing systems by setting $E_{\mathrm{C}} = E_{\mathrm{B}}$ and $x_{\mathrm{s}}^{\mathrm{C}} = 1$, where E_{B} is the enthalpy per atom of a pure solute phase.

Generally, a grain boundary segregated state at thermodynamic equilibrium is a complexion [59,60], i.e., a defined equilibrium atomic configuration at the interface separating grains. For the developments that follow, we find it useful to adopt the view that this complexion is more specifically a 2D compound [77-78] as it will exhibit a chemically ordered configuration that, similar to a 3D ordered phase, can be described using an effective enthalpy per atom, E_{GB}, and a stoichiometry, $x_{\mathrm{s}}^{\mathrm{GB}}$, which is the fraction of atoms in the grain boundary compound that are solute. Therefore, the enthalpy of a nanocrystalline alloy, H_{GB}, with a solute-enriched grain boundary can also be written in the same format as the previous equation:

$$H_{\mathrm{GB}} = \left(1 - \frac{X}{x_{\mathrm{s}}^{\mathrm{GB}}}\right) E_{\mathrm{A}} + \frac{X}{x_{\mathrm{s}}^{\mathrm{GB}}} E_{\mathrm{GB}} \tag{11}$$

Under this representation, the enthalpy of the nanocrystalline alloy follows a common tangent line as shown in Fig. 14, between the pure solvent phase and the grain boundary compound. The implication of this common tangent line is that at compositions below the stoichiometry of the grain boundary compound, the volume fraction of the grain boundary compound decreases proportionally according to a lever rule. In a system with fixed grain boundary area, one might envision patches of grain boundary with the equilibrium grain boundary compound that grow in area as the global concentration is increased. In the more general case where grain boundary area is unconstrained and can equilibrate, one expects the area density of grain boundaries to increase with composition and the entire grain boundary to be at the grain boundary compound

stoichiometry. This representation is consistent with the behavior of the regular solution models of nanocrystalline stability, where increasing solute content monotonically decreases the equilibrium grain size [41,47]. At the stoichiometric composition, this approach predicts a system fully composed of the grain boundary segregated state/compound, which is not a well-defined condition. For example, in prior work the grain boundary segregated state has been likened to an amorphous configuration near stoichiometry [41,47,68]. In the present work we will consider systems with solute concentrations well below the grain boundary compound stoichiometry; the grain boundary compound thus forms in a lever-rule fashion with the terminal solvent phase.

Finally, we must consider whether forming a grain boundary segregated state is preferred with respect to forming a bulk ordered phase. This would occur using the above definitions when $H_{\mathrm{GB}} < H_{\mathrm{ord}}$. The stability criterion for forming a nanocrystalline state is thus:

$$\frac{1}{x_{\mathrm{s}}^{\mathrm{GB}}}(E_{\mathrm{GB}} - E_{\mathrm{A}}) < \frac{1}{x_{\mathrm{s}}^{\mathrm{C}}}(E_{\mathrm{C}} - E_{\mathrm{A}}) \tag{12}$$

To translate this into alloy design terms, the per-atom enthalpies of the ordered states ($E_{\mathrm{GB}}, E_{\mathrm{C}}$) should be replaced by expressions for the global enthalpies of compound formation, ΔH_{form}, and grain boundary segregation, ΔH_{seg}. For the compound, this relationship is:

$$\Delta H_{\mathrm{form}} = E_{\mathrm{C}} - (1 - x_{\mathrm{s}}^{\mathrm{C}})E_{\mathrm{A}} - x_{\mathrm{s}}^{\mathrm{C}} E_{\mathrm{B}} \tag{13}$$

An enthalpy of formation can also be defined for the grain boundary segregated state, however it is better to define the grain boundary compound energy as a function of ΔH_{seg} as this is the more traditional thermodynamic parameter, defined as the change in enthalpy of the system upon swapping a solute atom at the grain boundary with a solvent atom in the grain, and defined such that grain boundary segregation is expected when $\Delta H_{\mathrm{seg}} > 0$. Substituting a solute atom at the grain boundary for a solvent atom replaces one unit of the grain boundary compound with a region of pure solvent grain boundary. This results in an enthalpy change of $\frac{1}{x_{\mathrm{s}}^{\mathrm{GB}}}\left(E_{\mathrm{GB}}^{\mathrm{A}} - E_{\mathrm{GB}}\right)$, where $E_{\mathrm{GB}}^{\mathrm{A}}$ is the enthalpy per atom of a pure solvent grain boundary. In the crystalline region, removing a solvent atom from a pure solvent matrix requires an energy of $2E_{\mathrm{A}}$ and after substitution of a solute atom, the energy of the site, $E_{\mathrm{B\,in\,A}}$, can be written in terms of the enthalpy of mixing: $\Delta H_{\mathrm{mix}} = E_{\mathrm{B\,in\,A}} - E_{\mathrm{B}} - E_{\mathrm{A}}$. As a result, a general expression for the enthalpy of grain boundary segregation is:

$$\Delta H_{\text{seg}} = \Delta H_{\text{mix}} + E_B - E_A - \frac{1}{x_{\text{s}}^{\text{GB}}}\left(E_{\text{GB}} - E_{\text{GB}}^{\text{A}}\right) \quad (14)$$

Using the relationships ΔH_{form} and ΔH_{seg} the criterion for the stability of a grain boundary segregated state with respect to forming second phases can be written as:

$$\Delta H_{\text{seg}} > \Delta H_{\text{mix}} - \frac{1}{x_{\text{s}}^{\text{c}}}\Delta H_{\text{form}} + k\gamma \quad (15)$$

where $k\gamma$ is the excess energy of a pure A grain boundary, $\frac{1}{x_{\text{s}}^{\text{GB}}}\left(E_{\text{GB}}^{\text{A}} - E_{\text{A}}\right)$, where k converts the grain boundary energy from energy/area to energy/atom.

The criterion of Eq. 15 satisfies basic intuition for stabilizing grain boundaries with solute: a larger enthalpy of grain boundary segregation is required if the excess grain boundary energy that must be overcome is larger and if the crystal can undergo a larger drop in enthalpy by compound formation $\left(\Delta H_{\text{mix}} - \frac{1}{x_{\text{s}}^{\text{c}}}\Delta H_{\text{form}}\right)$. If this criterion is met, the energy of the system has a minimum at a particular grain size that depends on the solute concentration as seen by Chookajorn and Schuh [68]; decreasing the grain size from equilibrium results in an energetic penalty for forming pure solvent grain boundary and increasing the grain size results in an increase in energy for forming the bulk ordered phase instead of the grain boundary compound. For stability against phase separation into a solute precipitate in positive enthalpy of mixing systems, this same criterion holds with $\Delta H_{\text{form}} = 0$. Alternatively, a grain boundary segregated state can be stable with respect to grain growth alone, but only metastable with respect to forming a second phase. The metastability criterion thus does not include the enthalpy associated with second-phase formation:

$$\Delta H_{\text{seg}} > k\gamma \quad (16)$$

The metastability criterion attained in this manner is essentially the same as the one proposed by Weissmüller (Eq. X), though Eq. 16 does not consider the entropy associated with forming a solid solution and thus is expected to underestimate the threshold for metastability.

The criteria for nanocrystalline stability established in Eqs. 15 and 16 are conveniently written in terms of bulk thermodynamic parameters that can be estimated for most binary alloy systems and guide the selection of alloying elements for nanocrystalline materials. The enthalpies of grain boundary segregation and solid-state mixing can be estimated empirically using a

Miedema approach [31,79]. The enthalpies of formation of binary compounds can be calculated by density functional theory and are readily attainable from the Open Quantum Materials Database [74]. While many compounds are often stable in the same binary system at different compositions, we suggest using the compound that is stable at the lowest stoichiometry as alloying for nanocrystalline stability is typically done at low compositions and this is the regime for which Eqs.15 and 16 apply. For the enthalpic penalty of the grain boundary, $k\gamma$, the pure element grain boundary energy can be estimated as one-third of the surface energy calculated from a Miedema model [79]. The coefficient, *k*, can be approximated as the molar volume [80] divided by the grain boundary thickness (estimated as 5 Å). This approximation of *k*, which was also used in previous work [68] to convert the units of grain boundary energy to energy per mole, could be treated more completely, for example by more directly incorporating the packing density of atomic planes and the excess volume of the grain boundary.

Section 2.1.2: Maps for selecting alloys to form stable nanocrystalline states based on the stability criterion

The criteria from Eqs. 15 and 16 delineate a stability map as shown in Figure 15 (on the right), which classifies the stability of the grain boundary segregated state as a function of bulk thermodynamic parameters. On this stability map, one axis measures the enthalpy gained by forming a grain boundary segregated state (ΔH_{seg}) and the other measures the enthalpy gained by forming a crystalline second phase ($\Delta H_{\mathrm{mix}} - \frac{1}{x_{\mathrm{s}}^{\mathrm{c}}}\Delta H_{\mathrm{form}}$). The Weissmüller criterion is shown on the same axes on the left as a point of reference. The key added consideration in this generalized stability criterion is the energetic benefit for the solute to form any ordered phase in the bulk.

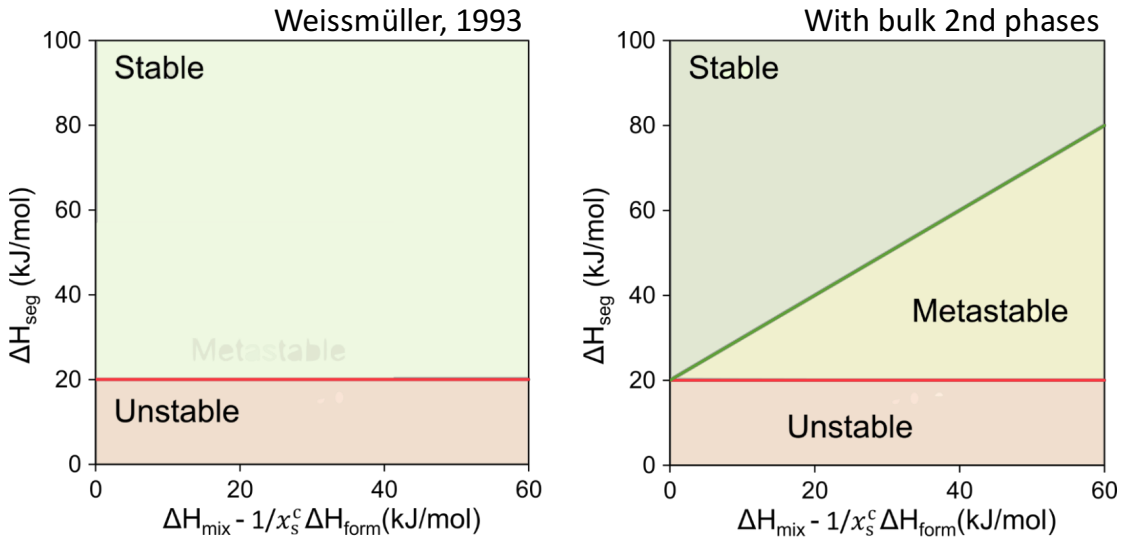

Figure 15: A stability map for selecting nanocrystalline alloys based on the bulk thermodynamic parameters of the alloy pair (only enthalpic considerations of stability). On the left is the map produced by the Weissmüller criterion where the only configurations considered are the grain boundary segregated nanocrystalline state and a bulk solid solution. On the right is the map produced by the criterion derived in Section 2.1.1 where two phase states are also incorporated in the phase space considered.

The existence of alloying combinations that meet the stability criterion thus requires that some alloys possess an enthalpy of grain boundary segregation that is sufficiently larger than the enthalpy gained by forming a second phase. This may seem unlikely due to the experimentally-observed relationship (Figure 16) between the terminal solubility of a crystalline second phase and the enrichment factor (measure of excess solute) at the grain boundary [81,82], which is often interpreted as meaning that the enthalpies of grain boundary segregation and second phase formation are highly correlated, or $\Delta H_{\mathrm{seg}} \approx (\Delta H_{\mathrm{mix}} - \frac{1}{x_{\mathrm{s}}^{\mathrm{c}}} \Delta H_{\mathrm{form}})$ in the terms of our criterion.

To test whether this correlation is too strong for the stability criterion to be satisfied in physically realizable alloys, we determined ΔH_{seg}, ΔH_{mix}, and $\frac{1}{x_{\mathrm{s}}^{\mathrm{c}}} \Delta H_{\mathrm{form}}$ values (as described in the previous section) for a large number of transition metal – transition metal binary alloy pairs and plotted them on the same axes as the stability map (Figure 17). Indeed, a positive correlation between the second phase and grain boundary segregation energies seems to exist as the points

largely follow the trend of the solid line. However, there is a substantial amount of spread; the dashed line represents the stability criterion when $k\gamma$ is 20 kJ/mol and it is observed that a number of alloy pairs satisfy the criterion for a stable nanocrystalline state.

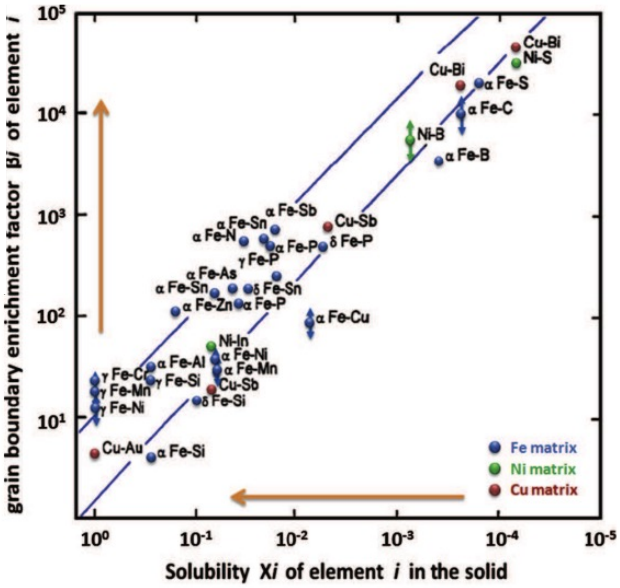

Figure 16: The experimentally-observed relationship between the terminal solubility of an alloy (which is related to the tendency for second phase formation) and the enrichment factor of the grain boundary (which is related to the enthalpy of grain boundary segregation). Reproduced with permissions from publisher [81].

The relatively large data spread in Figure 17 is not entirely surprising. The experimentally-observed correlation between terminal solubility and enrichment factor at the grain boundary has a spread of roughly one order of magnitude in the enrichment factor. Furthermore, different ordered configurations in crystalline phases of the same alloy often vary in energy by dozens of kJ/mol, and thus it is reasonable to expect ordered 2D compounds to differ in energy from 3D compounds by energies on that order of magnitude as well.

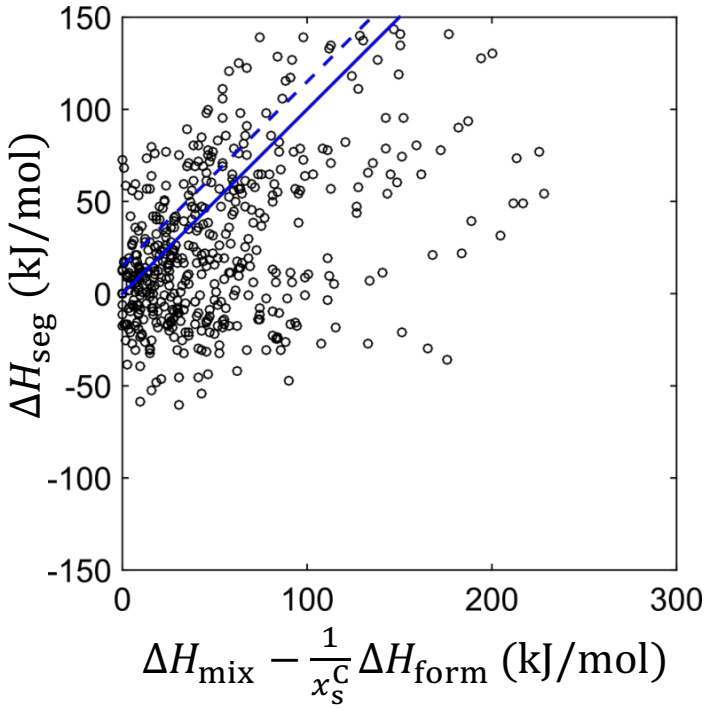

Figure 17: Transition metal – transition metal binary alloys plotted using Miedema estimates [31,79] of ΔH_{mix} and ΔH_{seg} and density functional theory calculations of ΔH_{form} for compounds (attained from the Open Quantum Materials Database [74]) to observe the strength of correlation between the two axes of the stability map for physical alloy pairs. The solid line corresponds to perfect correlation between the axes, and the dashed line represents the stability criterion.

Section 2.2: Incorporating entropic effects into the stability criterion: devising a more general lattice Monte Carlo simulation for nanocrystalline alloys

Our stability and metastability criteria as developed in Section 2.1 are enthalpic and do not consider the entropy of the different ordered states or the presence of interphase boundaries. We favor the inclusion of configurational entropy effects using a lattice-based model, as it is a classical method for accounting for such effects and also opens the door to Monte Carlo exploration of the preferred structural configurations as a function of temperature and composition (see Section 1.4.3).

Equilibrium states of a bulk, single crystalline alloy in a lattice model (an Ising model for binary alloys) are determined by identifying the configuration of chemical species that minimizes the free energy of the alloy system. To incorporate the possible presence of grain boundaries, each lattice site carries two pieces of information: 1) the chemical identity of the species, and 2) a grain number denoting the grain allegiance of the atom at that site. Crystalline bonds are defined between neighboring atoms with the same grain number, and alternatively grain boundary bonds exist if the atoms have different grain numbers. The phase space of this model is thus any chemical configuration on the lattice sites, with any set of bonds between lattice sites being grain boundary bonds. The equilibrium configuration can be determined using a Monte Carlo algorithm (see Section 1.4.4.2).

The equilibrium configuration is based on the defined interatomic potential. For positive enthalpy of mixing systems, a nearest neighbor, pairwise potential with six bond energies was sufficient to provide distinct energies for grain boundary segregated states, solute precipitates, and solid solution phases, which could then be sampled by Monte Carlo to select the lowest free energy configuration. These six pairwise bond energies are $\{E^{\mathrm{c}}_{\mathrm{AA}}, E^{\mathrm{c}}_{\mathrm{AB}}, E^{\mathrm{c}}_{\mathrm{BB}}, E^{\mathrm{gb}}_{\mathrm{AA}}, E^{\mathrm{gb}}_{\mathrm{AB}}, E^{\mathrm{gb}}_{\mathrm{BB}}\}$ where the subscript specifies the chemical identity of the two atoms bonded – solvent (A) and solute (B) – and the superscript denotes the nature of the bond – crystalline (c) and grain boundary (gb).

However, the pairwise potential does not correctly produce bulk ordered phases in a lattice model, and multi-body terms are generally required using a cluster expansion [83-91]. The next section explains the compound unit method, a simplified approach that we developed to incorporate bulk ordered phases into a lattice model when the bulk phase diagram is already known and thus a full cluster expansion is not necessary.

Section 2.2.1: The compound unit approach for incorporating known equilibrium ordered states into the energy space of a lattice model

Section 2.2.1.1: A summary of the key features of the compound unit model

In order to permit stable compounds in a pairwise model, a distinction has to be drawn between solute-solvent bonds in a solid solution and those in an ordered phase (for more clarity on why this is, see the introduction to our publication on the compound unit model [92]). Rather

than add multiple higher order terms as in a standard cluster expansion [83-91], we directly include an ordered compound with known structure and formation energy into a nearest-neighbor pairwise formalism by identifying its structure through a "compound unit". A compound unit is defined here as a repeating group of atoms from which the entire superstructure of the compound can be formed. For example, we may define the compound unit shown in Figure 18a to identify the ordered compound shown in Figure 18b.

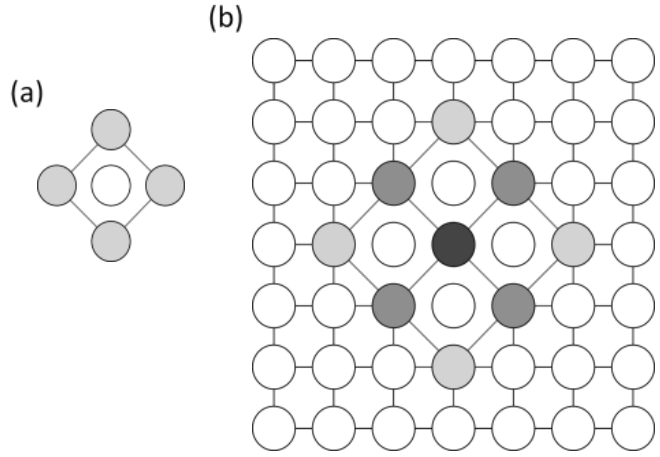

Figure 18. (a) A possible definition of a compound unit for the ordered compound pictured in (b) where dark atoms are solute. (b) In addition to showing the equilibrium compound, the shading in this image shows a schematic of how the energy of an atom is calculated in the compound unit model, where darker atoms have a larger compound unit contribution to their energy.

Many potential compound units may be defined for a given ordered compound, but the key feature of the unit is that when it appears in the structure, it will be assigned a lower enthalpy than what the pairwise potential would return, and which is related to the compound formation energy. If a compound unit, α, is found in the lattice, the energy of the system includes an additional term including the contribution from the compound energy:

$$E_m = N^{\mathrm{c}}_{\mathrm{AA}}E^{\mathrm{c}}_{\mathrm{AA}} + N^{\mathrm{c}}_{\mathrm{AB}}E^{\mathrm{c}}_{\mathrm{AB}} + N^{\mathrm{c}}_{\mathrm{BB}}E^{\mathrm{c}}_{\mathrm{BB}} + N^{\mathrm{gb}}_{\mathrm{AA}}E^{\mathrm{gb}}_{\mathrm{AA}} + N^{\mathrm{gb}}_{\mathrm{AB}}E^{\mathrm{gb}}_{\mathrm{AB}} + N^{\mathrm{gb}}_{\mathrm{BB}}E^{\mathrm{gb}}_{\mathrm{BB}} + N_{\alpha}E^{\mathrm{c}}_{\mathrm{A_xB}} \qquad (17)$$

where N_α is the number of compound units found on the lattice and $E^{\mathrm{c}}_{\mathrm{A_xB}}$ is the energy of those compound units. To do implement this properly, the energy used for $E^{\mathrm{c}}_{\mathrm{A_xB}}$ should be the energy

per atom based on the compound formation energy minus the pairwise energies that make up the compound unit. It is important to note that when calculating the energy of an individual atom, the energy is calculated entirely from pairwise interactions if none of the environment around the atom resembles a compound unit, but if the atom is part of a compound unit then that portion of its energy is replaced by the compound unit energy. This is illustrated in Figure 18(b), where the interior atom of the compound has its complete energy described by the compound unit energy, as opposed to atoms on the edges and corners which respectively have one-half and one-quarter of their energies described by the compound unit energy, with the remainder calculated from pairwise bonds. This leads to faceted ground state precipitates. The reader is referred to [92] to see the full derivation of the compound unit model Hamiltonian, but as this is not critical to understand its implementation we move on to a simple demonstration of the model to show that it captures the necessary bulk ordering behavior for our nanocrystalline lattice model.

Section 2.2.1.2: The compound unit model captures the necessary order-disorder phenomena in the bulk phase for the nanocrystalline lattice model

The goal of the compound unit model is to capture accurate order-disorder phenomena in alloys with a stable ordered compound, such that these energies can be captured accurately in our nanocrystalline lattice model.

The pairwise potential cannot accurately capture ordering in two-phase fields, and the addition of a compound unit term is a purposeful mend to this problem. Monte Carlo simulations were conducted to determine the 0 K equilibrium behavior of the compound unit model, with compound units defined for the $D0_3$ and B2 compounds (stoichiometries of 25 and 50 at. %) on a BCC lattice. The superstructure for these compounds is best described by 4 interpenetrating FCC lattices, as shown in Figure 19(a), where the positions on the lattice with the same number below to the same FCC sublattice. The compound units defined for the $D0_3$ and B2 compounds are shown in Figure 19(b). For details on why these particular compound units are used, the reader is referred to our publication on this topic [92].

Figure 20 shows the solute atoms in the (100) plane of equilibrated structures with and without the compound unit term at different compositions. At the 25 at.% and 50 at.%

compositions, the $D0_3$ and B2 compounds are the equilibrium phases in both cases. However, deficiencies in the pairwise model are already evident; in Figure 20a at 25 at.%, two antiphase boundaries are observed and indicated with arrows. These defects should not be present at equilibrium in a single phase compound, and appear because they are trapped in this simulation. This difficulty in achieving long range order is a common problem when studying compounds in the Ising model with a pairwise potential [93,94]. However, in the compound unit approach, antiphase boundaries are more energetic and not easily trapped, which yields the correct equilibrium microstructure as shown in Figure 20b at 25 at.%.

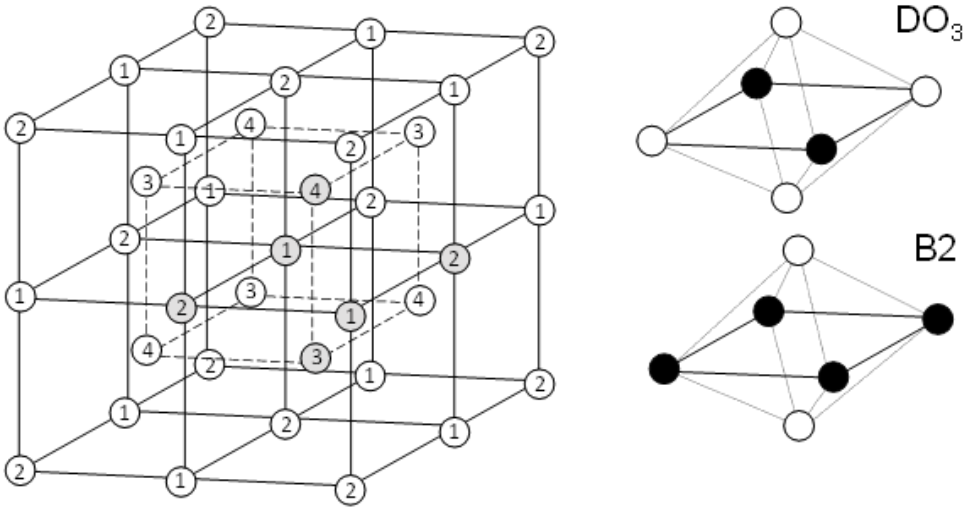

Figure 19: (a) A schematic of the compound superstructure for $D0_3$ and B2 compounds in body-centered cubic binary alloys, with numbers signifying different interpenetrating FCC sublattices. Convenient compound units for $D0_3$ and B2 are shown in (b), with solute in black. Shaded atoms in (a) illustrate the compound unit within the superstructure.

The more serious deficiencies of the pairwise model appear at off-stoichiometric compositions, where faceted precipitates in a two-phase equilibrium are thermodynamically expected at 0 K. The equilibrated structures in Figure 20(a) have non-zero entropies, as evidenced by the large degeneracy of the equilibrium states. At the stoichiometric composition, the equilibrium is a single-phase compound that is forced to form by geometry, and it does not require a non-zero interfacial energy. At slightly off-stoichiometric compositions, local ordering is observed via this same constraint, but a single consolidated phase is not preferred energetically

because there is no energetic penalty associated with forming an interface between the compound and solvent atoms. At low concentrations, this leads to a solid solution as there are many sites where solute can reside and still achieve ideal first and second nearest neighbor coordination.

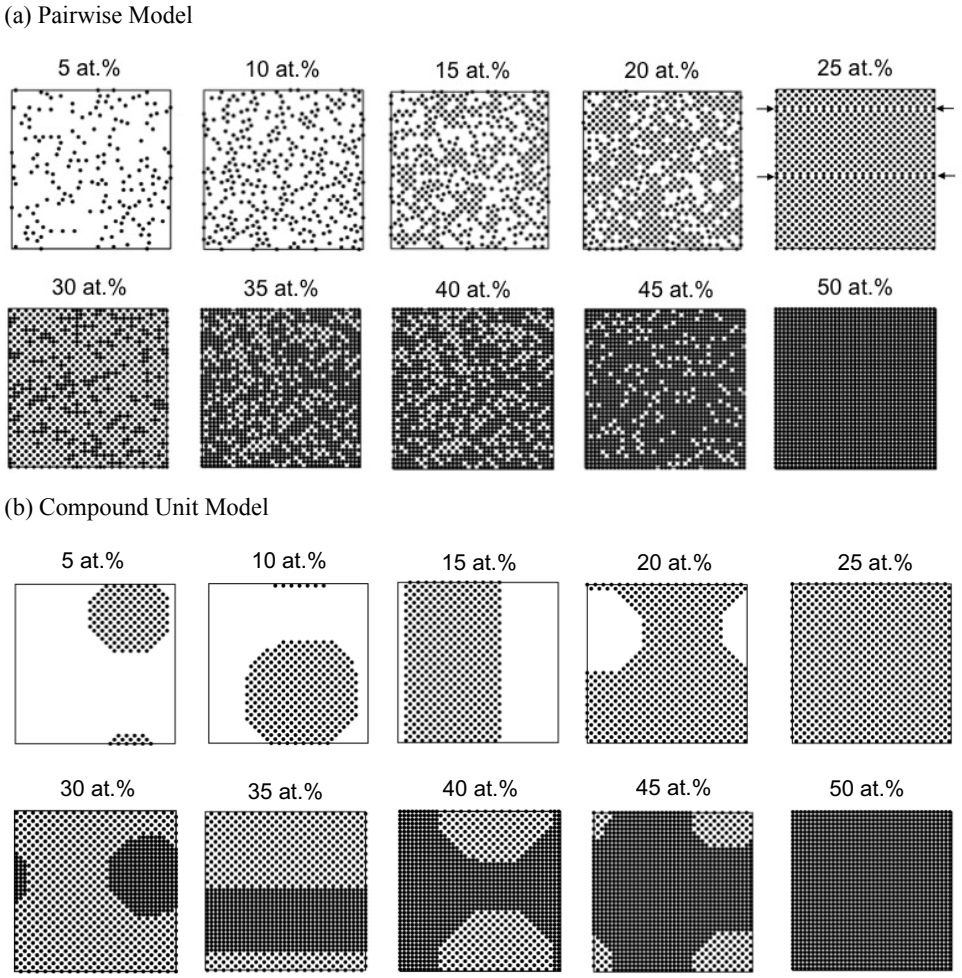

Figure 20. Equilibrium states computed at 0 K via a Monte Carlo simulation under (a) the pairwise model and (b) the compound unit model. Only solute atoms are shown in the image, on a single (100) plane of the simulation cell.

In contrast, and shown in Figure 20(b), the compound unit model produces equilibrium structures with the expected two-phase equilibrium at off-stoichiometric compositions at 0 K. Firstly, the addition of compound units fixes the energetics such that the ground state of the alloy is now two, separated phases at 0K. Secondly, this formulation makes it convenient for Monte Carlo simulations to find the correct equilibrium state even at low temperatures since each atom

at the interface possesses an interfacial energy; the system thus correctly coarsens into a single precipitate, and can avoid producing anti-phase boundaries.

The compound unit also reveals the desired phase transformation behaviors as the temperature is increased. Figure 21 shows the equilibrium states at compositions of 10 and 25 at.% during this disordering processes. As expected, at non-zero temperatures, each phase exhibits some solubility of the second phase, and as the temperature increases the amount of the ordered phase decreases until it disappears above the phase transition temperature. Phase diagrams were constructed both with and without the compound unit method (Figure 22). The critical temperature of a phase transition was determined by identifying the temperature at which an order parameter exhibits a discontinuity in slope, and was corroborated with visual evidence of phase changes in the equilibrium microstructures.

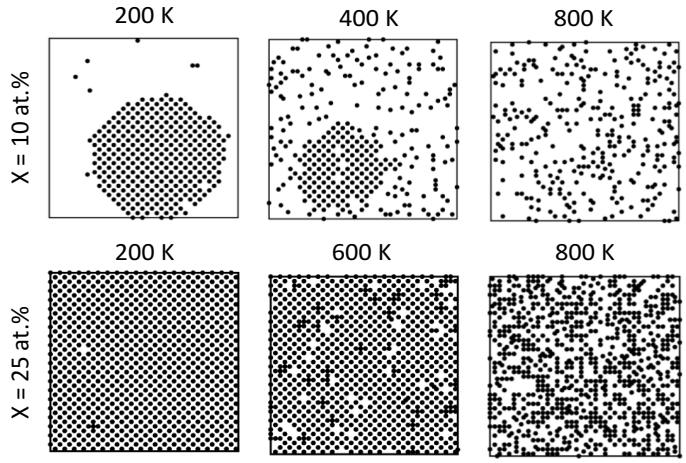

Figure 21. Equilibrium states as temperature is increased from 200 to 800 K at compositions of 10 and 25 at.%. Only solute atoms are shown in the image, with atoms

There are a few important differences between the two phase diagrams. At low concentrations, the compound unit model produces the expected two-phase equilibrium with the A-rich solid solution phase. The lack of this two-phase region in the pairwise model was the principle reason for incorporating compound units, and the phase diagram demonstrates that this approach fixes the anomalous thermodynamic behavior in the pairwise model. Similarly, there is a two-phase region that exists between the $D0_3$ and B2 phases in the compound unit model that is absent in the pairwise model. Other pairwise models simulating a system with $D0_3$ and B2 compounds produce a second order phase transition between the $D0_3$ and B2 phases [95,96], which

would also violate the third law of thermodynamics, as one or both phases would have to have a non-zero solubility at 0 K. Thus, the presence of this two-phase region also seems to be an improvement made by the inclusion of compound unit energies. The critical temperature for disordering is also lower for the compounds in the pairwise model than in the compound unit model, since only geometric considerations lead to ordering, whereas in the compound unit model both geometric and chemical interactions favor the ordered phases.

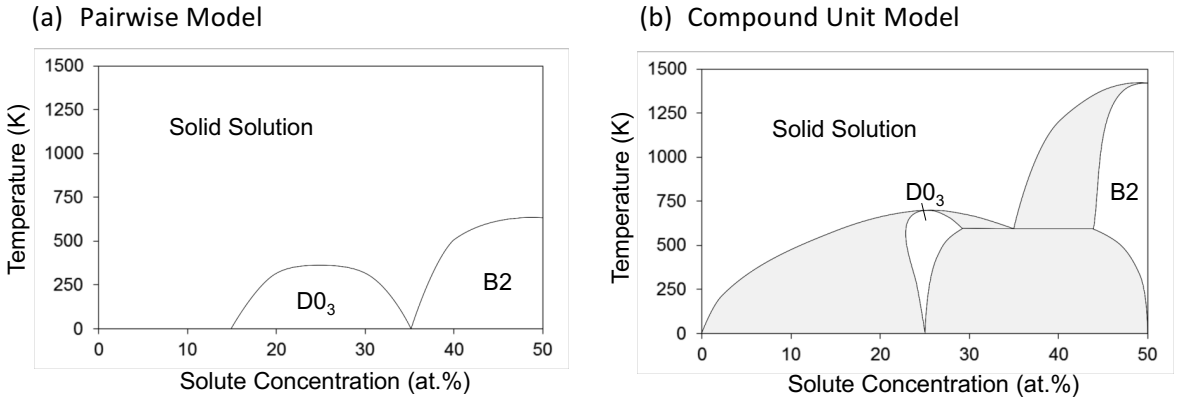

Figure 22. Phase diagrams in (a) the pairwise model and (b) the compound unit model calculated via Monte Carlo. Phase transitions are denoted with solid lines, and two-phase regions are shaded.

The adherence of the phase diagram produced by the compound unit model to basic thermodynamic principles provides confidence that this approach is a viable alternative to a full multi-body expansion for incorporating bulk ordering thermodynamics into lattice models of alloys.

Section 2.2.2: Defining the energetic parameters in the lattice model in terms of known alloy thermodynamic quantities

The compound unit approach introduces an additional energy (to the 6 pairwise bond energies) into our nanocrystalline lattice model, which can conveniently be represented as an effective pairwise bond energy, $E^{c}_{A_xB}$. In addition, we need to consider how ordering at the grain boundary in the lattice model effects the segregation behavior.

At low temperatures, grain boundary segregation occurs in the lattice model when the lowest enthalpy compound at the grain boundary has a stoichiometry that is higher than the global solute concentration. Fig. 22(a) shows the grain boundary compound observed by Chookajorn and Schuh in a body-centered cubic (BCC) lattice when $E_{\mathrm{AB}}^{\mathrm{gb}}$ is lower than the mean of $E_{\mathrm{AA}}^{\mathrm{gb}}$ and $E_{\mathrm{BB}}^{\mathrm{gb}}$. The enthalpy of grain boundary segregation can be determined for a set of bond energies by measuring the change in enthalpy of a bicrystal from a random distribution of solute atoms to the equilibrium configuration and dividing by the change in the number of solutes residing at the grain boundary [68]. In order to relate the lattice model to physical systems, however, the inverse relationship needs to be determined: a known enthalpy of grain boundary segregation for an alloy system must be described in terms of appropriate bond energies in the lattice model such that the enthalpy of segregation is achieved accurately in the simulation. Here, we estimate this relationship for this particular grain boundary compound by calculating the change in energy from swapping a solute atom in the crystal with a solvent atom in the grain boundary (z is the coordination number):

$$\Delta H_{\mathrm{seg}} = \frac{z}{2}\left(E_{\mathrm{AB}}^{\mathrm{c}} - E_{\mathrm{AA}}^{\mathrm{c}} + E_{\mathrm{AA}}^{\mathrm{gb}} - E_{\mathrm{AB}}^{\mathrm{gb}}\right) \tag{18}$$

This relationship can equivalently be produced from Eq. 14 by using standard relationships ($\Delta H_{\mathrm{mix}} = z\left(E_{\mathrm{AB}}^{\mathrm{c}} - \frac{E_{\mathrm{AA}}^{\mathrm{c}} + E_{\mathrm{BB}}^{\mathrm{c}}}{2}\right)$, $E_{\mathrm{A}} = \frac{z}{2}E_{\mathrm{AA}}^{\mathrm{c}}$, $E_{\mathrm{B}} = \frac{z}{2}E_{\mathrm{BB}}^{\mathrm{c}}$) and average grain boundary compound energies, which in this case are: $E_{\mathrm{GB}}^{\mathrm{A}} = \frac{z}{6}\left(E_{\mathrm{AA}}^{\mathrm{gb}} + 2E_{\mathrm{AA}}^{\mathrm{c}}\right)$ and $E_{\mathrm{GB}} = \frac{z}{6}\left(E_{\mathrm{AB}}^{\mathrm{gb}} + E_{\mathrm{AA}}^{\mathrm{c}} + E_{\mathrm{AB}}^{\mathrm{c}}\right)$, where three layers of atoms are necessary to define the grain boundary compound ($x_{\mathrm{s}}^{\mathrm{GB}} = 1/3$).

The efficacy of this equation is evaluated by comparing the enthalpy of grain boundary segregation as calculated by this equation with the enthalpy of grain boundary segregation measured through a fixed bicrystal Monte Carlo simulation with the same pairwise bond energies. Fig. 23(b) shows the results of this validation, where $E_{\mathrm{AB}}^{\mathrm{gb}}$ is varied to produced different enthalpies of grain boundary segregation at different fixed values of $E_{\mathrm{AB}}^{\mathrm{c}}$, which controls the enthalpy of mixing (all other bond energies were fixed at 0 eV). Regardless of the enthalpy of mixing, the enthalpy of segregation calculated by Eq. 18 compared reasonably well with the enthalpy of segregation produced in the simulations.

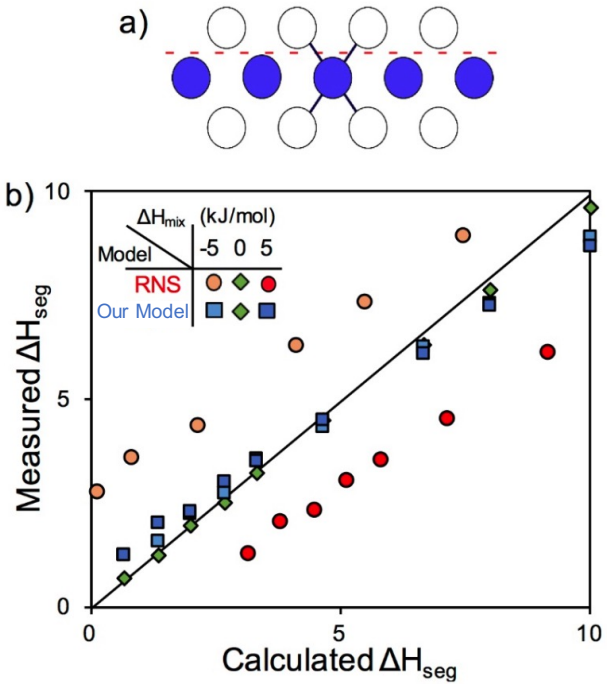

Figure 23: a) Schematic of ordering at a fixed grain boundary in the lattice model for a BCC lattice (blue – solute). b) Verification of Eq. 18 for calculating pairwise bond energies for the lattice model from a known enthalpy of segregation and a known grain boundary compound.

The regular nanocrystalline solution (RNS) model also produces a similar equation for the enthalpy of grain boundary segregation [39]:

$$\Delta H_{\text{seg}} = \frac{z}{2}\left(2E^{\text{c}}_{\text{AB}} - E^{\text{c}}_{\text{AA}} + E^{\text{gb}}_{\text{AA}} - E^{\text{gb}}_{\text{AB}} - \frac{1}{2}(E^{\text{c}}_{\text{AA}} + E^{\text{c}}_{\text{BB}})\right) \tag{19}$$

When the enthalpy of mixing is zero, both Eqs. 18 and 19 are equivalent, but for non-zero enthalpies of mixing, the RNS model produces a systematic error because it assumes a random solution configuration and thus fails to account for the ordering preferred at the grain boundary. While the RNS equation is useful at the continuum level, when ordering at the grain boundary is present the approach outlined above produces a more reliable equation for grain boundary segregation enthalpy. For a given grain boundary compound, stability and metastability criteria can be derived from Eqs. 15 and 16 using the relationship in Eq. 18, $\Delta H_{\text{form}} =$

$\frac{z}{2}\left[E^{c}_{A_xB} - (1-x^c_s)E^{c}_{AA} - x^c_s E^{c}_{BB}\right]$, and $k\gamma = \frac{z}{2}[E^{gb}_{AA} - E^{c}_{AA}]$. The criteria for the stability and metastability of this grain boundary compound are thus:

$$\text{Stability: } E^{gb}_{AB} + E^{c}_{AB} - 2E^{c}_{AA} < \frac{1}{x^c_s}\left(E^{c}_{A_xB} - E^{c}_{AA}\right) \quad (20)$$

$$\text{Metastability: } E^{gb}_{AB} < E^{c}_{AB} \quad (21)$$

Under the assumption that the alloy has a positive enthalpy of mixing and that BB and AA bonds have the same energy this criterion is exactly the same as that established by Chookajorn and Schuh [68], but it is substantially more general in the present form, as it applies to any second phase and can be derived for any grain boundary compound in a lattice model.

Section 2.3: Comparison of the analytical model with Monte Carlo simulations

The lattice model is solved through a Monte Carlo simulation to find the thermodynamic equilibrium behavior of nanocrystalline alloys given their thermodynamic properties. The Monte Carlo simulation allows us to study more complicated behavior of both the grain boundary and the bulk states as a function of composition and temperature. Monte Carlo doesn't require an assumption that grain boundary complexions behave energetically like phases. Thus using Monte Carlo, we can similarly explore the generality of both the stability and metastability criteria established in the previous sections, this time including configurational entropy and geometric constraints, and unearth more nuanced behavior within the stable and metastable regimes for nanocrystalline alloys.

Monte Carlo simulations were conducted on a 72x72x8 BCC lattice. The lattice was initiated with a random distribution of solute and with a unique grain number assigned to each lattice site. Atom and grain swaps, as proposed by Chookajorn and Schuh [68], were used to explore the configuration space until $4x10^9$ Monte Carlo swaps were attempted, starting from a temperature of 10,000 °C and reducing the temperature towards a final temperature of 500 °C at a rate of 0.1% every Monte Carlo step (equivalent to $4x10^4$ swap attempts). Using the compound unit approach [92] (Section 2.2), a $D0_3$ compound (25 at.% stoichiometry) with an enthalpy of formation of -20 kJ/mol was incorporated into the configuration space of the model. Simulations

were conducted varying the ΔH_{mix} and ΔH_{seg} as shown by the circles in the stability map in Figure 23, with $k\gamma$ = 20 kJ/mol and for a solute concentration of 10 at.%.

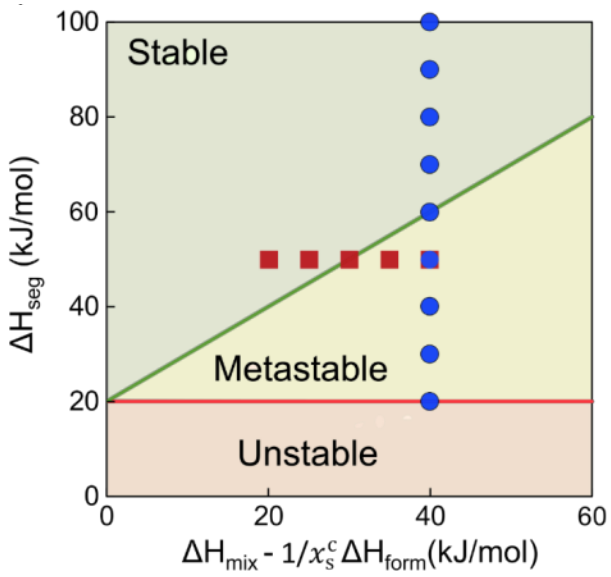

Figure 24: Stability map based on Eqs. 15 and 16, when $k\gamma$ = 20 kJ/mol. Blue dots correspond to the ΔH_{seg} series and the red squares correspond to the ΔH_{mix} series for which equilibrium nanostructures are shown in Figs. 24 and 26, respectively.

Two series of simulations are described on Fig. 24, and will be discussed in turn in what follows:

- ΔH_{seg} series: the effect of grain boundary segregation tendency on equilibrium nanostructure.
- ΔH_{mix} series: the effect of second-phase formation tendency on equilibrium nanostructure.

Section 2.3.1: The effect of ΔH_{seg} on the equilibrium nanostructure

Figure 25 shows the results of increasing ΔH_{seg} at a fixed ΔH_{mix} = -40 kJ/mol. Our analytical stability criterion expects that a nanocrystalline state will be stable against grain growth and compound formation when $\Delta H_{\text{seg}} > 60$ kJ/mol. Below ΔH_{seg} = 60 kJ/mol, bulk single crystalline states with a stable $D0_3$ compound are found, as expected. However, at 50 kJ/mol, a

nanocrystalline state is found, wherein both grain boundary segregated states exist and $D0_3$ precipitates form. This state resembles a duplex nanocrystalline state [72] where the nanocrystallinity is stabilized entropically; rather than the ordered precipitate disordering into a solid solution at higher temperatures, it can instead disorder into a grain boundary segregated state, which can occur at a lower enthalpic cost when ΔH_{seg} is close to meeting the stability criterion. Evidence of the entropic nature of this stabilization is seen in Figure 26, where in the region between 40-60 kJ/mol, the enthalpy of the equilibrium state increases as there is still an enthalpic cost to forming grain boundaries.

Above ΔH_{seg} = 60 kJ/mol, stable nanocrystalline states are formed without the presence of an ordered precipitate, because a grain boundary compound is preferred to bulk ordering as predicted by the stability criterion. The grain boundary regions in the alloy at ΔH_{seg} = 60 kJ/mol are thick, and this thickness is reduced as ΔH_{seg} is increased. Correspondingly, there is less solute dissolved in the crystalline regions, which suggests that at higher ΔH_{seg} the alloy prefers thinner complexions because it can attain more entropy without having to dissolve into the grains at a higher enthalpic cost.

Metastability can be simulated by setting the formation energy of the $D0_3$ compound to zero; the resulting equilibrium microstructures are also shown in Figure 25. Above 20 kJ/mol, grain boundary states are seen in the equilibrated structure, which matches the metastability threshold provided by Eq. 16. Interestingly, rather than forming a grain boundary network, at low ΔH_{seg} a precipitated "grain boundary phase" clusters together. This is an expected behavior for a system in which it is energetically degenerate to add grain boundary area or thicken existing grain boundaries. Such a "grain boundary phase" has been discussed in the regular nanocrystalline solution (RNS) model, which also exhibits this degeneracy, and can be interpreted as, e.g., an amorphous phase [41,47].

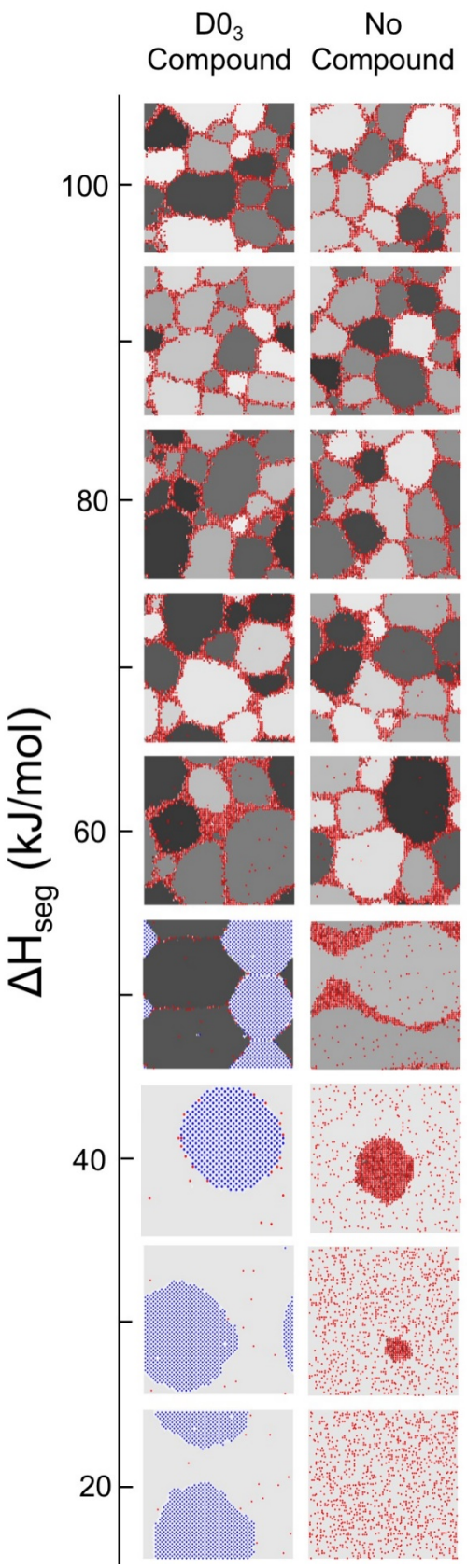

Figure 25. Equilibrium states of the ΔH_{seg} series with a stable $D0_3$ compound (on left) and systems without any stable compound (on right). Different grains have different shades of gray. Solute atoms are in blue if they are part of a $D0_3$ precipitate and red otherwise.

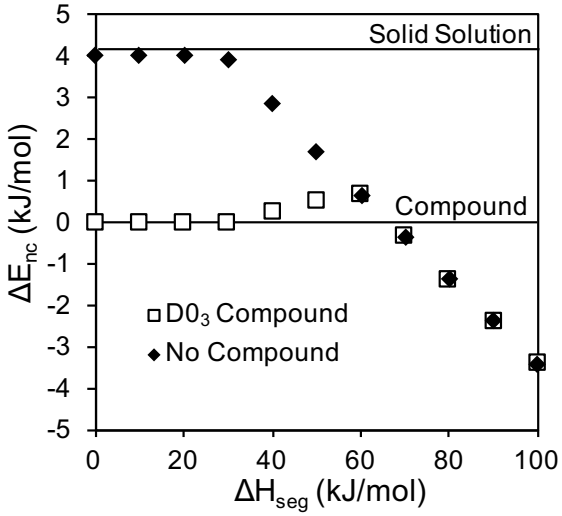

Figure 26. The enthalpy relative to the bulk equilibrium state with increasing enthalpy of segregation for alloy systems with a stable $D0_3$ compound and without any stable compound.

However, there remains the general trend of stabilizing thinner grain boundaries when an alloy possesses a higher ΔH_{seg}, and in a similar way the states with a "grain boundary phase" have a higher solute concentration in the grain. At higher ΔH_{seg}, the grain boundary segregated state becomes more favorable (and forming a solid solution becomes less favorable), and as a result the alloy seems to prefer forming a grain boundary network which has more configurational entropy than the "grain boundary phase". This transition occurs when ΔH_{seg} is roughly 60 kJ/mol, where there is a corresponding change in slope in Figure 26. The slope of the "grain boundary phase" is larger, which suggests that a lower enthalpy could be effected by forming such a precipitate even at higher enthalpies of segregation, and thus the stability of a grain boundary network would only be expected if entropy is playing a significant role. The network has a much larger interfacial area with the surrounding crystalline regions than does the precipitate, thus the solute configurational entropy should be higher for the network configuration because solute at this interface will have a larger range of degenerate sites.

However, the grain topology space is explored in the present Monte Carlo simulations only through local changes to the grain numbers, which may not produce an ergodic sampling of grain boundary configuration space and prohibits detailed exploration of the preference for the network configuration. Chapter 4 explores a different Monte Carlo sampling mechanisms for exploring the

nanocrystalline alloy configuration space to produce more robust thermodynamic equilibrium observations. We are not aware that the configurational entropy of grain boundary networks has been elaborated in detail, although for nanostructured systems this is clearly a necessary component of their thermodynamics and is worthy of further study.

Section 2.3.2: The effect of ΔH_{seg} on the equilibrium nanostructure

The behavior when changing ΔH_{mix} is quite different than when changing only the enthalpy of grain boundary segregation (Figure 27).

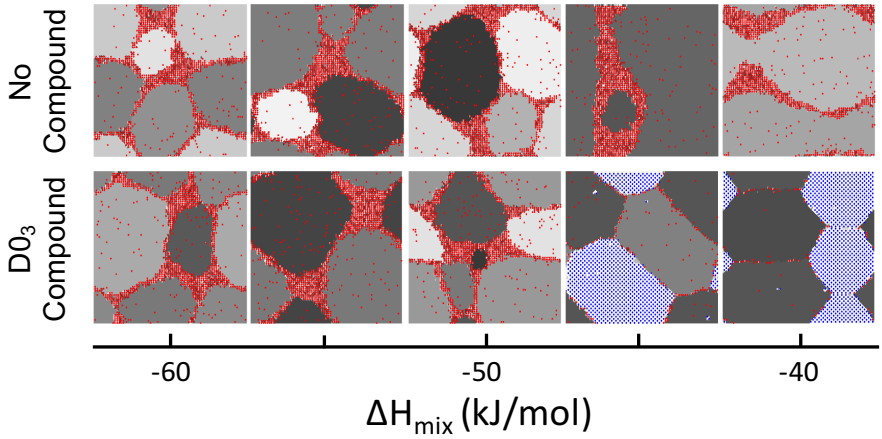

Figure 27. Equilibrium states of the ΔH_{mix} series with a stable $D0_3$ compound (bottom) and without any stable compound (top). Different grains have different shades of gray. Solute atoms are in blue if they are part of a $D0_3$ precipitate and red otherwise.

When the $D0_3$ compound is present, there is a change from a duplex structure to a fully grain boundary segregated structure as the tendency for forming a second phase decreases, which occurs in accordance with Eq. 15. However, while the stability is increased as the enthalpic benefit for bulk ordering is decreased, the equilibrium nanostructure is roughly unchanged. This is similarly observed when metastable equilibrium is studied, where grain sizes remain relatively large and unchanged with ΔH_{mix}. This suggests that it is the relative stability of the alloy with respect to the metastability criteria that governs behavior, which is reasonable since the stability criterion accounts for the possibility of compound formation, and if the compound is not formed, its existence in the phase space should not affect the equilibrium properties. Figure 28 shows the

effective grain boundary energy at different solute concentrations, calculated in the same manner as in Ref. [68], when two key quantities in the stability criteria are changed: $\Delta H_{\mathrm{mix}} - \frac{1}{x_{\mathrm{s}}^{\mathrm{c}}}\Delta H_{\mathrm{form}}$ and $\Delta H_{\mathrm{seg}} - k\gamma$. This quantitatively shows that changing $\Delta H_{\mathrm{mix}} - \frac{1}{x_{\mathrm{s}}^{\mathrm{c}}}\Delta H_{\mathrm{form}}$ does not affect the energy of the grain boundary segregated state, and only $\Delta H_{\mathrm{seg}} - k\gamma$ is relevant. Typically ΔH_{mix} is necessary for determining the critical temperature at which an ordered state will disorder, but in this case ΔH_{seg} already incorporates this effect (see Eq. 14) and as a result it is the key alloying parameter that governs the thermodynamic behavior of the nanocrystalline state.

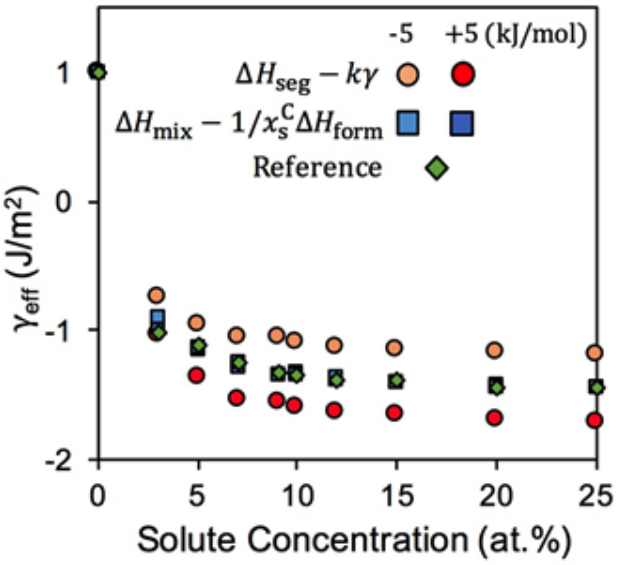

Figure 28. Effect on the excess enthalpy of the grain boundary segregated state, upon varying the enthalpy of grain boundary segregation and the enthalpy of mixing independently.

Section 2.4. Guidelines for nanocrystalline alloy selection

A selection of binary alloys for which stabilization of the nanocrystalline state by grain boundary segregation has been studied experimentally [36,38,71,72,82,97-100] are listed in Table 1 with the relevant bulk thermodynamic parameters for each alloy system (obtained as described in Section 2.1.1). The position of each system with respect to the present stability and metastability criteria is also indicated.

Table 1. Predicted stability classification according to Eqs. 15 and 16 for alloy systems for which the thermal stability has been experimentally studied. ΔH_{seg} critical is the enthalpy of grain boundary segregation needed for the alloy system to be stable. If the enthalpy of grain boundary segregation is within 5 kJ/mol of satisfying or failing either criteria, both likely classifications are specified.

Alloy	ΔH_{seg} (kJ/mol)	ΔH_{mix} (kJ/mol)	x_s^C	ΔH_{form} (kJ/mol)	kγ (kJ/mol)	ΔH_{seg} critical (kJ/mol)	Stability
Fe-Zr	61	-35	1/3	-27	12	58	Stable/Metastable
Fe-Mg	86	76	1	0	12	84	Stable/Metastable
Fe-Ag	58	128	1	0	12	140	Metastable
Fe-Cu	19	52	1	0	12	64	Metastable
Fe-Ta	15	-10	1/3	-19	12	59	Metastable/Unstable
W-Ti	65	20	1	0	24	44	Stable
W-Cr	61	38	1	0	24	62	Metastable/Stable
Ni-W	10	-3	1/5	-10	10	57	Metastable/Unstable
Hf-Ti	28	14	1	0	19	33	Metastable

First examining the Fe-based alloys, Darling and coworkers found that alloying with 1 at.% Zr stabilized a grain size of 50 nm up to 1000 °C without the formation of any precipitates [97]. However, when alloying with 10 at.% Zr, the precipitation of an Fe_2Zr phase was observed at 700 °C leading to a loss of thermal stability [36]. Similar behavior was observed by Clark et al. when alloying Fe with 10 at.% Mg [99] and by Liu when alloying Fe with 3.2 at.% Ag [100], i.e. grain boundary segregation is observed to help retain nanometer-scale grain sizes and upon annealing second phase precipitation is found. The stability criterion predicts Fe-Zr and Fe-Mg to be borderline stable candidates and Fe-Ag to be metastable as the grain boundary segregated state does not present a substantial decrease in enthalpy compared to the alternative of forming second phases. This is reasonably consistent with the experimental observations considering the approximate nature with which thermodynamic parameters have been determined for these systems. It is important to also note that, unlike in the Fe-Zr system, the grain size in the Fe-Mg and Fe-Ag systems is not observed to become constant with increasing temperature. Thus, more data is needed to determine whether the Mg and Ag-alloyed systems are metastable or unstable, as

their behavior is also similar to Fe-Cu [99], Fe-Ta [97], Hf-Ti [101], and Ni-W [98] nanocrystalline alloys which have a much lower enthalpy of grain boundary segregation. For example, Fe with 1 at.% Ta underwent rapid, abnormal grain growth at 800 °C without the precipitation of a second phase, which may be evidence that the nanostructure stability at lower homologous temperatures is in part due to solute drag. Alternatively, the temperature dependence of segregation may come into play in systems such as this, where dissolution into the bulk is favored upon heating (this behavior is modeled in Chapter 4).

In W-based alloys, the addition of 20 at.% Ti was found to stabilize a 20 nm grain size after annealing at 1100 °C for 1 week [46] through grain boundary segregation with no second phase precipitation. In contrast, annealing tungsten with 15 at.% Cr at 950°C [72] also provides stability through grain boundary segregation but also leads to second phase formation and is thus metastable. While the enthalpy of grain boundary segregation is similar in both alloys, the enthalpy of mixing is almost twice as high for W-Cr, which explains the difference in behavior of these systems in accordance with Eqs. 15 and 16.

Many alloying systems studied for stabilizing nanocrystalline materials through grain boundary segregation are positive enthalpy of mixing couples. This is in part due to a general, albeit weak, correlation expected between enthalpy of mixing and enthalpy of grain boundary segregation, but also a consequence of many stability models being limited to only considering positive enthalpy of mixing alloys. The criteria presented in this chapter, with the consideration of ordered phases to treat negative enthalpy of mixing systems should enable a more systematic and unconstrained exploration of alloy systems for the development of bulk nanocrystalline materials.

Chapter 3: Thermodynamics of Ni-Ti-W Nanocrystalline Alloys: A Case Study

One of the big advantages of the Monte Carlo simulation developed in Chapter 2 over the existing models for nanocrystalline stability (Section 1.4) is the ability to treat more complex alloy systems that include compound forming elements. In this chapter, the lattice Monte Carlo simulation is used to analyze the thermodynamics of Ni-Ti-W nanocrystalline alloys. This work was done in collaboration with Dr. Aslan Ahadi working at the National Institute for Materials Science in Tokyo Japan, who was characterizing nanocrystalline Ni-Ti-W thin films to understand the role of W in stabilizing this nanocrystalline NiTi shape memory alloy at elevated temperatures.

Section 3.1: Background and experimental analysis

Due to excellent work output per unit volume and ultralow fatigue [102], NiTi-based shape memory alloy (SMA) thin films are increasingly used in micro-machines as micromanipulators and fluid micro-valves. The control of grain size as an influential microstructural parameter has recently received increased attention due to the emergence of novel properties when grain sizes are in the nanocrystalline regime, where the martensitic phase transformation is observed both experimentally and theoretically to occur in a fundamentally different fashion [103-107]. There are a number of promising properties that have been observed in nanocrystalline SMAs such as a small and vanishing thermal hysteresis (during thermally-induced phase transformations) for high speed microactuators [108].

Retaining a nanocrystalline grain size during heat treatment and thermal cycling presents a serious challenge. Empirically, a few alloying elements have been found to lead to smaller grain sizes and improved thermal stability in NiTi thin films [108-111], the best performing being W, which was observed by Buenconsejo et. al. to maintain a grain size around 25 nm after annealing for 1 hour at 700 °C [108,109]. Characterization after annealing revealed BCC W precipitates in NiTi, which suggests that Zener pinning may play a role in the thermal stability of nanocrystalline NiTi-W, but an understanding of how W interacts with grain boundaries is necessary to attain a complete picture of the thermal stability of this alloy. The goal of our study was to use our Monte Carlo simulations in conjunction with the thorough characterization of this alloy system conducted

by Dr. Ahadi to develop a more complete picture of how W stabilizes the NiTi grains against grain growth.

In addition, we were interested in applying the Monte Carlo simulation to this system because the considerations for thermal stability in nanocrystalline NiTi alloys are more complex than most alloys that have been modeled to date. The nanocrystalline matrix is an intermetallic, B2 NiTi phase and the effect of the alloying element on thermal stability requires a ternary model capable of capturing ordering as well as grain boundary segregation. Additionally, the Ni-W and W-Ti binary systems that make up this ternary alloy are two of the best studied nanocrystalline systems for thermodynamic stability against grain growth. This system was therefore a particularly interesting candidate for applying the extended lattice-based Monte Carlo simulation.

Section 3.1.1: Summary of experimental findings

The detailed experimental findings (from experiments performed by Dr. Ahadi) on characterizing the stability of nanocrystalline Ni-Ti-W SMA thin films can be found in our publication [112]. Here we show the most important data to contextualize the analysis from the Monte Carlo simulations, in particular noting the nanostructures formed and the observations of grain boundary chemistry after annealing at different temperatures.

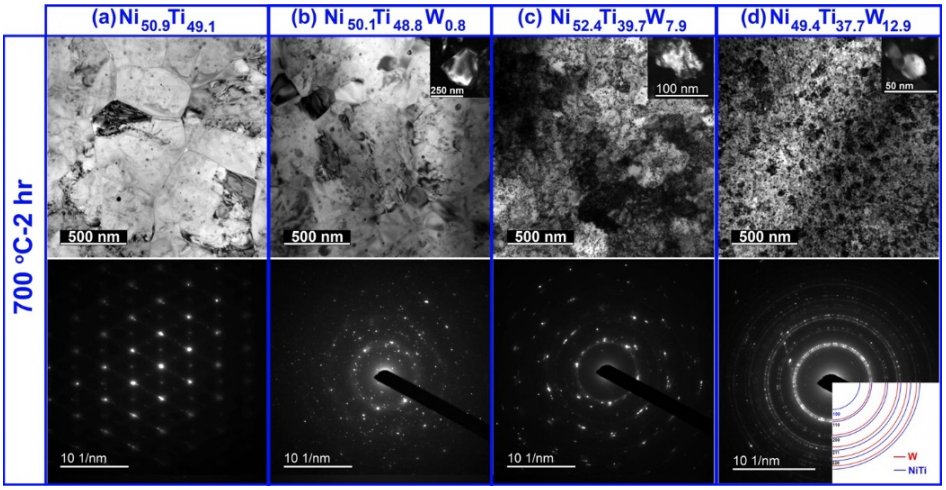

Figure 29: Transmission electron microscope (TEM) microstructures and corresponding SAEDs after annealing at 700 °C for 2 hours showing the effect of W addition on the grain growth behavior of (a) $Ni_{50.9}Ti_{49.1}$, (b) $Ni_{50.3}Ti_{48.8}W_{0.8}$, (c) $Ni_{52.4}Ti_{39.7}W_{7.9}$, and (d) $Ni_{49.4}Ti_{37.7}W_{12.9}$ films.

Films of varying W concentration were prepared by sputtering (using Carousel-type RF magnetron sputtering) with film thicknesses around 9 μm. Figure 29 shows the microstructures of these films after annealing for 2 hours at 700 °C. The Ni-Ti binary alloy is observed to exhibit substantial grain growth, resulting in grain sizes on the order of 1 μm. As the concentration of W present in the system increases, the grain size decreases substantially. Annealing studies were performed at increasing temperatures from 700 °C to 1050 °C, and the average grain sizes measured by XRD for these thin films are shown in Figure 30.

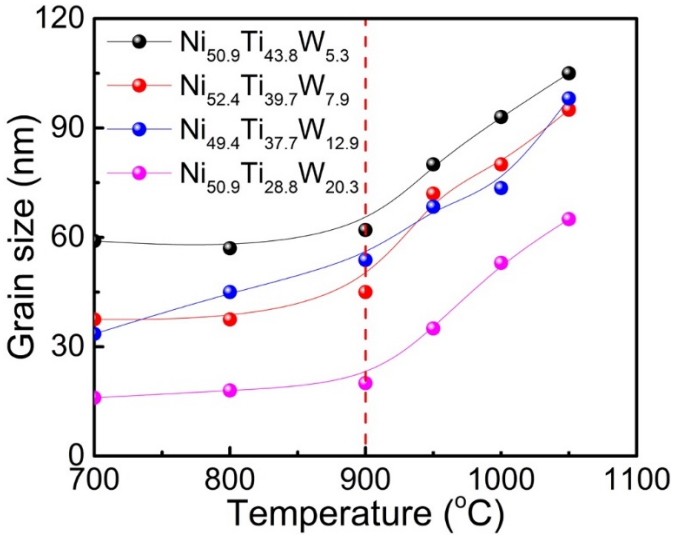

Figure 30: Variation of NiTi grain size with temperature measured with XRD (Scherer equation). Annealing was done for 2 hours at each temperature.

At around 900 °C, the rate of grain growth accelerates in all of the films analyzed. To characterize why this occurs, in-situ TEM measurements were conducted at and above 900 °C. Snapshots from these annealing studies for the 12.9 at.% W film are shown in Figure 31. From the in-situ videos (can be found in our publication [112]), it is observed that as the temperature is increased from 1000 °C to 1100 °C, the W-rich particles start to coarsen while the NiTi grains grow in size (Figures 31(c) and 31(d)). After 4 minutes at 1100 °C, the precipitates are much less densely packed and larger in size. The rate of evolution is even faster at 1200 °C, where after 70 seconds the austenite grains are roughly 50 nm in size (Figures 31(e-f)). These observations suggest that at temperatures above 1000 °C, coarsening of the precipitates occurs at a fast enough rate to cause a loss of thermal stability against grain growth.

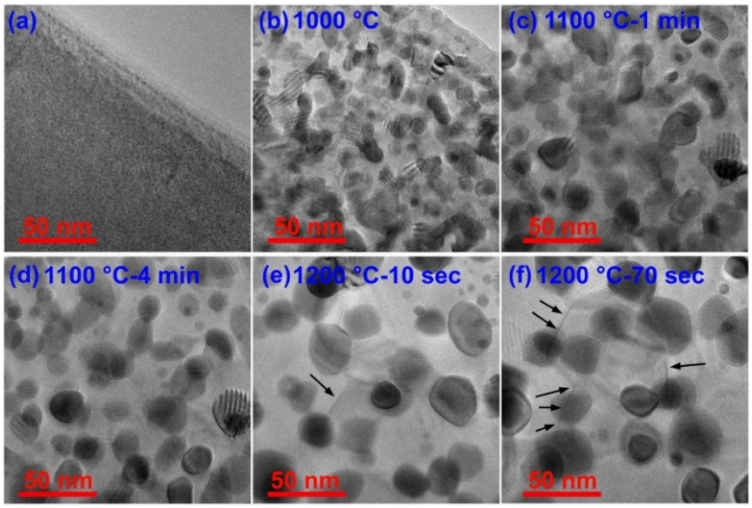

Figure 31: In-situ TEM images of the $Ni_{49.4}Ti_{37.7}W_{12.9}$ thin film in the (a) as-deposited amorphous state, and after annealing (b) to 1000 °C, (c) at 1100 °C for 1 min, (d) at 1100 °C for 4 min, (e) at 1200 °C for 10 sec, (f) and at 1200 °C for 70 sec.

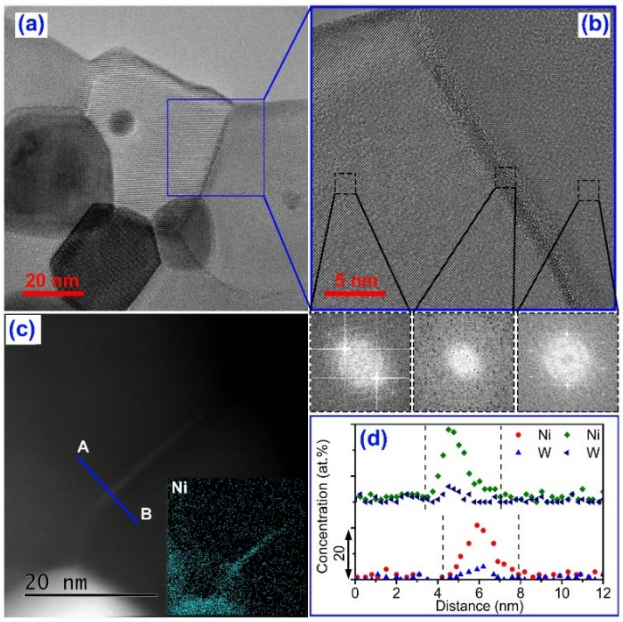

Figure 32: Thermal stability analysis of the $Ni_{49.4}Ti_{37.7}W_{12.9}$ thin film, showing (a) a nanocrystal with size of about 50 nm stable at 1200 °C with clear grain boundary segregation and W-rich precipitates, (b) an HRTEM image of the squared area in (a) showing a thick, amorphous grain boundary with a thickness of ~ 3 nm at 1200 °C, (c) room temperature HAADF-STEM image of the amorphous region showing Ni segregation at the grain boundary, and (d) two typical room temperature EDX compositional line scans across the grain boundary complexions showing both Ni and W segregation.

The grain boundary in Figure 32(a) is one of many that is visually observed to darken and thicken during in-situ TEM. The fast Fourier transform (FFT) analysis of this grain boundary in Figure 32(b) indicates that the boundary is of an amorphous nature with a thickness of ~ 3 nm. The transition of grain boundaries into amorphous complexions [59] at elevated temperatures has been observed in other processing studies such as in Cu-Zr [113,114] and is generally attributed to the increased entropy generated by forming this grain boundary complexion. Figures 32 (c-d) show the chemistry at this grain boundary to be significantly rich in Ni and to a lesser extent rich in W. The Ni excess reaches to ~ 30 at.% higher than that of the matrix while the W segregation reaches to ~ 8 at.% above the matrix. This changing chemistry at the grain boundary at elevated temperature is important to understanding the thermodynamics associated with thermal stability of nanocrystalline NiTi-W thin films. This was one of the key questions that we employed Monte Carlo simulations of this ternary nanocrystalline alloy to better understand.

Section 3.2: Constructing the Monte Carlo simulation of Ni-Ti-W

Monte Carlo simulations were performed using a lattice model to study the equilibrium nanostructures of the NiTi-W system at different W concentrations and temperatures, using the method developed in Chapter 2. In the lattice model, each site contains two pieces of information, a grain number and a chemical identity. However, here we need to update the model to include a ternary element. We do so by treating this system using the energies from the different binary pairs that make up the ternary system, as outlined in our publication on ternary nanocrystalline systems [48]. Nearest-neighbor lattice sites interact through pairwise bonds, namely Ni-Ni, Ti-Ti, W-W, Ni-Ti, Ni-W, and Ti-W bonds that are crystalline bonds (denoted with superscript 'c') if the adjacent sites have the same grain number and grain boundary bonds (denoted with superscript 'gb') otherwise. The values of the pairwise bond energies, $E_{ij}^{(c,gb)}$, between different elements are determined based on the enthalpy of mixing, $\Delta H_{\text{mix}}^{ij}$, and enthalpy of segregation, $\Delta H_{\text{seg}}^{ij}$, of each pairwise couple using the following relationships:

$$\Delta H_{\text{seg}}^{AB} = \frac{z}{2}(E_{\text{AB}}^{\text{c}} - E_{\text{AA}}^{\text{c}} + E_{\text{AA}}^{\text{gb}} - E_{\text{AB}}^{\text{gb}}) \tag{22}$$

$$\Delta H_{\text{mix}}^{AB} = z\left(E_{\text{AB}}^{\text{c}} - \frac{E_{\text{AA}}^{\text{c}} + E_{\text{BB}}^{\text{c}}}{2}\right) \tag{23}$$

The $\Delta H_{\text{seg}}^{AB}$ and $\Delta H_{\text{mix}}^{AB}$ for a binary pair are determined using Miedema estimates or from another similar source (if specified), and are listed in Table 2. One important added consideration in this system is the behavior of W in the NiTi phase, which affects the level of precipitation observed in this system (as the matrix phase in this system is NiTi). The compound unit approach from Section 2.2.1 was used to incorporate the B2 ordered configuration of NiTi, which matches the NiTi phase observed through X-ray diffraction experimentally in these thin films. Bonds between NiTi compound units and W were defined with a distinct energy based on the $\Delta H_{\text{seg}}^{NiTi-W}$ and $\Delta H_{\text{mix}}^{NiTi-W}$, to capture the correct behavior for W precipitation and grain boundary segregation in this phase. These enthalpies of mixing and segregation were treated with a pseudo-binary Miedema model, where NiTi was treated as the solvent element and W was treated as the solute element. Grain boundary bond energies between identical atoms were determined from the grain boundary energies (approximated as 1/3 of the surface energy from a Miedema model [79]): $E_{\text{Ni-Ni}}^{\text{gb}}$ = 2.7, $E_{\text{Ti-Ti}}^{\text{gb}}$ = 3.7, and $E_{\text{W-W}}^{\text{gb}}$= 5.3 kJ/mol.

Table 2: Thermodynamic parameters for the Ni-Ti-W systems used for the Monte Carlo simulations.

Atomic bonds	ΔH_{seg} (kJ/mol)	ΔH_{mix} (kJ/mol)	ΔH_{form} (kJ/mol)
Ni-Ti	11.8	-40 [39,53]	-40.3[54] (NiTi)
Ni-W	10.0[24]	41.4	-
Ti-W	-35.2	-16.1	-
NiTi-W	42.6	79.1	-

Monte Carlo simulations were used to determine the equilibrium alloy configuration using the algorithm described in Chapter 2. Simulations were performed on an 8x120x120 body-centered cubic lattice with varying amounts of Ni, Ti, W to match the experimentally measured compositions, and each system was equilibrated for 11×10^9 Monte Carlo swaps through cooling from a very high temperature to a target in the range of the experiments. It should be emphasized that there are no kinetics in the present simulations, which only explore configuration space to identify energetically preferred microstructures. The extension of this simulation to incorporate

ternary elements, the NiTi B2 compound, and the NiTi-W interactions increased the simulation time from 15 minutes to 90 minutes on a single core of a standard desktop computer with an i5 intel processer (using C++ programming and GCC compiler).

Section 3.3: Thermodynamic analysis of stability against grain growth in Ni-Ti-W thin films

The lattice-based Monte Carlo simulations were used to study the observed nanostructure from a thermodynamic perspective. Simulations were conducted at the same concentrations as the experimental samples at 600, 900, and 1200 °C. The equilibrium microstructures are shown in Figure 33, where white areas represent W atoms, black areas represent NiTi compound atoms, and gray areas represent excess Ni atoms not in their ordered positions within the compound.

For the $Ni_{50.9}Ti_{49.1}$ alloy, the light gray grain boundaries represent the segregation of Ni to the grain boundaries of the NiTi intermetallic phase. This is due to the off-stoichiometric composition of the alloy. In a single crystal, this alloy forms precipitates of Ni in the NiTi matrix, as the amount of excess Ni is above the solubility limit of the NiTi phase.

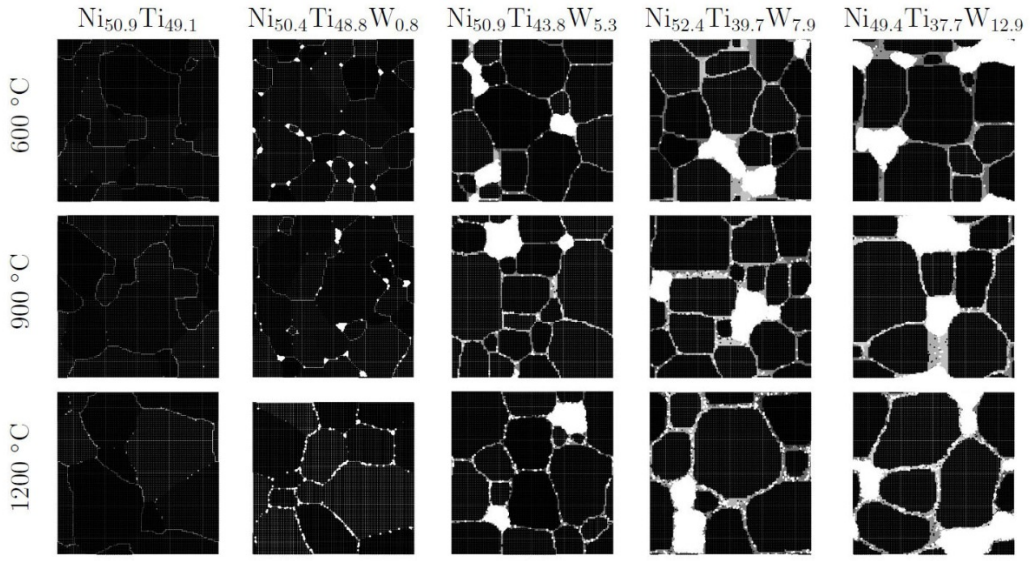

Figure 33: Equilibrium microstructures from Monte Carlo simulations of $NiTiW_x$ with different W concentrations at 600, 900, and 1200 °C. W atoms are colored gray and white, respectively, different shades of gray represent Ni with different grains, and black regions representative of atoms in the NiTi compound.

In the nanocrystalline state, Ni can reduce the energy of the grain boundary, as it has a lower grain boundary energy than Ti, and thus segregates to the grain boundary instead of forming precipitates. At 600 °C, W precipitates are found at the grain boundaries, with a volume fraction that scales in proportion to the global W concentration, along with W segregation to the grain boundary. The microstructures in Figure 33 correspond well to the TEM observations in Figures 29 and 32. The chemistry at the grain boundary as a function of W concentration is shown in Figure 34(a).

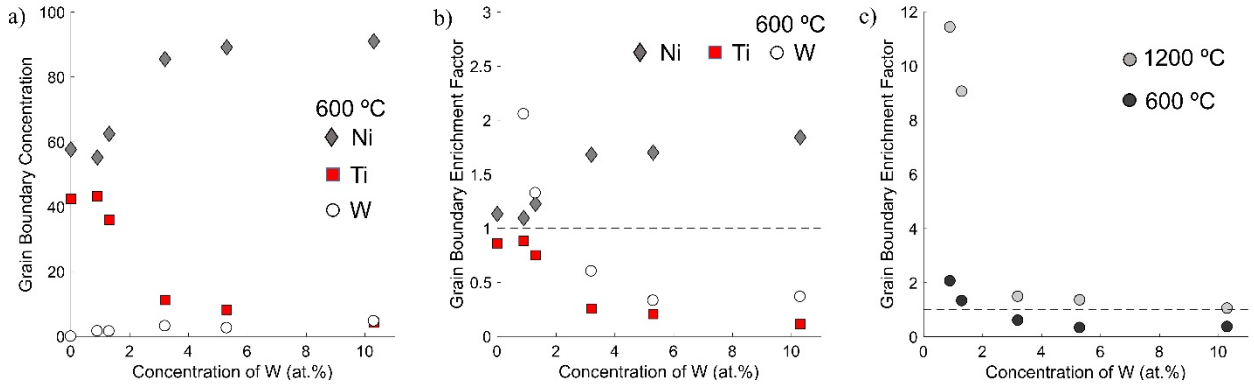

Figure 34: Thermodynamic analysis of grain boundary segregation in the NiTi-W alloy system, with (a) the concentration of solute at the grain boundary at 600 °C and (b) the grain boundary enrichment of solute at the grain boundary at 600 °C, and (c) the grain boundary enrichment of W at 600 °C and 1200 °C. Dashed lines at enrichment factors of 1 are used to visually compare (b) and (c).

Ni is the dominant species at the grain boundary, while the amount of W at the grain boundary is relatively small. The amount of Ni at the grain boundary is generally determined by the stoichiometry, as the higher W level alloys in the set of alloys studied in this work also happen to be more rich in Ni relative to the stoichiometric concentration of NiTi. This helps explain the observation of high excess Ni concentrations and low excess W concentrations at the grain boundary in the EDX line scans in Figure 32(d).

Figure 34(b) shows the grain boundary enrichment factors, the ratio of the concentration at the grain boundary to the concentration in the crystalline regions, at 600 °C as a function of W concentration. The enrichment factors are all relatively low, which means that the driving force

and extent of grain boundary segregation is relatively weak, in this case due to the competing preference for forming W precipitates. Note that in this context an enrichment factor of less than one does not mean that grain boundary segregation is not occurring, as W atoms in precipitates count towards the concentration in the crystalline regions. In fact, W segregation to the grain boundary is observed in all ternary microstructures in Figure 33. Interestingly, W segregation shows a clear trend that is not apparent when only looking at the concentration at the grain boundary: the W enrichment factor decreases with increasing W content, which means a smaller fraction of W atoms are segregated to the grain boundary at higher W concentrations.

This effect is even stronger at elevated temperatures, as observed in Figure 33 where more W is present at the grain boundary with increasing temperature. Figure 34(c) shows that the W enrichment factors are an order of magnitude larger for the lower concentrations at 1200 °C compared to 600 °C. This trend is counter to what would be expected according to dilute limit segregation theories (such as the McLean isotherm), where the amount of segregation to the grain boundary is expected to decrease with increasing temperature. The opposite trend observed in this system is due to the presence of high concentrations of W, which leads to the formation of W precipitates, and the particular alloy energetics associated with the interaction of W with the NiTi intermetallic, i.e. ΔH_{mix}, ΔH_{seg}. Based on the enthalpies listed in Table 2, the enthalpy of grain boundary segregation is not larger than the enthalpy of mixing, which means that precipitation is enthalpically preferred to grain boundary segregation. This is in line with the observations at high W concentrations at 600 °C where the grain boundary segregation of W is low and the vast majority of the W resides in W precipitates. However, the enthalpy of grain boundary segregation is still relatively large, and in particular large enough to offset the grain boundary energy in the absence of W precipitation, leading to strong segregation of W to the grain boundary. As the temperature is increased, entropy begins to play a more dominant role in the equilibrium microstructure, as W atoms begin to leave precipitates to find higher entropy configurations. Because the enthalpy of grain boundary segregation is large in this system, it becomes thermodynamically favorable to segregate to the grain boundary rather than directly dissolve into the crystal, as has been shown previously in binary duplex nanocrystalline alloys. This increased preference for grain boundary segregation coincides with the observation of amorphous complexions forming at 1200 °C in Section 3.3.2.

While both W and Ni grain boundary segregation are observed in these simulations, the grain size does not change substantially with increasing W concentration, which contradicts with what was observed experimentally (see Figure 29). In this lattice-based Monte Carlo simulation, an increase in solute concentration can lead to large decreases in grain size, but only when the nanocrystalline alloy is thermodynamically stabilized due to grain boundary segregation. In the NiTi-W system, precipitation of W is enthalpically preferred to W grain boundary segregation, which limits the effects of stability from grain boundary segregation. This coincides with observations in Figure 31 that Zener pinning is likely the dominant mechanism for stability against grain growth in this system.

At 1200 °C, W precipitates were observed experimentally to coarsen, leading to a loss of stability against grain growth. The flux of W through the grain boundary, which drives coarsening of the W precipitates, depends on both the grain boundary enrichment factor as well as the grain boundary diffusivity. Diffusivity through the grain boundary increases according to an Arrhenius dependence in the grain boundary, and this effect seems to be further enhanced in this system due to the increase in grain boundary segregation with temperature. Thus, in this case, the tendency to segregate to the grain boundary may actually lead to a decrease in the thermal stability of the NiTi-W system. The relationship for the flux of solute through a grain boundary does not depend on solely the grain boundary diffusivity, D_{gb}, but also the enrichment factor for solute at the grain boundary, β, and the grain boundary thickness, λ [115]:

$$P = D_{gb}\lambda\beta \tag{24}$$

In both our model and in the experimental observations, the chemistry of the grain boundary is observed to transition above 900 °C to become both thicker and contain a larger amount of W solutes. This change in grain boundary chemistry, explained by the thermodynamics of nanocrystalline alloys, seems to lead to the onset of accelerated diffusion that leads to W precipitate coarsening and loss of stability of the nanocrystalline grain size.

The NiTi-W alloy system also highlights some considerations that are important for models of thermal stability against grain growth. Whereas most prior models of this phenomenon are for binary alloys, for ternary, intermetallic systems a variety of new considerations emerge. When the compound is off-stoichiometry, self-segregation of one of the elements in the intermetallic to the grain boundary can affect the grain boundary chemistry. The minority alloying element can either

dissolve into the intermetallic, precipitate or segregate to the grain boundary. This behavior is relatively similar to that observed in binary systems; the NiTi-W case falls roughly in line with the duplex nanostructure case identified for binary alloys.

Section 3.4: Conclusions

We conducted thermodynamic analysis using our Monte Carlo simulations on the role of W in stabilizing nanocrystalline NiTi shape memory alloys against grain growth. This marked a major extension in the complexity of our simulations, as we were able to consider a ternary, intermetallic-forming system, which is among the most complex nanocrystalline alloy for which thermodynamic analyses have been conducted to date. We were able to add the following insights to the experimental analysis of grain size stabilization in these films:

- The consistency of the grain size with varying W concentration in the Monte Carlo simulations helped to rule out the possibility of thermodynamic stabilization of the nanocrystalline state due to W grain boundary segregation, supporting the case for Zener pinning from W precipitates being the dominant mechanism for stabilization.
- We found that while W segregation was expected thermodynamically in these films, the self-segregation to grain boundaries is also favored in this system due to the Ni-rich composition of these films. The Monte Carlo simulations can be used to guide the selection of compositions in the Ni-Ti-W alloy to produce grain boundaries with desired chemistries.
- The Monte Carlo simulations revealed increased segregation of W at elevated temperatures as well as a thickening of grain boundaries above 900 °C that coincided with in situ TEM observations. This suggests that a chemical transition is occurring in the alloy, namely that as more W is dissolved into the NiTi phase for entropic reasons a higher concentration of W is driven to the grain boundary. This behavior seems to lead to the acceleration in the rate of diffusion of W through the grain boundary observed experimentally, leading to the loss of stability against grain growth in this alloy.

Chapter 4: Developing Phase Diagrams of Nanocrystalline Alloys

Section 4.1: Why doesn't the lattice Monte Carlo simulation always reach ergodicity?

The swaps in the lattice model are meant to sample the phase space according to the equilibrium probabilities described by statistical mechanics (see Section 1.4.3). After an initial period in which the Monte Carlo system calibrates from the initial alloy configuration towards equilibrium, any instance of the system (i.e. any observation of the system) is a sample of an equilibrium alloy configuration. If the Monte Carlo simulation reaches ergodicity, this instance should occur with the same probability as that predicted by the Boltzmann distribution for the phase space of the alloy.

The nanocrystalline lattice model that has been used to this point has major shortcomings in robustly finding the thermodynamic equilibrium state. For instance, in the previous chapter, Figure 33 shows nanocrystalline states that are in a local minimum in free energy, but almost certainly not in a global minimum in free energy. For example, the Ni-Ti binary alloy, which does not meet the stability criterion in Chapter 2, still exhibits grain sizes in the nanocrystalline regime when a single crystalline state is likely more thermodynamically favorable even after entropic considerations. It is for this reason that we restricted our analysis to the grain boundary chemistry in this metastable nanocrystalline state (local minimum) and could not make any comments on equilibrium grain size. Similarly, Clark et. al. applied the Chookajorn-Schuh model to the Fe-Cu system and found the equilibrium state shown in Figure 35, which they describe as non-nanocrystalline stable [99].

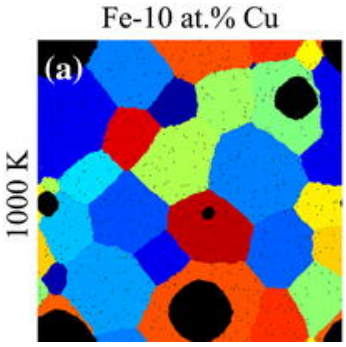

Figure 35: Monte Carlo simulation of the Fe-Cu system conducted by Clark et. al. where the equilibrium predicted by the simulation is not the thermodynamic equilibrium state. (Reproduced with permission from the publisher [99]).

The thermodynamic equilibrium state for Fe-Cu is also a single crystal, but the Monte Carlo simulation again gets trapped before reaching the global minimum in free energy.

The difficulty in finding the true thermodynamic equilibrium configuration is not unique to the nanocrystalline lattice model. Even the simple Ising model (binary alloy without grain boundaries) can get trapped in a local equilibrium (see the antiphase boundaries in Figure 20a and the uncoarsened precipitates in Figure 13a). Reaching true equilibrium is however decidedly more difficult in the nanocrystalline lattice model due to the local nature of the grain swaps. The grain swaps are meant to explore the topological configuration space of the grain boundary network. However, the simulations use a Potts model-inspired mechanism to move the grain boundaries through local grain boundary motion. This Monte Carlo event is far too localized to reliably explore the grain boundary configuration space (especially given how easily the Potts model itself can be trapped due to faceting [70]), and is the culprit for the non-equilibrium states in Figures 33 and 35, even when cooling into the equilibrium temperature. I note here that this is likely also what leads to the observation of the phase separated nanocrystalline state in Figure 12(c) where clear evidence of faceting is observed.

To develop reliable guidelines for the selection and processing of nanocrystalline alloys, these Monte Carlo simulations need to be adjusted to perform more robust searches of the grain boundary network configuration space. One manner in which to do this without changing the basic principles of the nanocrystalline lattice model simulation is to cool the simulation even slower. Chookajorn and Schuh found that a cooling rate of 0.1% from 10,000 K to 773 K worked reasonably well for their W-Ti system, which has become the standard used by following works [68]. However, the slower the cooling rate, the less likely the Monte Carlo simulation is to fall into a local minimum in free energy and find the true global minimum in free energy. When using the slower cooling rate we do find the global minimum in free energy for the alloy system, but it is one where each solute atom acts as an individual grain (to maximize the number of solute-solvent grain boundary bonds which have the lowest energy in the system). This unphysical state is shown in Figure 36. We experimented with different methods of defining the lattice Hamiltonian, for instance penalizing solute atoms with more than a certain number of solute-solvent grain boundary bonds to try to be more physically accurate, but finding the correct balance without guidance from any more detailed physical model ultimately makes any resulting model equally not robust.

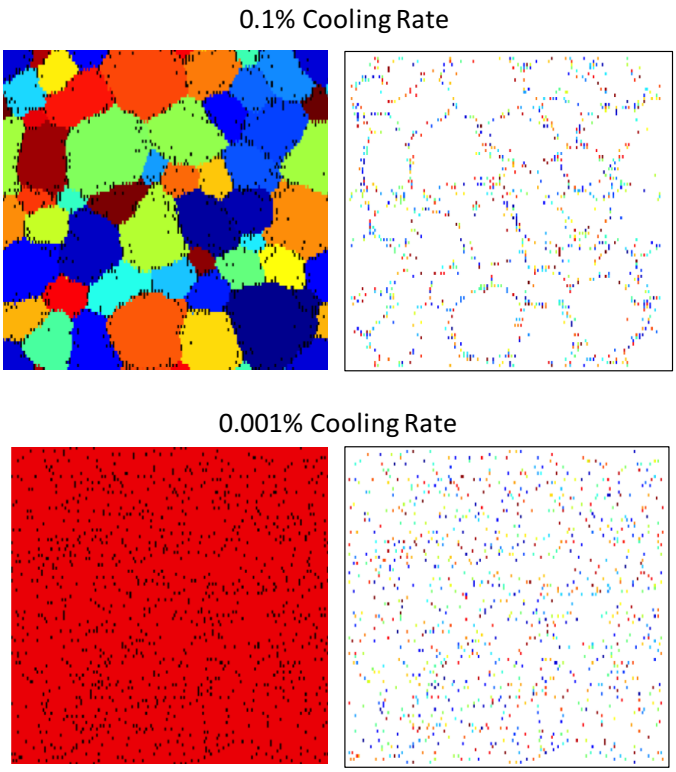

Figure 36: On the left for each simulation is the equilibrated system where solute are in black and colors denote the grain numbers of the solvent. On the right, the grain numbers of the solute are shown in color. In both cases, the grain numbers of the solute are random, where solute are maximizing their coordination of grain boundary solute-solvent bonds. This leads to unphysical ground states that complicates the development of a robust Monte Carlo simulation.

The above challenges to the Monte Carlo approach of simulating nanocrystalline alloys remain in need of further methodological developments. One method is to use the basic concept of the atomistic Monte Carlo simulations described in Section 1.4.4.1 (see Figure 10). To analyze stability in these simulations, nanocrystalline states with different grain sizes were simulated independently and compared to identify which one possessed the lowest energy. The main issue with this method is that only internal energies were available for comparing the different states, which would only be valid at 0 K. If instead of internal energy, a free energy was calculated for the different fixed grain topologies, not only could one decouple exploration of the grain boundary network configuration space and the solute configuration space, but one also could explicitly evaluate the role of entropy in nanocrystalline structures. In this chapter, we develop a more

rigorous method for investigating the thermodynamic equilibrium behavior of stable nanocrystalline alloys with explicit consideration of entropic and enthalpic effects and employ it to observe the nature of phase transitions in stable nanocrystalline states.

Section 4.2: A new method for identifying thermodynamic equilibrium considering nanocrystalline states

Section 4.2.1: Model formulation of the Nanocrystalline Ising model

The advantage of the Chookajorn and Schuh model [68] is that both grain boundary network configuration space and solute configuration space are sampled within the Monte Carlo simulation and as a result the equilibrium state produced by the simulation is one which minimizes the free energy with respect to both configuration spaces, simultaneously. However, as described above, due to the difficulty of exploring the grain boundary network configuration space well, it can be beneficial to decouple the free energy minimization onto each configuration space separately. The Monte Carlo simulation is relatively robust for sampling the solute configuration space, particularly if certain protocols that enhance the ability of the simulation to explore the configuration space freely are introduced. By performing these calculations over a set of grain boundary network configurations that cover (an appropriate swath of) the network configuration space we can determine the minimum free energy configuration with respect to both configuration spaces. Since the grain boundary network is not changed within each Monte Carlo simulation of solute configuration space, the lattice effects from performing grain swaps are entirely avoided. A schematic of this framework is shown in Figure 37 for a simplified view of grain boundary network space that only changes the relative area of a single planar boundary [116].

The grain boundary network configuration space can be surveyed with respect to any set of parameters describing the grain boundary network, such as the grain boundary area density, triple junction linear density, and the grain size distribution. In strongly grain boundary segregated systems, grain boundary area is expected to have the largest influence on the thermodynamic properties of a particular grain boundary network configuration space [39, 47, 65, 68], and thus we focus on surveying the space with respect to grain boundary area. While this neglects many topological features, such as thickened grain boundaries and triple junctions which will be addressed in future work, it provides the simplest physical starting point for quantitative

thermodynamic analysis of nanocrystalline systems. It also makes for easy comparison with the RNS models, which also restrict their exploration of grain boundary network configuration space to the grain size.

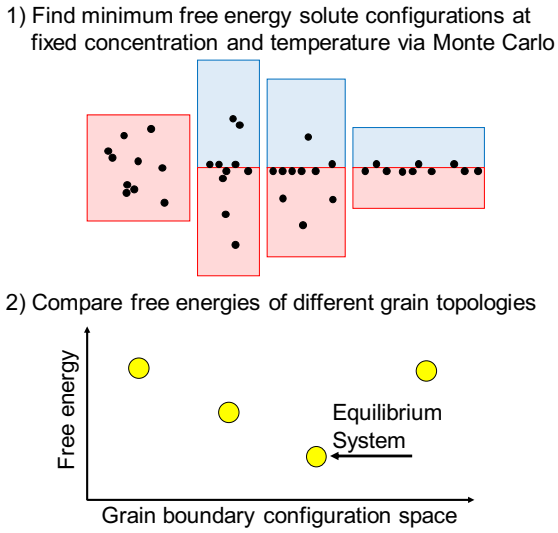

Figure 37: Schematic representation of the framework for identifying free energy minimizing nanocrystalline states by separately exploring solute and grain boundary network configuration spaces. The four configurations shown are all of the same volume (area), but have different relative proportions of grain boundary area (length); comparing across them at constant composition therefore speaks to the energetics of the boundary area and its interaction with the solute.

To this end, we construct a number of bicrystal systems where the grain boundary volume fraction is varied by altering the dimensions of a bicrystal cell, each with a BCC atomic lattice. For comparison we also simulate a single crystal cell without a grain boundary. Each cell has roughly 30,000 atoms (+/- 10%) and the grain boundary 'volume fractions' in the bicrystals (i.e., the fraction of atoms at the boundary) range from 0.004 to 0.5. If the atoms are taken to be a BCC metal such as W, the resulting relative grain boundary areas corresponding to this range spans from 30 to 2500 nm^2, which relates to grain sizes ranging from 1.4 to 175 nm. The bicrystal lattice has periodic boundary conditions in each direction, though in the dimension normal to the grain boundary where the periodic boundary conditions would normally form a second grain boundary the grain boundary bonds are replaced with crystalline bonds to limit the system to just a single

grain boundary plane for more consistent results and finer control. The internal energy of a particular solute configuration is determined just as in the Chookajorn-Schuh model, by summing pairwise bonds within the lattice.

The Monte Carlo simulation on a fixed bicrystal geometry is conducted by randomly swapping a solute and solvent atom within the lattice and accepting the swap with a probability of 1 if it lowers the internal energy of the system or with a probability $e^{\frac{-\Delta U}{k_b T}}$ if the internal energy of the system increases by ΔU, where T is the temperature and k_b is the Boltzmann constant. By performing millions of such swaps, the free energy minimizing configuration is produced. The simulation, however, does not directly provide the free energy of this configuration, which we require in order to compare the free energy of all the equilibrium systems with different grain boundary volume fractions. To extract the free energy from the Monte Carlo simulation of a particular bicrystal geometry with a fixed solute concentration at a temperature, T, we first calculate the specific heat, C, from the thermodynamic fluctuations of the internal energy for a number of temperatures from 0 K to T:

$$C(t) = \frac{\sigma_{U(t)}^2}{k_b t^2} \tag{25}$$

where $\sigma_{U(t)}^2$ is the variance of the internal energy at constant temperature, t. When calculating this variance, each of the samples of internal energy should ideally be uncorrelated from one another; defining a Monte Carlo step as occurring when the number of attempted swaps equals the number of lattice sites in the system, we use internal energy values after every 10 Monte Carlo steps to compute the variance. Intervals larger than 10 Monte Carlo steps were tested and found to be indistinguishable from using the 10 step protocol. We then perform a thermodynamic integration of the specific heat to determine the entropy, $S(T)$:

$$S(T) = \int_0^T \frac{C(t)}{t} dt + S_{\text{res}} \tag{26}$$

where the residual entropy, S_{res}, is the entropy of the 0 K configuration. The residual entropy is zero when the grain boundary is fully saturated, i.e. when there are exactly enough solute atoms to fully occupy the grain boundary segregation sites. When the grain boundary volume fraction is changed, there can be ground state degeneracy, Ω, in some lattices (such as body-centered cubic)

since a plane of N_t atoms that is partially filled with N_s solute atoms can be occupied in $\Omega = \frac{N_t!}{N_s!(N_t-N_s)!}$ ways. This results in a residual entropy of $S_{res} = k_b \ln(\Omega)$. From the entropy, the Helmholtz free energy, F, is simply:

$$F(T) = U_{avg}(T) - T \cdot S(T) \tag{27}$$

where $U_{avg}(T)$ is the average internal energy at temperature, T (computed with the same sampling as the specific heat) and $T \cdot S(T)$ is the entropic component of the free energy, which we will refer to as the entropic energy. Once the free energies are computed, the equilibrium system is selected by comparing the free energies across each of the simulation cells to identify the bicrystal/single crystal state with the lowest free energy.

To attain such free energies, we begin the simulation at 0 K with a solute configuration that is known to be the ground state based on the set of pairwise bond energies provided (for more information see Section 4.2.2). The temperature is then raised in increments of 10 K, performing 10,000 Monte Carlo steps at each temperature up to at least 2000 K. Increasing the temperature from 0 K is critical to getting robust, repeatable behavior from the Monte Carlo simulation. The Monte Carlo simulation has a tendency to get trapped at lower temperatures where the transition probabilities become smaller. By starting at the ground state at 0 K and increasing the temperature, the system already has the right low temperature state and the thermodynamic accuracy of the simulation is greatly increased. The first 3,000 Monte Carlo steps at each temperature are excluded from the specific heat and average internal energy calculations to allow the system to equilibrate to the new temperature (for low temperatures, often 3,000 Monte Carlo steps was not quite right and changes in the number of steps needed for the system to equilibrate were done manually by looking at the internal energy as a function of Monte Carlo steps).

As a model system, we choose an enthalpy of mixing of 20 kJ/mol and an enthalpy of grain boundary segregation of 65 kJ/mol, which matches the energies used by Chookajorn and Schuh (physically representing W alloyed with Ti) [68]. We use a BCC lattice with a grain boundary along the (100) plane and assign pairwise bonds energies as $E^c_{AA} = E^c_{BB} = 0$, $E^c_{AB} = 25.9, E^{gb}_{AA} = E^{gb}_{BB} = 54.8$, and $E^{gb}_{AB} = -61.8$ meV/bond. We calculate minimum free energy configurations over the range of temperatures from 0 to 2000 K for solute concentrations from 1 to 10 at.%. The results of these simulations are discussed in Section 4.3.

Section 4.2.2: Defining 0 K ground states configurations in lattice models

Finding the ground state ordering for a lattice model with even a slightly complex interatomic potential (as our model including grain boundary bonds) is not a trivial calculation. The problem requires finding the solute configuration that minimizes the internal energy. The space of possible configurations is large, with N choose N_s combinations where N is the number of atoms and N_s is the number of solute atoms. For even an extremely small system with 20 atoms and 8 solute atoms, there are 125970 configurations. Thus identifying the energy minimizing configuration in a large system requires a more efficient way of describing the space of configurations.

Dr. Peter Larsen (Technical University of Denmark) and I worked together to solve this problem, specifically to make it easier to initialize the nanocrystalline lattice model at 0 K. Our goal was to solve for all possible ground states for our interatomic potential and have a full one-to-one mapping between the parameters of the potential and the ground states. There are two key insights from this work for solving for all possible ground states given a lattice potential. First is realizing that the energy of a lattice model system is linearly dependent on the number of each type of bond, with an integrality constraint (i.e. you must have an integer number of each type of bond in the lattice). Given these conditions, integer programming solvers can be readily used to solve for the ground state of the lattice model given a set of pairwise bond energies. Secondly, while the configuration space is large, the space of the number of bonds of each type is tractably small for systems of interest. On a 12 by 12 hexagonal bicrystal lattice with 28 solute atoms (20 at.% solute) using our nearest neighbor potential, there are $\sim 10^{30}$ possible solute configurations but the number of possible sets of the number of each type of bond is only 12337, which is a small enough set to build our mapping between interatomic potential parameters and the ground state. The details of this method are found in our publication [117]. We found that there are several interesting ground states in the bicrystal lattice model. The ground states for the BCC lattice used for constructing the ground states for the Monte Carlo simulations is unpublished for the time being, but are similar to the hexagonal ground states shown in Figure 38. The ground state ordering for the energetic parameters for W-Ti described in the previous section fall under the class of Figure 38(c) known as a repulsive line, where solutes segregate to the grain boundary in a single layer. This matches the complexion we used to describe the behavior of the lattice model in Chapter 2.

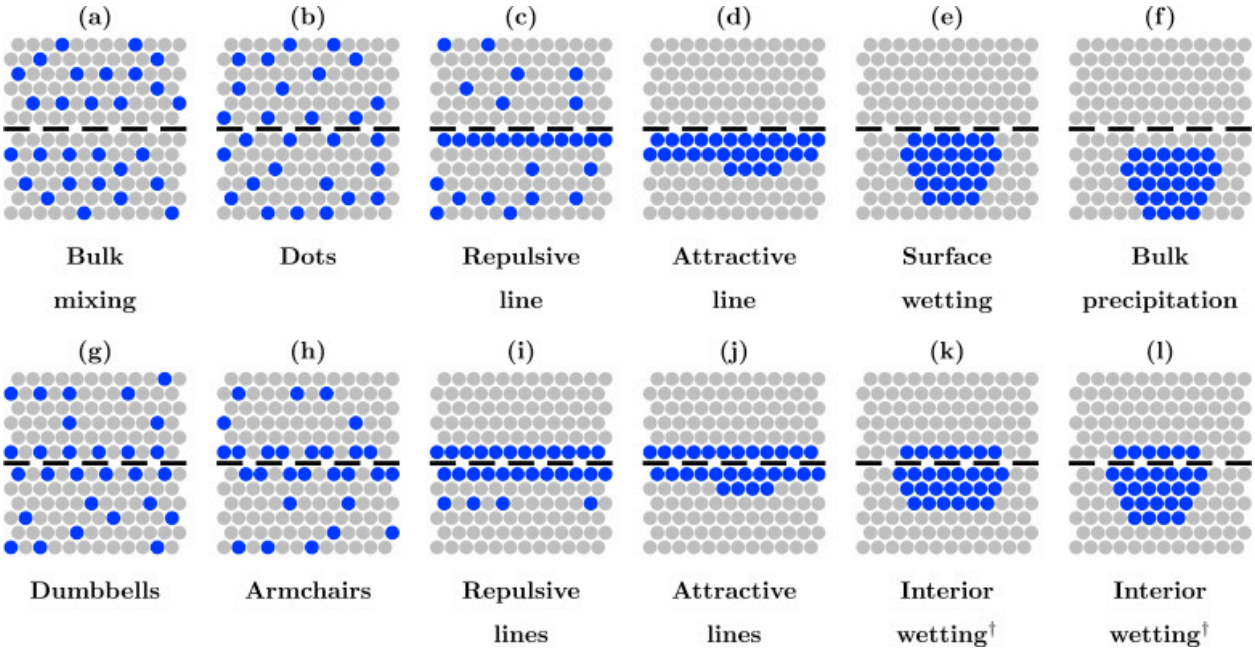

Figure 38: All minimizing configurations for a 2D hexagonal lattice with 28 solute atoms, with complexions with a preference for A-B grain boundary bonds and B-B grain boundary bonds placed in separate rows. Solvent and solute atoms are colored gray and blue respectively. †Wetting complexions form a continuum as the precipitate can intersect the grain boundary in several ways; as such, we have not given them different names.

Section 4.3: Case study in developing free energy and phase diagrams for W-Ti

Section 4.3.1: Order-disorder transitions at fixed grain boundary area

We first study the order-disorder processes that occur from 0 to 2000 K on each bicrystal system separately. At fixed solute concentration, there are four configurational families that are easily distinguished at 0 K for the alloys studied here (i.e., with positive heat of mixing and enthalpically favored grain boundary segregation) based on the grain boundary area of the system:

(1) the single crystal (grain boundary area of zero) where solute precipitation is enthalpically favorable.

(2) "oversaturated" systems where the grain boundary area is low, such that solute cannot be entirely accommodated at the grain boundary and excess solutes therefore form a second-phase precipitate (generally first along the boundary),

(3) A "saturated" system in which the grain boundary area is precisely enough to fully accommodate all solute atoms,

(4) "undersaturated" systems where the grain boundary area is higher than the saturated case and solute cannot occupy all of the available grain boundary sites.

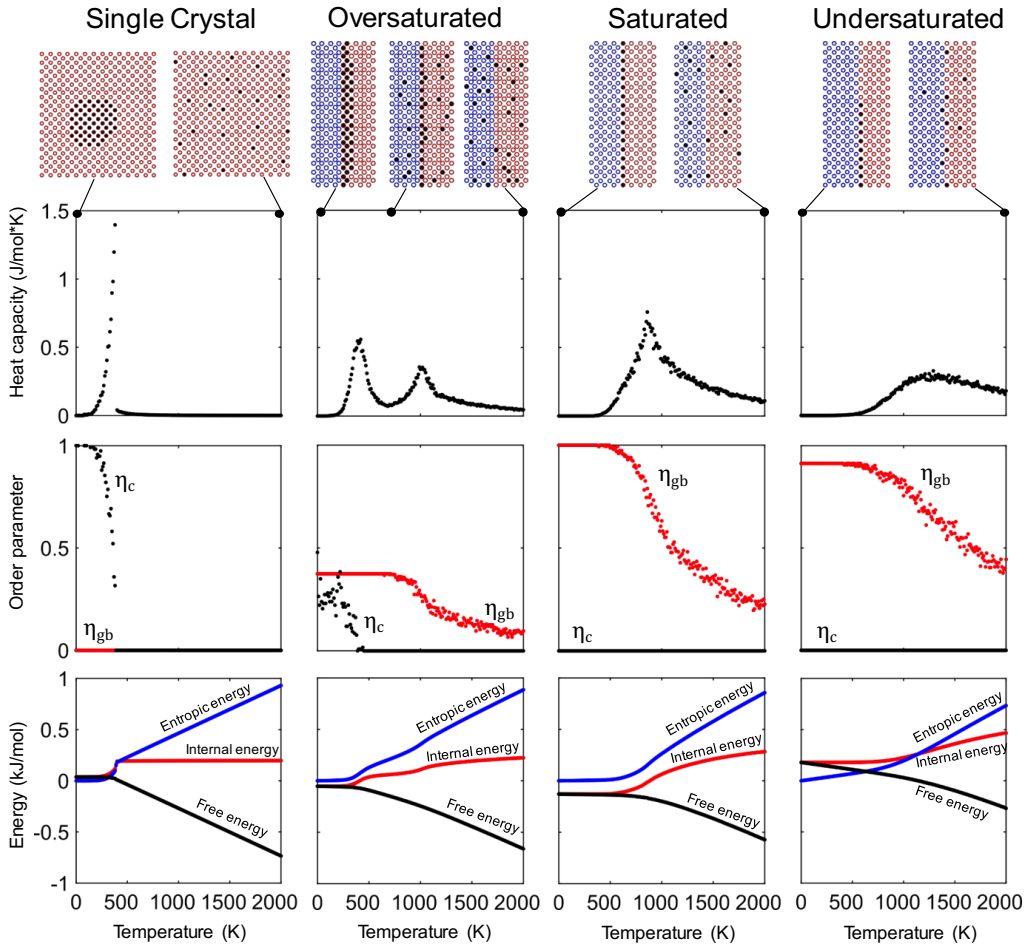

Figure 39: Order-disorder transitions of 1 at.% alloys at fixed grain boundary volume fraction for each of the four cases. Heat capacities are presented in the first row, followed by crystalline and grain boundary order parameters in the second row, and total system energy in the form of entropic energy, internal energy, and free energy in the third row.

Figure 39 shows the order-disorder behavior of each of these cases for a 1 at.% alloy. Two types of ordering emerge in these systems: bulk ordering in the form of phase separation and grain boundary segregation where solute and solvent atoms bond across the grain boundary. We can define order parameters for each of these forms of ordering: the crystalline precipitate order

parameter (η_c) is the fraction of solute atoms only bonded to solute atoms (all bonds are crystalline), and the grain boundary order parameter (η_{gb}) is the fraction of solute atoms that have four solvent grain boundary bonds (which is the lowest energy configuration for grain boundary segregation in the model).

At an order-disorder transition, heat capacity exhibits a peak. The first row of Figure 39 reveals two clearly distinct such order-disorder peaks when grain boundary area is fixed:

- The peak around 400 K corresponds to the dissolution (disordering) of the bulk solute precipitate as evidenced by the drop in the crystalline precipitate order parameter. Note that this transition occurs in the single crystal case as well as in the oversaturated case where the precipitate along the grain boundary also undergoes bulk disordering. The single crystal system has a much sharper peak in heat capacity, since all of the solute dissolves into solution at this transition point, as opposed to the oversaturated case where some solute atoms remain segregated at the grain boundary after the bulk disordering transition is completed. Nonetheless, the precipitate dissolution transition appears to occur at roughly the same temperature in this system whether the grain boundary is present or not.
- In the oversaturated case, there is a second disordering temperature at around 1000 K, also defined by a peak in the heat capacity, and related to the disordering of the grain boundary segregation state (i.e., dissolution of solute off the grain boundary and into the bulk). All of the three different bicrystal cases exhibit this transition, with the sharpest peak occurring for the saturated case.

These two transitions both reflect entropic disordering, but exhibit some key differences. The bulk phase transition is completed in a relatively small temperature window of ~100 K, while the grain boundary desegregation transition occurs over a much broader range of almost ~ 1000 K. The more gradual nature of the grain boundary desegregation transition is also evidenced in how the characteristic system energies change as a function of temperature, as shown in the third row of Figure 39. Whereas the free energy exhibits a change in slope at the critical temperature for bulk dissolution, emblematic of a first-order phase transition, that for the grain boundary desegregation reaction is broad and gradual, and thus more likely to be a second-order phase transition.

In Figure 39, for this specific alloy, the bulk transition occurs at lower temperatures than the grain boundary one. We expect that this should be generally true for a nanocrystalline alloy that is stabilized by grain boundary segregation; the internal energy gained by grain boundary segregation must be sufficiently larger than the internal energy gained by forming the bulk phase in order for the nanostructure to be stable in the first place. When the bulk phase transition occurs, the oversaturated and single crystal states undergo an increase in entropy when the solute precipitate dissolves into a solid solution, which allows these states to lower their free energy significantly at temperatures lower than the saturated and undersaturated systems. This behavior may also explain the duplex nanocrystalline behavior [72] described in Chapter 2 where a system with second phase bulk precipitates can disorder into a grain boundary-segregated polycrystal; the stable nanocrystalline state is thus an activated state in such alloys.

Figure 40 shows in more depth the effect of decreasing the grain boundary area from the saturated (grain boundary volume fraction of 0.02) to the single crystal case. Fig. 40(a) shows the heat capacity peaks for both the single crystal (which exhibits only the bulk dissolution peak), a saturated bicrystal (which exhibits only the grain boundary desegregation peak), and a variety of states in between these two.

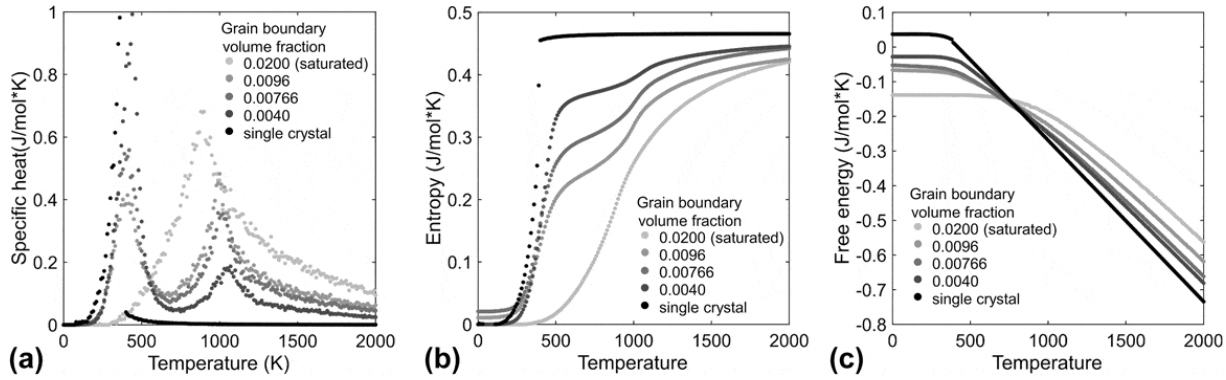

Figure 40. (a) Heat capacities from 0 to 2000 K for 1 at.% alloys with fixed grain boundary volume fraction in the saturated, oversaturated, and single crystal regime, and (b) the corresponding entropies and (c) free energies.

As grain boundary area (volume fraction) decreases, the peak in specific heat from the bulk phase transition increases in intensity, while the peak from the grain boundary desegregation transition shrinks, as fewer atoms participate in grain boundary desegregation. This corresponds,

according to Eq. 26, to larger rises in entropy for more oversaturated bicrystals, as shown in Fig. 40(b). As the grain size rises, these entropy rises trend towards the maximum entropy jump possible, i.e., that for the single crystal, which reaches the neighborhood of the ideal solution entropy, 0.465 J/mol-K. However, the enthalpies follow a similar trend, which can be read from the free energy curves in Figure 40(c) at low temperatures; the enthalpies increase with decreasing grain boundary area. This trade-off leads to the oversaturated bicrystals becoming equilibrium configurations first before the solid solution's higher entropy fully dominates as temperature increases. This transition is discussed in more detail in the next section.

Section 4.3.2: Order-disorder transitions for stable nanocrystalline states

The true equilibrium state at a given temperature and solute concentration is the state with the grain boundary area that attains the lowest free energy compared with any other at that temperature and concentration. Figure 41(a) shows how the free energy behaves as a function of grain boundary volume fraction at 0 K, 600 K, 840 K, and 2000 K for the same 1 at.% alloy. The grain boundary volume fraction that provides the lowest free energy at a given temperature is the equilibrium state. At 0 K, the saturated state has the lowest internal energy and therefore the lowest free energy as expected.

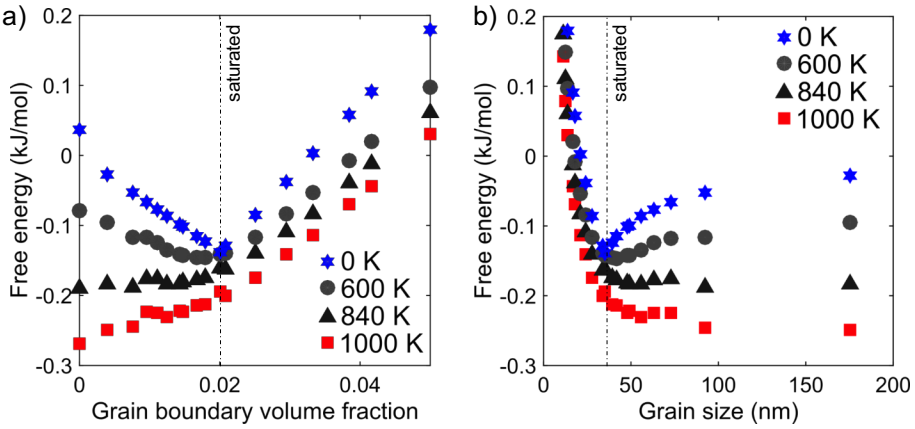

Figure 41. (a) Free energy as a function of grain boundary volume fraction at three temperatures: 0 K, 600 K where the stable grain boundary volume fraction is lower, 840 K where the solid solution phase first becomes stable, and 2000 K. (b) The same free energies are also shown with respect to grain size.

The dependence of free energy on grain boundary volume fraction at 0 K is linear both in the oversaturated regime, where the precipitate is growing, and in the undersaturated regime, where the pure solvent grain boundary is increasing in volume fraction. Systems in the undersaturated regime are not observed to become the equilibrium state at any temperature as free energy increases with grain boundary volume fraction above the saturated state, even beyond the range of values shown in Figure 41(a).

At 600 K, the oversaturated cases have undergone their first disordering transition, and entropy plays a significant role in the free energy of the states with grain boundary volume fractions below 0.02, as evidenced by the reduction in free energy relative to the 0 K states. A grain boundary volume fraction of 0.016 is now the lowest free energy configuration, lower in free energy than the saturated state which has not been able to access as much entropy; entropy and the loss of some solute from the grain boundary favors grain growth by a small degree to a somewhat larger equilibrium grain size. The preference for a grain boundary area between the saturated state and the single crystalline state comes from the balance between the enthalpic advantage of grain boundary segregation, which benefits from a larger number of available grain boundary sites, and the entropic advantage of disordering into a solid solution, which benefits from a smaller grain boundary area where more solute atoms originally reside in a bulk precipitate and thus disorder during the first transition. At 840 K, the free energy of the single crystalline state becomes the lowest free energy state, marking a completed transition away from the stable nanocrystalline configuration. As temperature continues to increase, the solid solution state continues to be the lowest free energy state as it has the highest entropy.

Chookajorn and Schuh [68] calculated the internal energy as a function of grain size in their nanocrystalline lattice model and found the minimum internal energy to be at a saturated nanocrystalline state. Their internal energy dependence on grain size resembles the free energy dependence on grain size at 0 K in Figure 41(b), which suggests that the bicrystal model is a reasonable approximation of even more complex nanocrystalline topologies. The free energy calculated by this method, however, captures temperature effects and shows that as temperature increases, larger grain sizes become more energetically favorable. In addition, at a critical temperature grain growth to a single crystal is entirely downhill in free energy and the nanocrystalline state is no longer stable.

To determine the true equilibrium behavior of the alloy and attain useful relationships, such as equilibrium grain size as a function of temperature, we need to merge the decoupled sampling of the grain boundary network configuration space and the solute configuration space. This is accomplished by defining the properties of the equilibrium state (e.g. energy, configuration, grain boundary volume fraction) at a given temperature to be equal to the properties of the free energy minimizing bicrystal/single crystal at that temperature. Figure 42 shows the equilibrium behavior of the alloy system, now defined as the free energy minimizing configuration across both solute configuration space and grain boundary network configuration space. Overall, the observed behavior is much more similar to a bulk phase transition than the grain boundary desegregation transition. The free energy in Figure 42(a) shows a more discontinuous change in slope at the transition temperature of 840 K. The corresponding enthalpies and entropies also have an increasing slope as the transition temperature is approached, as opposed to the more gradual increase in internal energy in the saturated bicrystal in Figure 39. The order parameter in Figure 42(b) also has an abrupt drop that is similar to the crystalline order parameter in Figure 39 for the single crystal. This suggests that the transition marking the loss of nanocrystal stability is much like crossing a standard alloy solvus transition and is similarly a first-order transition.

As the crystalline order parameter decreases in the single crystal case, the volume fraction of the precipitate correspondingly decreases as more solid solution phase is formed. In the case where grain boundary segregation stabilizes a nanocrystalline state, as the grain boundary segregation order parameter decreases, the volume fraction of segregated grain boundary decreases as well, again to form more solid solution phase. This corresponds to a decrease in the grain boundary area as shown in Figure 42(c), and in the equilibrium microstructures in Figure 43. Effectively, this means that as temperature increases, the equilibrium grain size of a nanocrystalline state should rise. It is also important to note that in each of the microstructures in Figure 43 the grain boundary remains relatively fully segregated, which is necessary in order for the nanocrystalline state to remain energetically favorable.

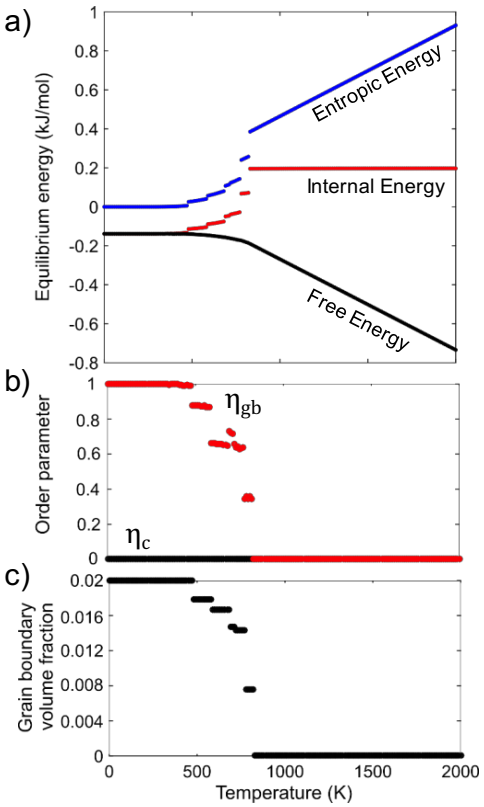

Figure 42: Order-disorder transitions for a 1 at.% stable nanocrystalline alloy. (a) The free energy, entropic energy, and internal energy, accompanied by (b) the grain boundary and crystalline order parameters, and (c) the grain boundary volume fraction are shown as a function of temperature from 0 K to 2000 K.

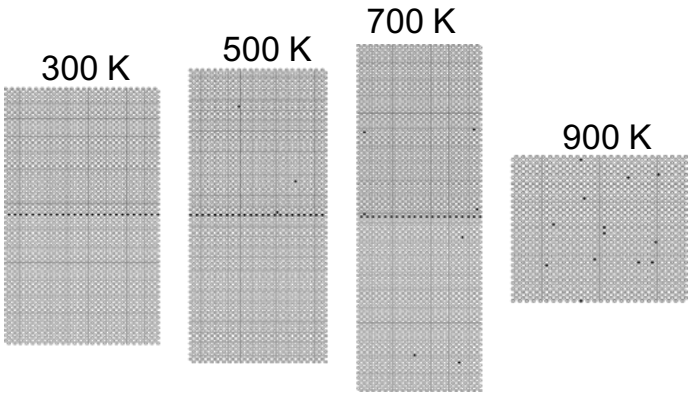

Figure 43: The equilibrium microstructures at 300 K, 500 K, 700 K, and 900 K.

One of the difficulties with exploring grain boundary network configuration space by performing separate Monte Carlo simulations is that it relies on accurate measurement of free energy from these simulations, which requires fine sampling of temperature to numerically integrate the specific heat, and fine sampling of grain boundary network configuration space. Each

of the curves in Figure 5, particularly the entropic energy, internal energy, and grain boundary volume fraction, have several small jumps where in fact it is more likely that each of those parameters is actually continuous with temperature. The small jumps emerge because in actuality the grain boundary area should change continuously, and our sampling is not fine enough to fully capture the continuous curve. In addition, the calculation of entropy depends on how the specific heat is sampled when the numerical integration is conducted, and this leads to some error in the estimation of entropy and correspondingly in the free energy. Thus, even if grain boundary area is sampled more finely these equilibrium curves would likely still not be perfectly continuous due to the differences in the magnitude of the error in free energy in each simulation. Developing a way to overcome this resolution issue is an area for future work in improving the simulation framework. Nonetheless, this method is able to observe the thermodynamic disordering of a stable nanocrystalline state, which previous simulations could not, and is thus a useful tool for understanding how the equilibrium grain size changes during the disordering process.

Section 4.3.3: Free energy and phase diagrams for stable nanocrystalline states

The equilibrium free energy was similarly determined for solute concentrations from 2 to 10 at.%; the general behavior is very similar to the 1 at.% alloy that has been described thus far. Figure 44 shows the free energy diagram that results from these calculations at three temperatures. At 2000 K, the equilibrium phase for all systems in this concentration range is a solid solution, and the free energy curve has a decreasing slope as the solute concentration increases, as is expected for a solid solution phase. At 1550 K, the 7 at.% alloy is at its critical temperature, and the free energy curve above and below this composition exhibits different behaviors. From 1 at.% to 7 at.% where the solid solution phase is stable, the free energy curve has the same decreasing slope behavior as the solid solution phase at 2000 K. From 7 at.% to 10 at.%, the free energy curve becomes a straight line. This is even more evident at 1100 K, where the 3 at.% alloy is at its critical temperature and a straight line emerges from 3 at.% to 10 at.%.

The equilibrium state along these straight line regions is a stable bicrystal, resembling the bicrystal microstructures in Figure 44. A straight line in a free energy diagram is indicative of a two-phase equilibrium state, with the free energy determined from the common tangent line between the two equilibrium phases. The two phases for the bicrystal state are the crystalline solid

solution phase and the grain boundary "phase", where the grain boundary "phase" in our model is best likened to a 2D compound. Just as in a standard alloy free energy diagram, the lever rule can be used to determine the volume fraction and concentrations of the two phases present at equilibrium. In the case of nanocrystalline stability, the grain boundary volume fraction is determined by the volume fraction of the grain boundary "phase" and the concentration of solute in the grains is determined by the concentration of the solid solution phase thus defining the configuration of the equilibrium bicrystal/nanocrystalline state.

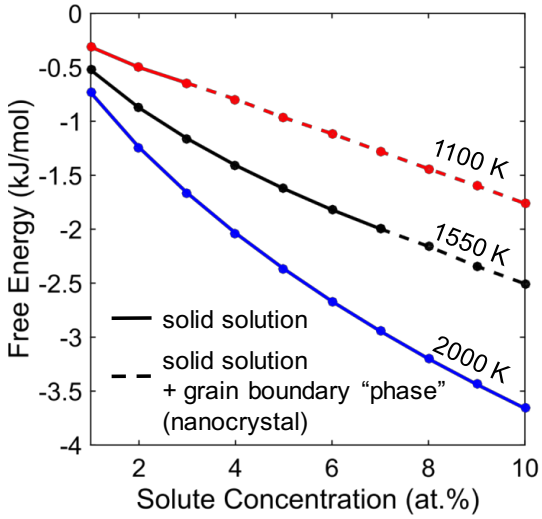

Figure 44: The free energy diagram at 1100 K, 1550 K, and 2000 K for solute concentrations from 1-10 at.%, where the solid lines represent systems where the solid solution is stable and the dashed lines represent systems with stable grain boundaries in equilibrium with a solid solution.

By collecting the group of critical temperatures for transitioning from the nanocrystalline state to the single crystal solid solution at each solute concentration, we construct a phase diagram for a stable nanocrystalline alloy as shown in Figure 45(a). The solid black dots represent the critical temperatures above which the single crystal solid solution phase is stable and below which a nanocrystalline state is stable. The corresponding solid black line is the solvus for the grain boundary segregated state and it is important to note that this nanocrystal solvus is different than the single crystal solvus we would determine if only single crystalline states are considered (shown by the blue dashed line in Fig. 45(a)). The single crystal solvus is the solvus traditionally read from a binary phase diagram, denoting the solubility limit with respect to the bulk solute precipitate

phase. However, in this system the single crystal solvus has a lower temperature than the nanocrystal solvus at all concentrations as a consequence of the nanocrystalline state being stable in this system and the bulk solute precipitate phase being metastable. The single crystal solvus depends on the enthalpy of mixing; the nanocrystal solvus similarly depends on the enthalpic benefit of the segregated nanocrystal, which is equal to the enthalpy of grain boundary segregation minus the enthalpy of the pure solvent grain boundary.

The nanocrystal solvus can be used to determine the composition of the two-phase equilibrium state in the same manner as in a standard binary alloy phase diagram. To illustrate this, take as an example an alloy with 4 at.% solute at 1000 °C (marked by the star in Fig. 45(a)), microstructure shown in Fig. 45(b)). The solvus at 1000 °C corresponds to a solute concentration of 2.4 at.%, which is the concentration of solute in the crystalline regions of the stable nanocrystalline state at 1000 °C. The volume fractions of the crystalline and grain boundary phases are determined by the lever rule between the solvus and the grain boundary "phase"; in our model the grain boundary "phase" has an effective concentration of one-third (a plane of solute atoms is sandwiched between two planes of solvent to form the segregated grain boundary) and is expected to be essentially a line compound. Based on the volume fractions of each phase, the grain boundary volume fraction is determined, which dictates the grain size of the nanocrystalline state. Thus, the nanocrystalline phase diagram can be directly read to understand the equilibrium grain size and the solute concentration in the grain interiors at a given temperature and solute concentration.

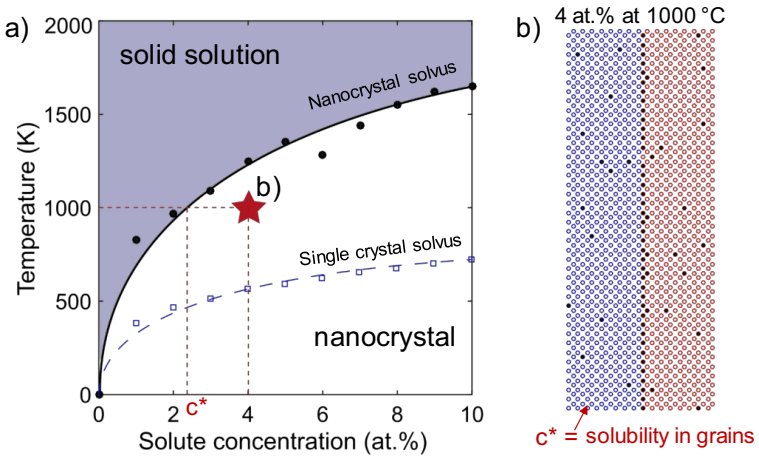

Figure 45: (a) The phase diagram for a stable nanocrystalline alloy, where the solid line and black dots represent the transition temperature for forming a solid solution from the nanocrystalline state (nanocrystal solvus). The blue squares represent the transition temperature for forming a solid solution from a bulk precipitate, which form the single crystal solvus for when nanocrystalline states are not considered. The white region is a two-phase region. (b) The equilibrium microstructure for a 4 at.% alloy at 1000° C (denoted by a star in (a)) for which the concentration of solute in the crystalline region is that of the nanocrystal solvus when read from the phase diagram according to the lever rule.

The nanocrystal solvus is essentially a curve where the grain boundary area goes to zero as a function of solute concentration. We can draw equivalent curves for when the grain boundary area equals a constant greater than zero on the phase diagram, as shown in Figure 46. The dashed lines in Figure 46 represent such curves for fixed grain boundary volume fractions of 0.015, 0.05 and 0.1, which correspond to grain sizes of 7 ,14, and 48 nm. These are effectively curves of equal volume fraction of the second phase according to the lever rule, as all nanocrystals with the same volume fraction of the grain boundary phase have the same grain size. This is an interesting contrast from the phase diagram of Fe-Zr with a metastable nanocrystalline state calculated by Zhou and Luo [47] (Figure 8), where the constant grain size curves are constant functions of temperature and effectively vertical lines in the phase diagram. Vertical lines would imply a discontinuous change in grain size from the saturated grain boundary volume fraction to a solid solution state, whereas for the thermodynamically stable nanocrystalline states presented here, the phase transition occurs by passing through a two-phase region with increasing solubility and grain

sizes decrease accordingly with temperature. While we chose a positive enthalpy of mixing system in this study, this approach can be generalized to include negative enthalpy of mixing systems with stable intermetallics and ordered compounds by using the compound unit approach.

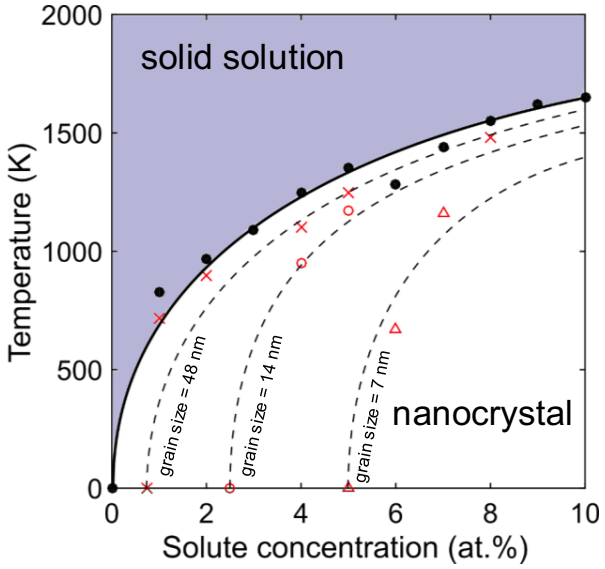

Figure 46: The phase diagram with curves of constant grain size (dashed lines) where red markers denote the temperature at which a particular grain size is stable for a given concentration.

The ability to construct phase diagrams of this type should improve the selection of alloying candidates for stabilizing grain size, as not only can systems be designed to have stable nanocrystalline states at low temperature but also selected based on their ability to retain a fine grain size up to higher temperatures. In addition, the similarities and differences between the order-disorder transition of the nanocrystalline state and that of a standard two-phase alloy allow us to better understand the thermodynamic implications of having a nanocrystalline ground state. The phase diagrams give researchers an important guide in processing their nanocrystalline material to their desired nanostructure.

This basic concept, demonstrated on a simple case of a bicrystal lattice model, can be readily extended to more complex systems to solve the challenges related to surveying the grain boundary configuration space. One extension, for example, is to use lattice models with more complex grain topologies to better incorporate effects of triple junctions (which will have different segregation energies) and more grains (which can accommodate precipitates). This method of calculating free energies is not limited to lattice models and can enable the use of the atomistic

Monte Carlo simulations (Section 1.4.4.1) to both analyze stability of alloy systems and to develop phase diagrams for processing desired nanocrystalline alloys. The method is also not limited to defining grain size as the key variable in the grain topology space to explore. For example, systems in an atomistic simulation can be developed with different grain boundary textures to identify preferences for particular textures among nanocrystalline alloys due to the segregation behavior of a solute element.

Section 4.4: Exploration of a more efficient method for sampling the grain topology space

Another method of approach is to find better "grain swap" definitions in order to get an ergodic sampling of the nanocrystalline configuration space. The key is to define the grain swap in such a way that you are able to get long range changes in the nanocrystalline configuration space through relatively few swaps. When doing this, it's generally necessary to define the grain swap as a multistep process, where after the grain topology is changed atom swaps are conducted to equilibrate the trial configuration before applying the Metropolis acceptance criterion. The reason for this is that if a long range change in the grain boundary network occurs without any change in the solute configuration, then these events would almost never be selected. This concept is similar to the protocols in atomistic Monte Carlo simulations where after performing an atom swap the local environment is structurally relaxed before determining whether to accept or reject the swap.

We experimented with a few basic ideas for events that will sample the grain topology space faster. One method that is promising for the lattice model is to move triple junctions as a grain swap instead of any random point on the grain boundary. Movements of the triple junction by even one point can change the grain number of a relatively large set of lattice sites leading to better sampling. Implementation of this idea is, however, made computationally expensive by the need to constantly redefine the grain numbers of all atoms on the lattice, as any conceived method of locally updating only the lattice sites in the area of the triple junction and its adjoining boundaries required several exceptions. The triple junctions also need to be able to be deleted or added in order to be able to consider systems with different numbers of grains. Maintaining well-defined grains through this process was a challenge.

The algorithm we implemented was a slight variation on the triple junction model, where rather than move an individual triple junction (more similar to our original Potts model), the grain structure of the system was generated with a weighted voronoi tessellation (Figure 47) and the location and weight of an individual node was changed in order to sample the grain topology space. This method has the added benefit of not having the "single solute grains" shown in Figure 36 within the phase space of the system, which allows us to probe for equilibrium without concern for unphysical states. The simulation was performed as follows:

1. The system is initialized with a small number of grains generated by a weighted voronoi tessellation.
2. Initialize solute positions by starting with a random distribution of solute on the lattice and performing 10,000 Monte Carlo steps of atom swaps at your desired temperature to reasonably equilibrate the solute to energetically favorable positions in this lattice.
3. Use the newly defined grain swap events to sample the nanocrystalline alloy phase space. Three types of grain swap events are defined: (i) a move, where a random voronoi node is moved to a random location within a 10 lattice site cut-off radius and given a new random weight, (ii) a deletion, where a grain is removed by removing a random voronoi node, and (iii) a creation, where a new voronoi node is added to the system at a random lattice site and with a random weight. After the operation on the node is conducted, perform 10,000 MC steps of atom swaps to reasonably equilibrate.
4. Perform these grain swaps at the desired temperature. In the simulations to follow where we aimed to understand the evolution of a nanocrystalline alloy at several temperatures, we performed simulations varying temperatures in a manner similar to that described for the bicrystal lattice in the previous section, but starting at elevated temperatures. We started at 1500 K and cooled by 100 K down to 0 K, performing 1000 Monte Carlo steps of grain swaps to reach equilibrium on a 48x48x96 BCC lattice. This is a relatively low number of Monte Carlo steps, but was a constraint due to the computational power available. As a result, these simulations should be seen as a simple exploration of using such a scheme for Monte Carlo simulations of thermodynamic equilibrium in nanocrystalline alloys.

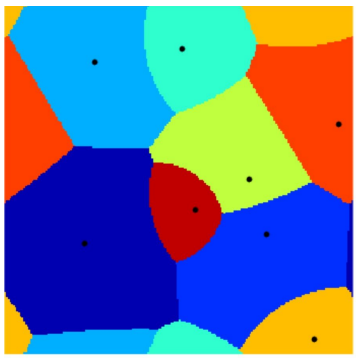

Figure 47: A weighted voronoi tessellation where black dots represent nodes used to generate the structure and different grains are colored differently.

As can be seen in Figure 48, the equilibrated system at ΔH_{seg} = 30 kJ/mol is a single crystal, as expected by the stability criterion, with a single, faceted precipitate representing the ground state. This was also observed for enthalpies of segregation below 30 kJ/mol. This is a promising result of this preliminary set of simulations, as it suggests that starting from a finite grain size, the grain swaps are efficient enough at exploring the grain boundary configuration space to distinguish between cases where the true equilibrium state should be a single crystal versus a nanocrystalline state with solute decorated grain boundaries.

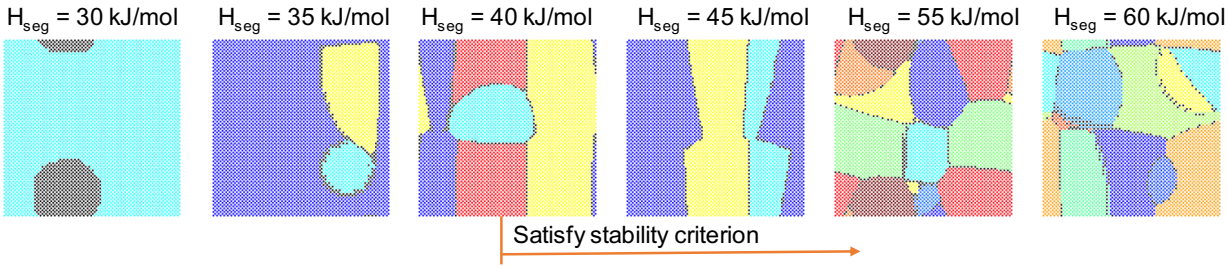

Figure 48: 0 K equilibrium microstructures as calculated by the Monte Carlo simulation. The ΔH_{mix} is 20 kJ/mol and the ΔH_{seg} is listed above each simulation. Systems above ΔH_{seg} = 40 kJ/mol are expected to satisfy the stability criterion. Different colors represent grains, black dots are solute. Grain boundary segregation is observed in all states with grain boundaries.

At the same time, the simulation is limited due to its current computational complexity, and there is an opportunity for future work to utilize this Monte Carlo algorithm if the time it takes

to perform grain swaps is reduced. Between 35 and 40 kJ/mol for the enthalpy of grain boundary segregation, there are grain boundaries at equilibrium. Similar behavior was found for simulations done with the enthalpy of mixing at 40 kJ/mol where the system that was 5 kJ/mol below the stability criterion still exhibited nanocrystallinity. It is likely that the grains in the 35 kJ/mol simulation are due to the simulation not reaching the true ground state.

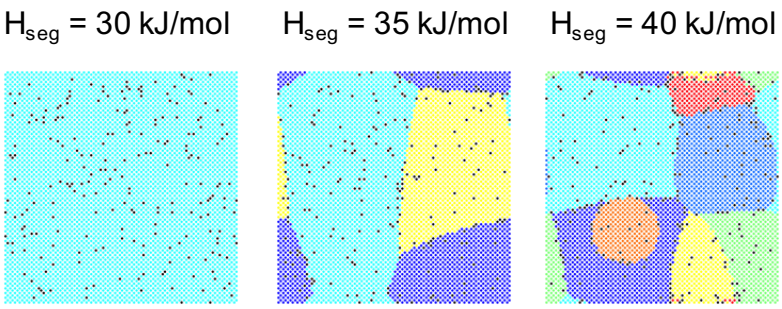

Figure 49: 1500 K equilibrium microstructures as calculated by the Monte Carlo simulation.

Figure 49 shows the equilibrated states at 1500 K, before the temperature was reduced in a stepwise fashion down to 0 K to produce the states shown in Figure 48. These equilibrated states do not show strong resemblance to the grain structures at 0 K in Figure 48. This is true not only for these simulations but simulations conducted at 40 kJ/mol enthalpy of mixing as well. This suggests that the grain swaps are still being accepted which means the simulation is likely not kinematically constrained at 1500 K. Studying the systems over the temperature range from 0 to 1500 K, it seems that such kinematic constraints set in close to 700 K, which is still a relatively high temperature for Monte Carlo simulations to be trapped. This is likely due to the low number of Monte Carlo swaps conducted; if closer to 50,000 grain swaps at each temperature were conducted, simulations at temperatures well below 700 K could be trusted.

Future work to do improve the runtime of this simulation could help answer many questions related to the thermodynamic stability of nanocrystalline alloys. First, the formal stability of duplex nanocrystalline alloys has not been rigorously confirmed by Monte Carlo simulations to date. The lattice-based methods of Chookajorn and Schuh show that this state may be stabilized for entropic reasons, but due to the aforementioned difficulty in getting robust ground states in that model, it is difficult to say for certain that the simulation simply does not get trapped in this state. The grain swaps in the algorithm described in this section are less likely to be trapped

in this manner since the grain swaps and atom swaps are all done in one single step and the changes in grain boundary topology space are generally more efficient due to the larger steps taken. Secondly, this model, in exploring the nanocrystalline phase space through grain swaps, may help us understand any entropy gained in nanocrystalline alloys due to the grain boundary topology configuration space. This could be an interesting added consideration in modeling the thermodynamics of stable nanocrystalline alloys.

Section 4.5: Conclusions

In this section, we understand some of the limitations of the existing lattice Monte Carlo simulations in exploring the thermodynamic phase space of nanocrystalline alloys. One of the key limitations is that the simulation is easily trapped in a local free energy minimum which hampers the reliability and robustness of the resulting calculations of the thermodynamic equilibrium state. To understand how grain size changes as a function of temperature and construct phase diagrams that can be used to understand how to process nanocrystalline materials with stable ground states, we develop a method that is more robust at identifying the thermodynamic equilibrium state. This method relies on sampling the grain boundary topology space by constructing a set of representative grain boundary topologies and performing Monte Carlo simulations of the solute configuration space to determine the free energy minimizing state. The simulation is used to construct nanocrystalline free energy and phase diagrams that show how the stable nanocrystalline states undergo a first-order order-disorder transformation, with many characteristics in common with bulk phase transformations. Finally, we explore alternative methods for exploring the grain boundary configuration space more efficiently to provide some ideas for future work in this field.

Chapter 5: Pathways for Grain Refinement in Alloys with Nanocrystalline Ground States

The processing of bulk nanocrystalline alloys through powder processing starts with the use of severe plastic deformation to decrease the grain size of the alloy to grain sizes in the 10 to 20 nm range. A phase diagram for a stable nanocrystalline alloy (such as the one in Figure 46) can then explain how annealing at a given temperature can lead to a nanocrystalline alloy with the desired grain size. For example, if the equilibrium grain size is around 35 nm, as shown in the free energy diagram in Figure 50 (representative of the low temperature free energy landscape for the W – 1 at.% Ti alloy from Figure 41b), the as-milled powder should undergo grain growth from its non-equilibrium state at 10 to 20 nm up to the equilibrium grain size of 35 nm. Grain growth in this case is expected to occur through standard grain coarsening kinetic mechanisms.

If the nanocrystalline alloy is instead processed to a state of 100 nm (green circle in Figure 50), this system is also a non-equilibrium state. However, the free energy landscape shows that in this case the free energy decreases with decreasing grain size. In such a state, the system should be stable against grain growth as increasing the grain size is thermodynamically unfavorable. Moreover, the system should favor a decrease in grain size, which can be referred to as grain refinement or grain shrinkage.

Formally, if the grain boundary energy is defined as $\gamma = dG/dA$, where G is the free energy and A is the grain boundary area, then a system under this condition has a "negative grain boundary energy", and this notion is often used to define systems in this condition [118-120]. However, the relationship $\gamma = dG/dA$ is only defined at a thermodynamic equilibrium, and since this system is not at equilibrium, it is more convenient to think of this system as a supersaturated state. Based on our analysis in Chapter 4, a system in this condition would be one that contains more solute in solution than would be thermodynamically preferred according to the equilibrium phase diagram. Thus, just as in the case of a typical supersaturated solution, the solutes in this state can decrease the free energy by forming more of the enthalpically preferred configuration. In the nanocrystalline alloy, this amounts to forming a larger grain boundary so that more of the solute species can segregate to the grain boundary and reach a lower free energy (Figure 51).

To date, observations of grain refinement in nanocrystalline materials have been limited to grain refinement in the case of recrystallization, which is driven by stored energy during plastic deformation. This section provides some early thoughts based on the thermodynamic analyses

conducted in this thesis as to why such behavior has not been observed and what considerations may help in devising a model to identify systems that could undergo grain refinement due to a chemical stored energy. If grain refinement in nanocrystalline alloys can be induced without plastic deformation and simply through proper alloy selection and thermal processing it will avail an exciting new processing pathway for producing bulk nanocrystalline alloys.

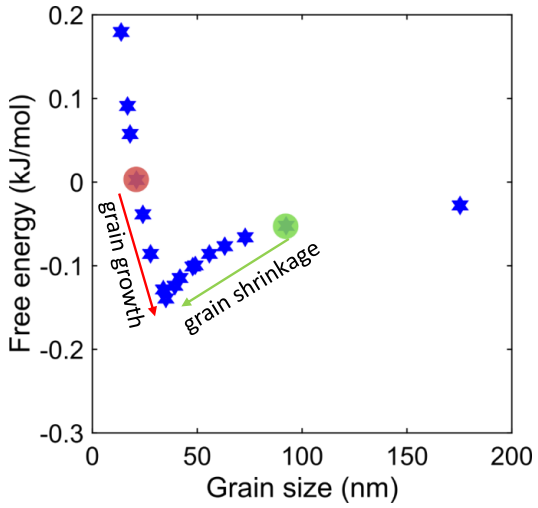

Figure 50: For grain sizes smaller than the equilibrium grain size, there is a driving force for grain growth. For grain sizes larger than the equilibrium size, the direction of the free energy gradient leads to a driving force for grain shrinkage instead of grain growth.

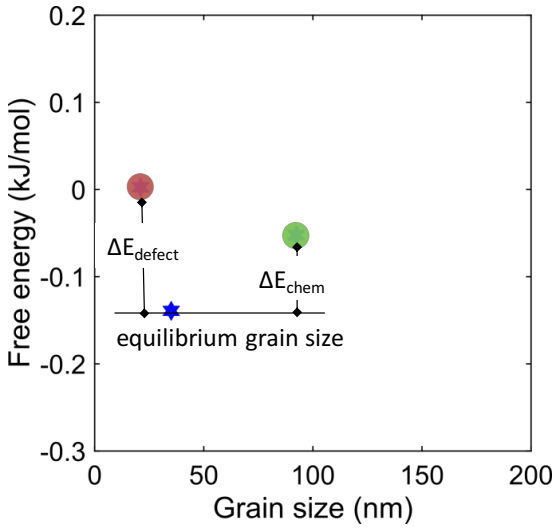

Figure 51: The driving force for grain growth is to decrease the grain boundary area (i.e. eliminate the excess energy due to defects). The driving force for grain shrinkage is to increase the amount of solute that is in a grain boundary segregated state, denoted as ΔE_{chem}.

A natural question to this entire premise is that if the models show that such a refinement is thermodynamically favorable, then why hasn't it been observed in any real materials? We explore this question first under the assumption that the theory presents reasonably accurate free energy landscapes, and then address reasons the theory may need to have additional considerations before it can be trusted in this context.

If in fact the free energy landscape shown in Figure 50 is present in alloys that meet the generalized stability criterion for nanocrystalline alloys (Figure 17), then there are some additional constraints that we can expect to make it difficult to observe chemically-induced grain refinement. First, there are typical challenges in processing nanocrystalline materials that could make isolating this type of behavior difficult. For instance, the influence of impurities on the nanocrystalline alloy phase space can change the free energy landscape. This is often observed through the presence of oxidation or the formation of carbides in nanocrystalline alloys that are otherwise expected to have strong stability against grain growth due to grain boundary segregation. Very few nanocrystalline alloy systems have been studied under pristine enough conditions where a formally stable nanocrystalline state (meeting the stability criterion) can be reasonably expected. As a result, the lack of observations of this phenomenon should not be used as the lone reason to dismiss it from being possible. Hopefully, with the advent of more accurate alloy selection and processing guidelines (such as the ones presented in this thesis) this will no longer be the largest bottleneck to studying this phenomenon.

The physical challenge to observing grain shrinkage may be that grain shrinkage involves kinetic mechanisms that require very precise thermal conditions to be active. Fischer et. al. developed a model of grain shrinkage driven by a negative grain boundary energy as a first attempt to treat such a kinetic process [119]. Their model studies the grain size distribution when evolved according to the Hillert grain growth model, but studied for the case where the grain boundary energy is negative. Their analytical model finds that in order for grain shrinkage to be possible there generally needs to be a nucleation event to produce new grains with smaller sizes. In the cases where no nucleation is present or the nucleation rate is relatively low, they find that the average grain size stays relatively steady, but the grain size distribution narrows sharply around the average grain size as without new grains the average grain size is heavily constrained. With a

sufficient nucleation rate, the grain size distribution moves to smaller grain sizes and becomes skewed to the right instead of to the left.

The nature of the nucleation mechanism for grain refinement requires further understanding of the energetic landscape for nucleated grains. In a classical nucleation process [13], the free energy of the nucleus as a function of nucleus size goes through a maximum at a critical radius, which can be defined as the nucleation barrier. The larger this nucleation barrier, and the more solutes needed to form a critical nucleus, the smaller the nucleation rate will be.

Figure 52 shows a schematic of how nuclei with different sizes forming at a triple junction would look for chemically-induced grain refinement.

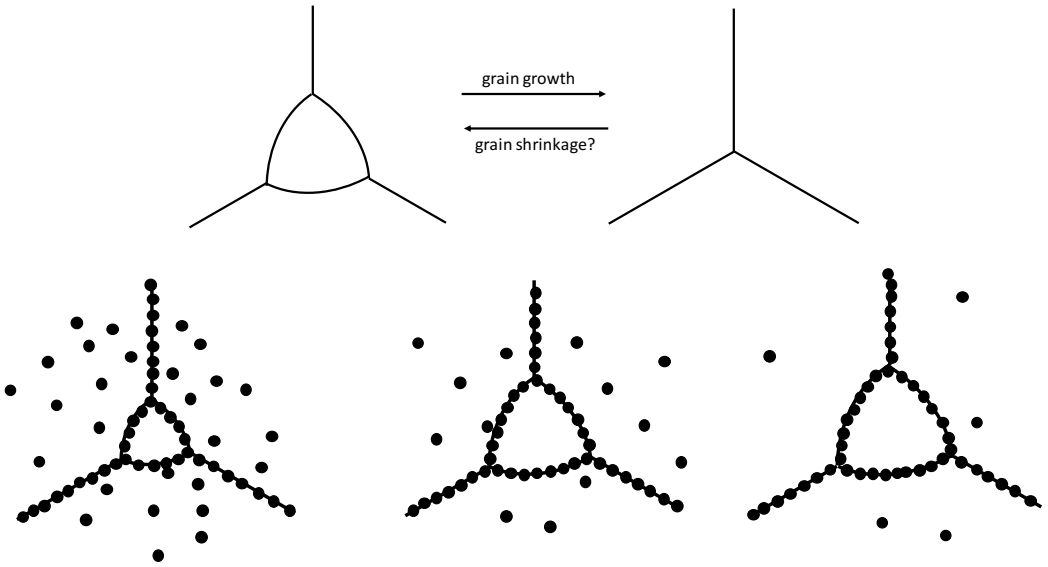

Figure 52: (Top) A schematic showing how nucleation of a grain at a triple junction could occur as the reverse of a grain growth process. (Bottom) A schematic of the solute distribution during nucleation of such a grain.

As the nucleus of the new grain grows, the grain boundary area also increases, allowing for more solute to segregate to the grain boundary. These solute, which leave the crystalline solution to form the ordered state at the grain boundary, will each gain an energy equal to $\Delta H_{seg} - k\gamma$ in accordance with the stability criterion (see Figure 28). From the perspective of a nucleation event, this energy is the driving force for nucleation, and would be considered the volumetric driving force if this were a phase transformation forming a precipitate. The second term expected

in classical nucleation is the interfacial energy, which increases with increasing size of the second phase, but at a slower rate than the volumetric term leading to the presence of a nucleation barrier. When modelling the process in Figure 52 in the nanocrystalline lattice model, however, there does not exist a clear interfacial energy in this system – in fact what is being formed is at first glance the interface itself.

Figure 53 shows a simple perturbation analysis on the lattice model to see how varying the interface area or curvature effects the energetics of the interface in this model. The perturbation consisted of a simple sine wave (Figure 53a). The wavelength and amplitude of this sine wave were varied and solute were allowed to segregate to the grain boundary (we used an enthalpy of mixing of 20 kJ/mol and an enthalpy of segregation of 60 kJ/mol, representative of W-Ti). Figures 53(b-c) show how the energy of the system varies with the wavelength and amplitude of the sine wave. In both cases, the energy decreases as the amount of area increases, monotonically, exhibiting no energetic barrier. This result is consistent with one of the challenges we faced with solute atoms wanting to have all grain boundary bonds to minimize their energy (Figure 36), which was deemed an unphysical result.

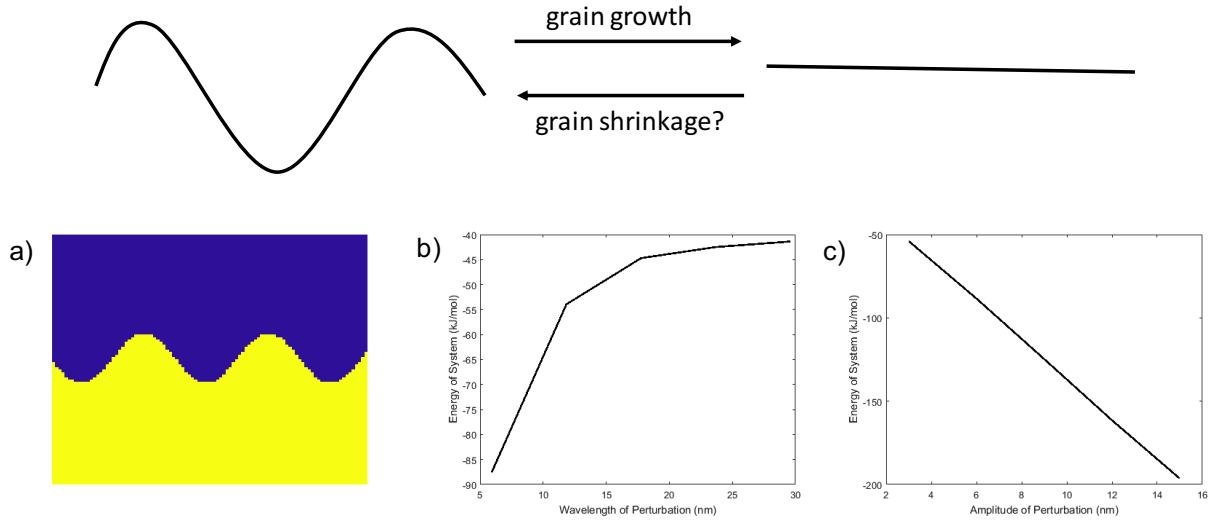

Figure 53: (Top) A schematic of how grain boundaries evolve in response to curvature in a case of grain shrinkage versus grain growth. The energetics of grain shrinkage from a flat surface in the lattice model were studied using a sinusoidal perturbation (pictured in (a)). The energy of the system decreases monotonically with decreasing wavelength (b) and increasing amplitude (c) of the perturbation.

This suggests that to model the nucleation of new grains in supersaturated, stable nanocrystalline alloys, the energetics of segregation need to be treated in more detail. This can be done within the lattice model through the consideration of longer-range interactions. If, for instance, there are longer range interactions that make it so that forming highly curved grain boundaries is energetically unfavorable, a nucleation barrier could be modeled. This may be expected in the case of highly ordered grain boundaries, where it is only below a certain curvature that the grain boundary can form the lowest energy complexion. For alloy-specific models, the use of an off-lattice model to understand the energetics of nucleation for a stable nanocrystalline alloy would provide even more detail regarding the nature of any nucleation barrier to the process of chemically-induced grain refinement. Alternatively, it is possible that no true nucleation barrier exists, which would mean that the schematic grain shrinkage transitions Figures 52 and 53 may be relatively easy to observe experimentally if stable nanocrystalline alloy systems are produced and if supersaturated states can be attained.

While the analytical and lattice model Monte Carlo simulations all produce free energy diagrams with thermodynamically stable grains, they each rely on a key assumption that the complex grain boundary network can be simplified to grain boundaries that all have roughly the same grain boundary energy and enthalpy of grain boundary segregation. The lattice Monte Carlo simulation provides some variety in grain boundary sites based on the coordination of grain boundary bonds, but this is still a very limited variation that misses out on the more important dependencies of grain boundary energies and segregation energies on the five-parameter description of a grain boundary, not to mention the degrees of freedom available in the local atomic environment (discussed in Section 1.4.4.1). Extending the theories developed in this thesis and prior to more accurate treatments of grain boundaries is an important area of future work and promises to help unearth important understanding regarding both the thermodynamics and kinetics of nanocrystalline alloys stabilized against grain growth by grain boundary segregation.

Chapter 6: Conclusions

Nanocrystalline materials have the potential to be lower cost, lighter-weight alternatives for applications requiring high hardness, wear resistance, and yield strength due to their fine grain size. In this thesis, we have developed thermodynamic models to identify alloy combinations that produce nanocrystalline materials that are stable against grain growth, which can enable the processing of bulk parts with nanocrystalline grain sizes as well as more reliable long-term use of nanocrystalline materials. The models developed here build upon previous works, with the ability to account for the presence of ordered compounds, include more detailed treatment of grain boundary segregation energies, and ensure ergodic sampling of the nanocrystalline configuration space for more reliable thermodynamic observations. Three different modeling frameworks were developed:

- An analytical model based on the free energy diagram for a binary alloy and the treatment of the grain boundary segregated state as an ordered 2D compound, was used to develop a generalized stability criterion for nanocrystalline alloys (Chapter 2).
- The lattice-based Monte Carlo simulation for nanocrystalline materials developed by Chookajorn and Schuh was improved to incorporate the presence of ordered compounds and a more rigorous treatment of grain boundary segregation energetics (Chapter 2).
- A statistical mechanics-based simulation framework where the grain boundary network configuration space and solute configuration space are decoupled for more rigorous analysis of thermodynamic equilibrium was developed to create equilibrium phase diagrams of stable nanocrystalline alloys (Chapter 4).

These models are useful tools for material scientists interested in the development of nanocrystalline materials. We learned a few new things from our own uses of these models to probe the thermodynamic behavior of nanocrystalline materials:

- A stability criterion for nanocrystalline alloys can be written in terms of macroscopic thermodynamic properties as: $\Delta H_{seg} > \Delta H_{mix} - 1/x_s^c \Delta H_{form} + k\gamma$ (Section 2.1).
- Ordered compounds with known structure and formation energy can be included in a lattice Monte Carlo simulation using the definition of simple compound units instead of a complete cluster expansion (Section 2.2).

- Stability as found through nanocrystalline lattice Monte Carlo simulations conforms to the analytical stability criterion (Section 2.3).
- Two-phase nanocrystalline alloys with ordered compounds, called ordered duplex nanocrystalline alloys, can be thermodynamically favored in alloy systems that are below the stability criterion but above the metastability criterion (Section 2.3).
- The lattice Monte Carlo simulation with ordered compounds can model complex alloy systems, such as the Ni-Ti-W shape memory alloy. While the nanograins in this system are stabilized by Zener drag, the Monte Carlo simulations show increased W segregation at elevated temperatures which coincides with the onset of rapid coarsening of the W precipitates and concomitant grain growth (Chapter 3).
- Thermodynamically stable nanocrystalline alloys undergo a first-order order-disorder transformation with increasing temperature, forming a solid solution at elevated temperatures (Chapter 4).
- Phase diagrams constructed for thermodynamically stable nanocrystalline alloys can be used to predict the equilibrium grain size as a function of temperature and solute concentration, which can inform both alloy selection and processing of nanocrystalline materials (Chapter 4).

References

1. Gleiter, H. (2000). Nanostructured materials: basic concepts and microstructure. *Acta materialia*, *48*(1), 1-29.
2. Suryanarayana, C. (1995). Nanocrystalline materials. *International Materials Reviews*, *40*(2), 41-64.3
3. Huang, T. Y., Kalidindi, A. R., & Schuh, C. A. (2018). Grain growth and second-phase precipitation in nanocrystalline aluminum–manganese electrodeposits. *Journal of Materials Science*, *53*(5), 3709-3719.
4. Hall, E. O. (1951). The deformation and ageing of mild steel: III discussion of results. *Proceedings of the Physical Society. Section B*, *64*(9), 747.
5. Petch, N. J. (1982). Citation classic-the cleavage strength of polycrystals. *Current Contents/Engineering Technology & Applied Sciences*, (19), 24-24.
6. Armstrong, R. W. (1970). The influence of polycrystal grain size on several mechanical properties of materials. *Metallurgical and Materials Transactions B*, *1*(5), 1169-1176.
7. Cordero, Z. C., Knight, B. E., & Schuh, C. A. (2016). Six decades of the Hall–Petch effect–a survey of grain-size strengthening studies on pure metals. *International Materials Reviews*, *61*(8), 495-512.
8. Cho, K., & Schuh, C. A. (2015). W-based amorphous phase stable to high temperatures. *Acta Materialia*, *85*, 331-342.
9. Frazer, L. (2006). Shiny science: a new substitute for hexavalent chromium. *Environmental Health Perspectives*, *114*(8), A482.
10. Murr, L. E. (1975). Interfacial phenomena in metals and alloys. Addison-Wesley Publishing Company, Reading, MA.
11. Murdoch, H. A. (2013). *Design of a stable nanocrystalline alloy.* (Doctoral dissertation, Massachusetts Institute of Technology).
12. Eckert, J., Das, J., Pauly, S., & Duhamel, C. (2007). Mechanical properties of bulk metallic glasses and composites. *Journal of materials research*, *22*(2), 285-301.
13. Balluffi, R. W., Allen, S., & Carter, W. C. (2005). *Kinetics of materials*. John Wiley & Sons.
14. Hillert, M. (1988). Inhibition of grain growth by second-phase particles. *Acta Metallurgica*, *36*(12), 3177-3181.

15. Srolovitz, D. J., Anderson, M. P., Grest, G. S., & Sahni, P. S. (1984). Computer simulation of grain growth-III. Influence of a particle dispersion. *Acta metallurgica*, *32*(9), 1429-1438.
16. Amram, Dor, and Christopher A. Schuh. "Interplay between thermodynamic and kinetic stabilization mechanisms in nanocrystalline Fe-Mg alloys." *Acta Materialia* 144 (2018): 447-458.
17. Chen, Y. Z., Herz, A., Li, Y. J., Borchers, C., Choi, P., Raabe, D., & Kirchheim, R. (2013). Nanocrystalline Fe–C alloys produced by ball milling of iron and graphite. *Acta Materialia*, *61*(9), 3172-3185.
18. Lücke, K., & Detert, K. (1957). A quantitative theory of grain-boundary motion and recrystallization in metals in the presence of impurities. *Acta Metallurgica*, *5*(11), 628-637.
19. Cahn, J. W. (1962). The impurity-drag effect in grain boundary motion. *Acta metallurgica*, *10*(9), 789-798.
20. Michels, A., Krill, C. E., Ehrhardt, H., Birringer, R., & Wu, D. T. (1999). Modelling the influence of grain-size-dependent solute drag on the kinetics of grain growth in nanocrystalline materials. *Acta materialia*, *47*(7), 2143-2152.
21. Koch, C. C., Scattergood, R. O., Darling, K. A., & Semones, J. E. (2008). Stabilization of nanocrystalline grain sizes by solute additions. *Journal of Materials Science*, *43*(23-24), 7264-7272.
22. Alexander, K. C., & Schuh, C. A. (2013). Exploring grain boundary energy landscapes with the activation-relaxation technique. *Scripta Materialia*, *68*(12), 937-940.
23. Wynblatt, P., & Chatain, D. (2006). Anisotropy of segregation at grain boundaries and surfaces. *Metallurgical and Materials Transactions A*, *37*(9), 2595-2620.
24. Hondros, E. D. (1965). The influence of phosphorus in dilute solid solution on the absolute surface and grain boundary energies of iron. In *Proc. R. Soc. Lond. A* (Vol. 286, No. 1407, pp. 479-498). The Royal Society.
25. Cahn, J.W. (1979). Surface Segregation in Metals and Alloys. ed. W. C. Johnson and J. M. Blakely (Metals Park, OH: ASM, 1979), p. 3.
26. Weissmüller, J. (1994). Alloy thermodynamics in nanostructures. *Journal of materials research*, *9*(1), 4-7.
27. Weissmüller, J. (1993). Alloy effects in nanostructures. *Nanostructured Materials*, *3*(1-6), 261-272.

28. Seidman, D. N. (2002). Subnanoscale studies of segregation at grain boundaries: Simulations and experiments. *Annual Review of Materials Research*, *32*(1), 235-269.
29. Foiles, S. M. (1989). Calculation of grain-boundary segregation in Ni-Cu alloys. *Physical Review B*, *40*(17), 11502.
30. Gibson, M. A., & Schuh, C. A. (2016). A survey of ab-initio calculations shows that segregation-induced grain boundary embrittlement is predicted by bond-breaking arguments. *Scripta Materialia*, *113*, 55-58.
31. Murdoch, H. A., & Schuh, C. A. (2013). Estimation of grain boundary segregation enthalpy and its role in stable nanocrystalline alloy design. *Journal of Materials Research*, *28*(16), 2154-2163.
32. Choi, P., da Silva, M., Klement, U., Al-Kassab, T., & Kirchheim, R. (2005). Thermal stability of electrodeposited nanocrystalline Co-1.1 at.% P. *Acta Materialia*, *53*(16), 4473-4481.
33. Choi, P., Al-Kassab, T., Gärtner, F., Kreye, H., & Kirchheim, R. (2003). Thermal stability of nanocrystalline nickel–18 at.% tungsten alloy investigated with the tomographic atom probe. *Materials Science and Engineering: A*, *353*(1-2), 74-79.
34. Mehta, S. C., Smith, D. A., & Erb, U. (1995). Study of grain growth in electrodeposited nanocrystalline nickel-1.2 wt.% phosphorus alloy. *Materials Science and Engineering: A*, *204*(1-2), 227-232.
35. Hentschel, T. H., Isheim, D., Kirchheim, R., Müller, F., & Kreye, H. (2000). Nanocrystalline Ni–3.6 at.% P and its transformation sequence studied by atom-probe field-ion microscopy. *Acta materialia*, *48*(4), 933-941.
36. Darling, K. A., VanLeeuwen, B. K., Koch, C. C., & Scattergood, R. O. (2010). Thermal stability of nanocrystalline Fe–Zr alloys. *Materials Science and Engineering: A*, *527*(15), 3572-3580.
37. Detor, A. J., & Schuh, C. A. (2007). Tailoring and patterning the grain size of nanocrystalline alloys. *Acta Materialia*, *55*(1), 371-379.
38. Eckert, J., Holzer, J. C., & Johnson, W. L. (1993). Thermal stability and grain growth behavior of mechanically alloyed nanocrystalline Fe-Cu alloys. *Journal of applied physics*, *73*(1), 131-141.

39. Trelewicz, J. R., & Schuh, C. A. (2009). Grain boundary segregation and thermodynamically stable binary nanocrystalline alloys. *Physical Review B*, *79*(9), 094112.
40. Porter, D. A., & Easterling, K. E. (1992). Phase transitions in metals and alloys. Chipman and Hall, London.
41. Murdoch, H. A., & Schuh, C. A. (2013). Stability of binary nanocrystalline alloys against grain growth and phase separation. *Acta Materialia*, *61*(6), 2121-2132.
42. Darling, K. A., Tschopp, M. A., VanLeeuwen, B. K., Atwater, M. A., & Liu, Z. K. (2014). Mitigating grain growth in binary nanocrystalline alloys through solute selection based on thermodynamic stability maps. *Computational Materials Science*, *84*, 255-266.
43. Saber, M., Kotan, H., Koch, C. C., & Scattergood, R. O. (2013). Thermodynamic stabilization of nanocrystalline binary alloys. *Journal of applied physics*, *113*(6), 063515.
44. Saber, M., Kotan, H., Koch, C. C., & Scattergood, R. O. (2013). A predictive model for thermodynamic stability of grain size in nanocrystalline ternary alloys. *Journal of Applied Physics*, *114*(10), 103510.
45. Saber, M., Koch, C. C., & Scattergood, R. O. (2015). Thermodynamic grain size stabilization models: an overview. *Materials Research Letters*, *3*(2), 65-75.
46. Chookajorn, T., Murdoch, H. A., & Schuh, C. A. (2012). Design of stable nanocrystalline alloys. *Science*, *337*(6097), 951-954.
47. Zhou, N., & Luo, J. (2014). Developing thermodynamic stability diagrams for equilibrium-grain-size binary alloys. *Materials Letters*, *115*, 268-271.
48. Xing, W., Kalidindi, A. R., & Schuh, C. A. (2017). Preferred nanocrystalline configurations in ternary and multicomponent alloys. *Scripta Materialia*, *127*, 136-140.
49. Kalidindi, A. R., Chookajorn, T., & Schuh, C. A. (2015). Nanocrystalline materials at equilibrium: a thermodynamic review. *JOM*, *67*(12), 2834-2843.
50. Millett, P. C., Selvam, R. P., & Saxena, A. (2007). Stabilizing nanocrystalline materials with dopants. *Acta Materialia*, *55*(7), 2329-2336.
51. Millett, P. C., Selvam, R. P., Bansal, S., & Saxena, A. (2005). Atomistic simulation of grain boundary energetics–Effects of dopants. *Acta Materialia*, *53*(13), 3671-3678.
52. Millett, P. C., Selvam, R. P., & Saxena, A. (2006). Molecular dynamics simulations of grain size stabilization in nanocrystalline materials by addition of dopants. *Acta materialia*, *54*(2), 297-303.

53. Landau, D. P., & Binder, K. (2014). A guide to Monte Carlo simulations in statistical physics. Cambridge university press.
54. Ceder, G. (1993). A derivation of the Ising model for the computation of phase diagrams. *Computational Materials Science*, *1*(2), 144-150.
55. Guttman, L. (1961). Monte Carlo Computations on the Ising Model. The Body-Centered Cubic Lattice. *The Journal of Chemical Physics*, *34*(3), 1024-1036.
56. Binder, K. (1980). Ordering of the face-centered-cubic lattice with nearest-neighbor interaction. *Physical Review Letters*, *45*(10), 811.
57. Binder, K. (1981). Monte Carlo study of entropy for face-centered cubic Ising antiferromagnets. *Zeitschrift für Physik B Condensed Matter*, *45*(1), 61-69.
58. Binder, K., Lebowitz, J. L., Phani, M. K., & Kalos, M. H. (1981). Monte Carlo study of the phase diagrams of binary alloys with face centered cubic lattice structure. *Acta Metallurgica*, *29*(9), 1655-1665.
59. Dillon, S. J., Tang, M., Carter, W. C., & Harmer, M. P. (2007). Complexion: A new concept for kinetic engineering in materials science. *Acta Materialia*, *55*(18), 6208-6218.
60. Cantwell, P. R., Tang, M., Dillon, S. J., Luo, J., Rohrer, G. S., & Harmer, M. P. (2014). Grain boundary complexions. *Acta Materialia*, *62*, 1-48.
61. Rittner, J. D., Foiles, S. M., & Seidman, D. N. (1994). Simulation of surface segregation free energies. *Physical Review B*, *50*(16), 12004.
62. Foiles, S. M. (1989). Calculation of grain-boundary segregation in Ni-Cu alloys. *Physical Review B*, *40*(17), 11502.
63. Udler, D., & Seidman, D. N. (1998). Monte Carlo simulation of the concentration dependence of segregation at vicinal grain boundaries. *Interface Science*, *6*(4), 259-265.
64. Udler, D., & Seidman, D. N. (1998). Solute segregation at [001] tilt boundaries in dilute fcc alloys. *Acta materialia*, *46*(4), 1221-1233.
65. Detor, A. J., & Schuh, C. A. (2007). Grain boundary segregation, chemical ordering and stability of nanocrystalline alloys: Atomistic computer simulations in the Ni–W system. *Acta Materialia*, *55*(12), 4221-4232.
66. Purohit, Y., Sun, L., Irving, D. L., Scattergood, R. O., & Brenner, D. W. (2010). Computational study of the impurity induced reduction of grain boundary energies in nano-

and bi-crystalline Al–Pb alloys. *Materials Science and Engineering: A*, *527*(7-8), 1769-1775.

67. Purohit, Y., Jang, S., Irving, D. L., Padgett, C. W., Scattergood, R. O., & Brenner, D. W. (2008). Atomistic modeling of the segregation of lead impurities to a grain boundary in an aluminum bicrystalline solid. *Materials Science and Engineering: A*, *493*(1-2), 97-100.
68. Chookajorn, T., & Schuh, C. A. (2014). Thermodynamics of stable nanocrystalline alloys: a Monte Carlo analysis. *Physical Review B*, *89*(6), 064102.
69. Anderson, M. P., Srolovitz, D. J., Grest, G. S., & Sahni, P. S. (1984). Computer simulation of grain growth—I. Kinetics. *Acta metallurgica*, *32*(5), 783-791.
70. Holm, E. A., & Battaile, C. C. (2001). The computer simulation of microstructural evolution. *Jom*, *53*(9), 20-23.
71. Chookajorn, T., & Schuh, C. A. (2014). Nanoscale segregation behavior and high-temperature stability of nanocrystalline W–20 at.% Ti. *Acta Materialia*, *73*, 128-138.
72. Chookajorn, T., Park, M., & Schuh, C. A. (2015). Duplex nanocrystalline alloys: entropic nanostructure stabilization and a case study on W–Cr. *Journal of Materials Research*, *30*(2), 151-163.
73. Kalidindi, A. R., & Schuh, C. A. (2017). Stability criteria for nanocrystalline alloys. *Acta Materialia*, *132*, 128-137.
74. Saal, J. E., Kirklin, S., Aykol, M., Meredig, B., & Wolverton, C. (2013). Materials design and discovery with high-throughput density functional theory: the open quantum materials database (OQMD). *Jom*, *65*(11), 1501-1509.
75. Jain, A., Ong, S. P., Hautier, G., Chen, W., Richards, W. D., Dacek, S., ... & Persson, K. A. (2013). Commentary: The Materials Project: A materials genome approach to accelerating materials innovation. *Apl Materials*, *1*(1), 011002.
76. Curtarolo, S., Setyawan, W., Wang, S., Xue, J., Yang, K., Taylor, R. H., ... & Mingo, N. (2012). AFLOWLIB. ORG: A distributed materials properties repository from high-throughput ab initio calculations. *Computational Materials Science*, *58*, 227-235.
77. Guttmann, M. (1977). Grain boundary segregation, two dimensional compound formation, and precipitation. *Metallurgical Transactions A*, *8*(9), 1383-1401.
78. Kirchheim, R. (1992). Physics and chemistry of segregation at internal interfaces. *Chapman & Hall(UK), 1992,*, 481-496.

79. Boer, F., Boom, R., Mattens, W. C. M., Miedema, A. R., & Niessen, A. K. (1988). Cohesion in Metals: Transition Metal Alloys, North Holland, Amsterdam.
80. Kittel, C. Introduction to Solid State Physics, fourth ed., Malden, Massachusetts, 2005.
81. Raabe, D., Herbig, M., Sandlöbes, S., Li, Y., Tytko, D., Kuzmina, M., ... & Choi, P. P. (2014). Grain boundary segregation engineering in metallic alloys: A pathway to the design of interfaces. *Current Opinion in Solid State and Materials Science*, *18*(4), 253-261.
82. Hondros, E. D., & Seah, M. P. (1972). Grain boundary activity measurements by Auger electron spectroscopy. *Scripta Metallurgica*, *6*(10), 1007-1012.
83. Connolly, J. W. D., & Williams, A. R. (1983). Density-functional theory applied to phase transformations in transition-metal alloys. *Physical Review B*, *27*(8), 5169.
84. Sanchez, J. M., Ducastelle, F., & Gratias, D. (1984). Generalized cluster description of multicomponent systems. *Physica A: Statistical Mechanics and its Applications*, *128*(1-2), 334-350.
85. Asta, M., Wolverton, C., De Fontaine, D., & Dreyssé, H. (1991). Effective cluster interactions from cluster-variation formalism. I. *Physical Review B*, *44*(10), 4907.
86. Wolverton, C., Asta, M., Dreyssé, H., & De Fontaine, D. (1991). Effective cluster interactions from cluster-variation formalism. II. *Physical Review B*, *44*(10), 4914.
87. Laks, D. B., Ferreira, L. G., Froyen, S., & Zunger, A. (1992). Efficient cluster expansion for substitutional systems. *Physical Review B*, *46*(19), 12587.
88. van de Walle, A., & Ceder, G. (2002). Automating first-principles phase diagram calculations. *Journal of Phase Equilibria*, *23*(4), 348.
89. Wei, S. H., Ferreira, L. G., & Zunger, A. (1990). First-principles calculation of temperature-composition phase diagrams of semiconductor alloys. *Physical Review B*, *41*(12), 8240.
90. Terakura, K., Oguchi, T., Mohri, T., & Watanabe, K. (1987). Electronic theory of the alloy phase stability of Cu-Ag, Cu-Au, and Ag-Au systems. *Physical Review B*, *35*(5), 2169.
91. Ozoliņš, V., Wolverton, C., & Zunger, A. (1998). Cu-Au, Ag-Au, Cu-Ag, and Ni-Au intermetallics: First-principles study of temperature-composition phase diagrams and structures. *Physical Review B*, *57*(11), 6427.

92. Kalidindi, A. R., & Schuh, C. A. (2016). A compound unit method for incorporating ordered compounds into lattice models of alloys. *Computational Materials Science*, *118*, 172-179.
93. Binder, K., & Landau, D. P. (1980). Phase diagrams and critical behavior in Ising square lattices with nearest-and next-nearest-neighbor interactions. *Physical Review B*, *21*(5), 1941.
94. Gahn, U. (1986). Ordering in face-centered cubic binary crystals confined to nearest-neighbour interactions—Monte Carlo calculations. *Journal of Physics and Chemistry of Solids*, *47*(12), 1153-1169.
95. Ackermann, H., Inden, G., & Kikuchi, R. (1989). Tetrahedron approximation of the cluster variation method for bcc alloys. *Acta Metallurgica*, *37*(1), 1-7.
96. Colinet, C., Inden, G., & Kikuchi, R. (1993). CVM calculation of the phase diagram of bcc Fe-Co-Al. *Acta metallurgica et materialia*, *41*(4), 1109-1118.
97. Darling, K. A., VanLeeuwen, B. K., Semones, J. E., Koch, C. C., Scattergood, R. O., Kecskes, L. J., & Mathaudhu, S. N. (2011). Stabilized nanocrystalline iron-based alloys: Guiding efforts in alloy selection. *Materials Science and Engineering: A*, *528*(13-14), 4365-4371.
98. Detor, A. J., & Schuh, C. A. (2007). Microstructural evolution during the heat treatment of nanocrystalline alloys. *Journal of Materials Research*, *22*(11), 3233-3248.
99. Clark, B. G., Hattar, K., Marshall, M. T., Chookajorn, T., Boyce, B. L., & Schuh, C. A. (2016). Thermal stability comparison of nanocrystalline Fe-based binary alloy pairs. *JOM*, *68*(6), 1625-1633.
100. Liu, F. (2005). Grain growth in nanocrystalline Fe–Ag thin film. *Materials Letters*, *59*(11), 1458-1462.
101. Polyakov, M. N., Chookajorn, T., Mecklenburg, M., Schuh, C. A., & Hodge, A. M. (2016). Sputtered Hf–Ti nanostructures: A segregation and high-temperature stability study. *Acta Materialia*, *108*, 8-16.
102. Chluba, C., Ge, W., de Miranda, R. L., Strobel, J., Kienle, L., Quandt, E., & Wuttig, M. (2015). Ultralow-fatigue shape memory alloy films. *Science*, *348*(6238), 1004-1007.

103. Ko, W. S., Maisel, S. B., Grabowski, B., Jeon, J. B., & Neugebauer, J. (2017). Atomic scale processes of phase transformations in nanocrystalline NiTi shape-memory alloys. *Acta Materialia*, *123*, 90-101.
104. Qiao, L., & Radovitzky, R. (2016). Computational modeling of size-dependent superelasticity of shape memory alloys. *Journal of the Mechanics and Physics of Solids*, *93*, 93-117.
105. Tsuchiya, K., Inuzuka, M., Tomus, D., Hosokawa, A., Nakayama, H., Morii, K., ... & Umemoto, M. (2006). Martensitic transformation in nanostructured TiNi shape memory alloy formed via severe plastic deformation. *Materials Science and Engineering: A*, *438*, 643-648.
106. Tsuchiya, K., Hada, Y., Koyano, T., Nakajima, K., Ohnuma, M., Koike, T., ... & Umemoto, M. (2009). Production of TiNi amorphous/nanocrystalline wires with high strength and elastic modulus by severe cold drawing. *Scripta Materialia*, *60*(9), 749-752.
107. Waitz, T., Tsuchiya, K., Antretter, T., & Fischer, F. D. (2009). Phase transformations of nanocrystalline martensitic materials. *MRS bulletin*, *34*(11), 814-821.
108. Buenconsejo, P. J. S., Zarnetta, R., & Ludwig, A. (2011). The effects of grain size on the phase transformation properties of annealed (Ti/Ni/W) shape memory alloy multilayers. *Scripta Materialia*, *64*(11), 1047-1050.
109. Buenconsejo, P. J. S., Zarnetta, R., König, D., Savan, A., Thienhaus, S., & Ludwig, A. (2011). A New Prototype Two-Phase (TiNi)–(β-W) SMA System with Tailorable Thermal Hysteresis. *Advanced Functional Materials*, *21*(1), 113-118.
110. Callisti, M. A. U. R. O., Mellor, B. G., & Polcar, T. (2014). Microstructural investigation on the grain refinement occurring in Cu-doped Ni–Ti thin films. *Scripta Materialia*, *77*, 52-55.
111. Kaur, N., & Kaur, D. (2013). Grain refinement of NiTi shape memory alloy thin films by W addition. *Materials Letters*, *91*, 202-205.
112. Ahadi, A., Kalidindi, A. R., Sakurai, J., Matsushita, Y., Tsuchiya, K., & Schuh, C. A. (2018). The role of W on the thermal stability of nanocrystalline NiTiWx thin films. *Acta Materialia*, *142*, 181-192.
113. Khalajhedayati, A., & Rupert, T. J. (2015). High-temperature stability and grain boundary complexion formation in a nanocrystalline Cu-Zr alloy. *JOM*, *67*(12), 2788-2801.

114. Khalajhedayati, A., Pan, Z., & Rupert, T. J. (2016). Manipulating the interfacial structure of nanomaterials to achieve a unique combination of strength and ductility. *Nature communications*, *7*, 10802.
115. Divinski, S., Ribbe, J., Schmitz, G., & Herzig, C. (2007). Grain boundary diffusion and segregation of Ni in Cu. *Acta Materialia*, *55*(10), 3337-3346.
116. Kalidindi, A. R., & Schuh, C. A. (2017). Phase transitions in stable nanocrystalline alloys. *Journal of Materials Research*, *32*(11), 1993-2002.
117. Larsen, P. M., Kalidindi, A. R., Schmidt, S., & Schuh, C. A. (2017). Alloy design as an inverse problem of cluster expansion models. *Acta Materialia*, *139*, 254-260.
118. Kirchheim, R. (2006). Comment on "Unexplored topics and potentials of grain boundary engineering" by LS Shvindlerman and G. Gottstein. *Scripta materialia*, *55*(10), 963-964.
119. Fischer, F. D., Zickler, G. A., & Svoboda, J. (2017). Modelling of grain refinement driven by negative grain boundary energy. *Philosophical Magazine*, *97*(23), 1963-1977.
120. Fabris, S., & Elsässer, C. (2003). First-principles analysis of cation segregation at grain boundaries in α-Al2O3. *Acta Materialia*, *51*(1), 71-86.